CALIFORNIA INSTITUTE OF TECHNOLOGY

ELECTRICAL ENGINEERING DEPARTMENT

LOW FREQUENCY, CONTINUOUS WAVE, IONOSPHERIC RESEARCH

by

C. W. Bergman
R. S. Macmillan
W. H. Pickering

FINAL TECHNICAL REPORT

October 15, 1953

A REPORT ON RESEARCH CONDUCTED UNDER
CONTRACT WITH THE OFFICE OF NAVAL RESEARCH

LOW FREQUENCY, CONTINUOUS WAVE, IONOSPHERIC RESEARCH

by

C. W. Bergman
R. S. Macmillan
W. H. Pickering

CALIFORNIA INSTITUTE OF TECHNOLOGY
PASADENA, CALIFORNIA

A FINAL REPORT TO THE OFFICE OF NAVAL RESEARCH

PREPARED FOR

OFFICE OF NAVAL RESEARCH CONTRACT Nonr-220(07)
(April 1, 1952 - March 31, 1953)

October 15, 1953

ABSTRACT

A new, continuous-wave, phase-measuring technique for ionospheric observations at low and very-low frequencies is described. The essential features of the system are (1) a horizontal transmitting antenna near the surface of the ground which is resonant at the operating frequency and which radiates no ground wave in the direction of the receiver and (2) a receiving station located within line-of-sight of the transmitter at which the phase of the low-frequency sky wave is directly compared with a reference phase transmitted over a very-high-frequency link.

Low-frequency ionospheric polarization, relative virtual height, and relative reflection coefficient measurements were made at near vertical incidence during October 1952. These measurements were made at a frequency of 50 kc/s.

The virtual height of the E-layer was found to change by approximately 7.5 km during the sunrise and sunset periods. Rapid fluctuations in the virtual height and reflection coefficients of the E-layer are attributed to (1) strong magneto-ionic splitting, (2) fluctuating ionization gradients in the lower nighttime E-region, (3) interference effects due to the presence of two or more partially reflecting layers (i. e., the fine structure of the E-layer), and (4) interference effects due to the interaction of the two magneto-ionic components.

Low-frequency noise measurements were also made during October 1952. The 50-kc/s atmospheric noise field strength reached a maximum value during the middle of the night. The atmospheric noise received in the east-west direction reached a much higher maximum value than that received in the north-south direction.

The applicability of the quasi-homogeneous, magneto-ionic theory to low-frequency-propagation problems is considered.

TABLE OF CONTENTS

LOW FREQUENCY, CONTINUOUS WAVE, IONOSPHERIC RESEARCH

I. INTRODUCTION

A number of radio methods have been developed for exploring the ionospheric regions. However, most of the investigations have been conducted by using radio frequencies in the range of 0.5 to 30 megacycles per second. During the past several years, a few stations have been established for investigating the properties of the ionosphere in the frequency range of 100 to 350 kilocycles per second. There are very few ionospheric data available at frequencies below 100 kc/s. Nearly all the work below 50 kc/s has been done in England, where use was made of the 16-kc/s GBR transmitter at Rugby. At 16 kc/s, the English investigators observed sudden phase anomalies which were strongly correlated with the appearance of solar flares and the fadeout of short radio waves.

During the past few years, there has been increasing interest in the properties of the ionosphere at very-low and low radio frequencies. Data of this type are needed for the design and establishment of low-frequency, high-precision navigational systems. Data on very-low-frequency propagation are needed by the United States Navy, which is using frequencies in this range to communicate with the fleet and submerged submarines. There are many unsolved problems regarding the constitution, circulation, and ionization processes in the lower regions of the ionosphere. It is expected that very-low-frequency and low-frequency radio measurements will help solve some of these problems.

The aim of the research program being conducted at the California Institute of Technology has been to design a practical, flexible, and inexpensive system for investigating the ionosphere at very-low and low radio frequencies.

One of the problems in studying the structure of the ionosphere with very-low-frequency radio waves is that of obtaining a suitable source for the transmissions. The usual approach is to utilize some existing transmitting station, or to build a "small" antenna and then pulse it with a large peak power.

The purpose of this report is to describe a new technique for investigating the ionosphere at low frequencies and to present some preliminary data. A new type of antenna is employed which appears to be of considerable value as a tool for low-frequency investigations. The significant feature of the antenna is that it is built over desert terrain where the rock is essentially a dielectric. Such an antenna radiates a horizontally polarized wave vertically upwards. At the same time no energy is radiated along the ground in the direction normal to the antenna. The antenna is cheap and simple to construct for any desired frequency, provided that desert terrain similar to the Mojave Desert of California is available. Furthermore the radiation efficiency is relatively high.

II. THE LOW-FREQUENCY IONOSPHERIC STATION

A complete low-frequency ionospheric sounding station has been constructed and successfully operated. The station is located in the Mojave Desert of California. The transmitting site is 10 miles southwest of Randsburg, California, and the receiving site is 15 miles northwest of Victorville, Calif. The distance between the sites is approximately 64 km. This location for the station was chosen because the characteristics of the ground are very favorable, and the noise level is relatively low.

A. The Principles of Operation on the System

The principles of operation of the system are illustrated in Figures 1 and 2. The transmitting antenna is a horizontal, resonant dipole placed near the surface of the earth. The properties of this antenna are such that no ground wave is propagated in the direction normal to the antenna. The receiving site is located in this direction, off the side of the transmitting antenna. A very-high-frequency, line-of-sight link is established between the transmitting and receiving stations. In principle, the very-high-frequency signal is modulated by the low-frequency transmitter, and a phase comparison is made between the low-frequency sky wave and the modulation of the very-high-frequency signal.

B. The Transmitting Antenna

The transmitting antenna consists of a wire 26,000 feet long supported about 11 feet above the ground. The antenna may be sectioned by switches which are located every 1,000 feet along the antenna. The antenna is tuned to the proper frequency by opening the appropriate switches. The antenna can be operated as a resonant dipole in the frequency range of 18 to 250 kc/s.

The field pattern in the plane normal to the length of the antenna is obtained by considering the direct and reflected waves radiated by the antenna. The two waves are added in order to obtain the total radiation field of the antenna. The magnitude and phase of the reflected wave are determined by the characteristics of the ground. When the reflected wave is added to the direct wave, a pattern such as that shown in Figure 3 is obtained.

The field strength above the antenna is a maximum when the ground conductivity and relative capacitivity are low. For this reason, a site for the transmitting antenna was chosen in the Mojave Desert, which is an arid region. The transmitting antenna is located on a long, high, granite ridge. The ridge is about 10 miles long and several miles wide. The cracks in the granite are dry to a depth probably in excess of 1,200 feet.

In addition to the pattern shown in Figure 3, the antenna excites a ground wave whose pattern is shown in Figure 4. It is important

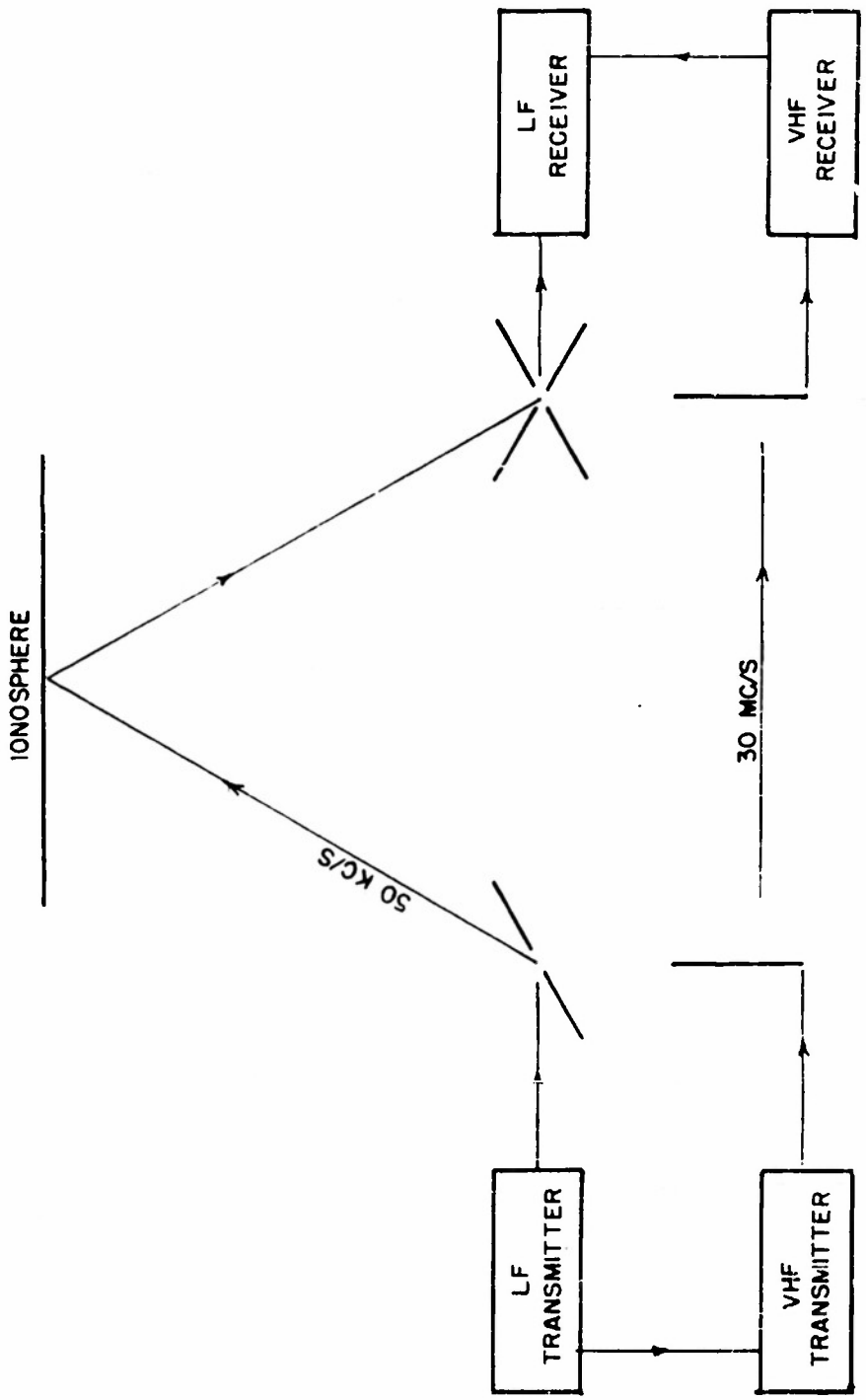

FIGURE 1 BLOCK DIAGRAM OF 50-KC/S IONOSPHERIC STATION

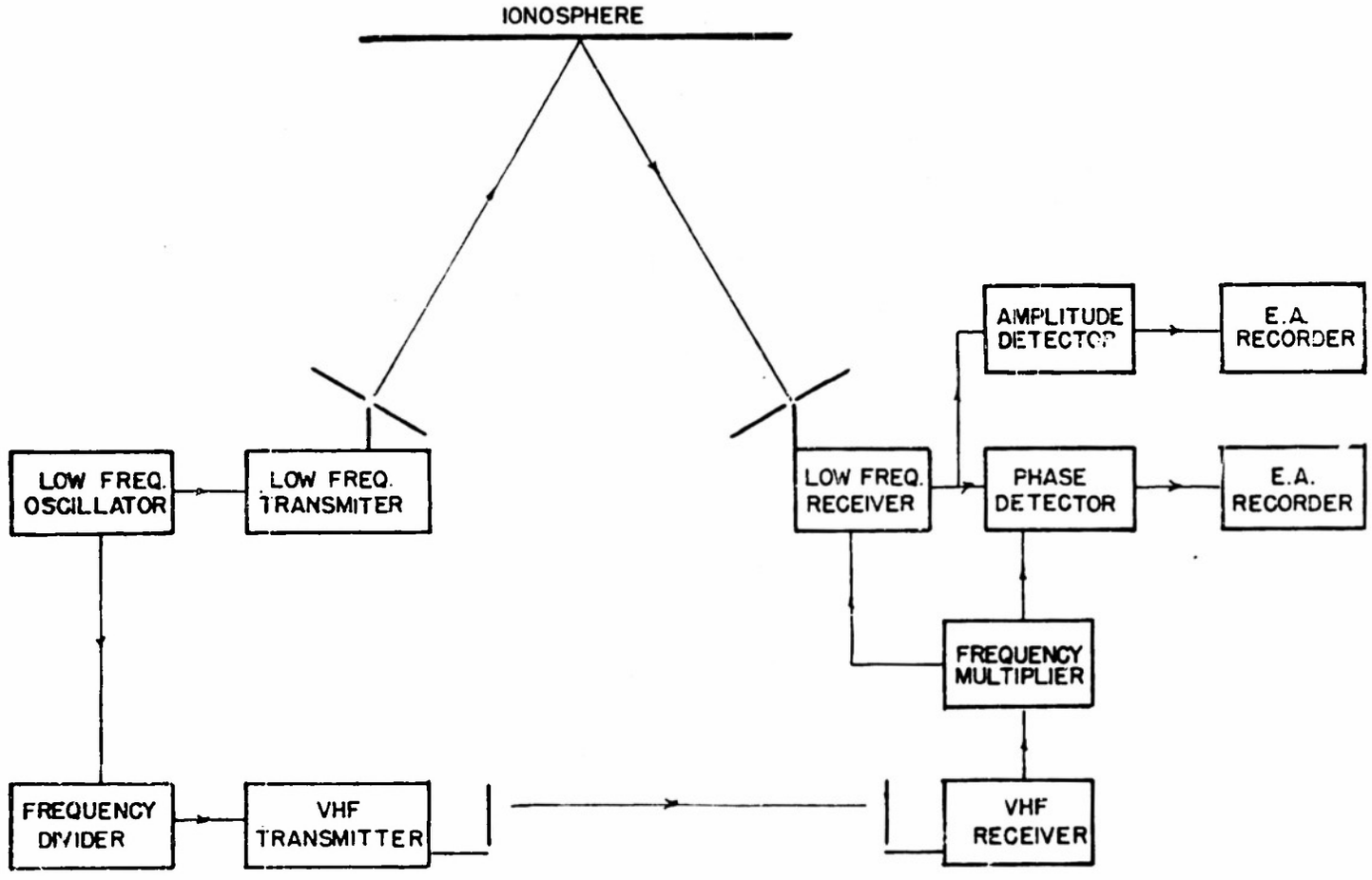

FIGURE 2. BLOCK DIAGRAM OF THE TRANSMITTING AND RECEIVING SYSTEM

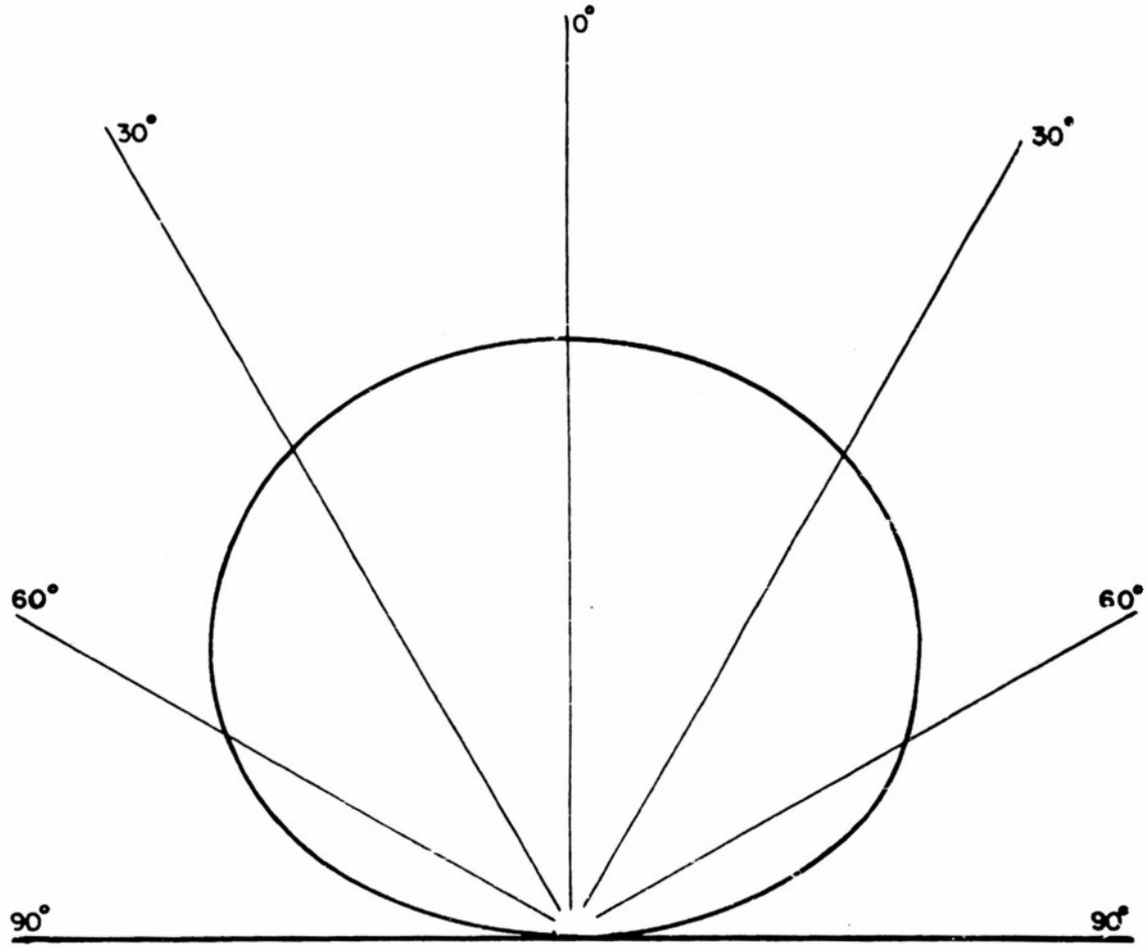

FIGURE 3. FIELD PATTERN IN THE PLANE NORMAL TO THE LENGTH OF THE DIPOLE

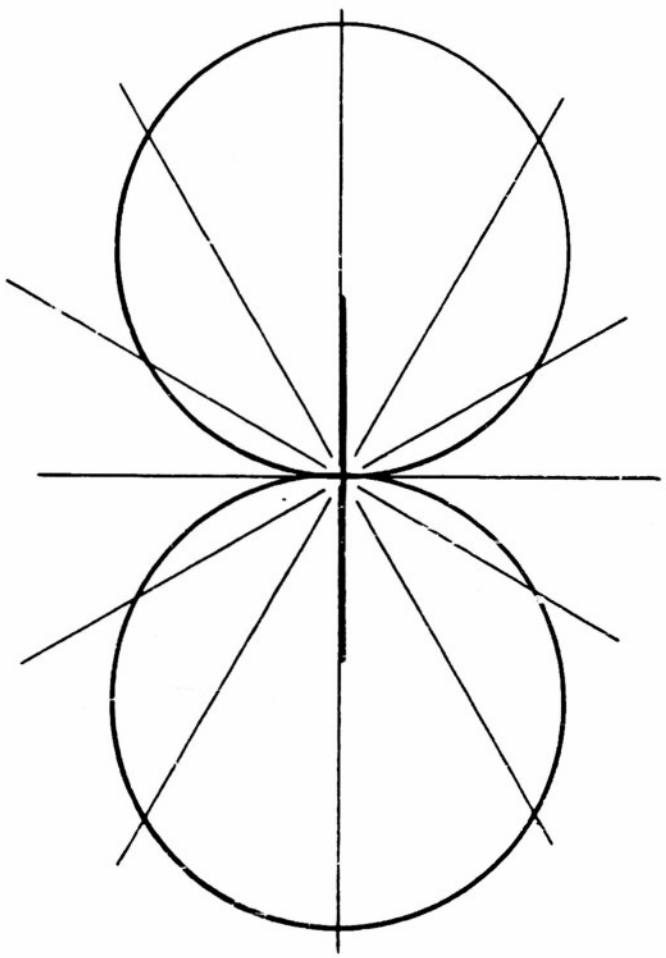

FIGURE 4. GROUND WAVE PATTERN OF A HORIZONTAL DIPOLE OVER THE EARTH

to note that there is no ground wave in the direction normal to the length of the antenna. As with the field strength above the antenna, the ground-wave intensity is determined by the ground constants.

The system has been operated at a frequency of 50 kc/s. At 50 kc/s, the resonant length of the antenna is 8,600 feet. In order to match the 100-ohm output impedance of the transmitter, the antenna was fed at a point 1,700 feet from the center. The center-fed antenna has an input impedance of 65 ohms, resistive. The measured quality factor Q of the antenna is 12.

A detailed analysis of the transmitting antenna is given in Section IV.

C. The Transmitting-Receiving System

The transmitting and receiving antennae are oriented as shown in Figure 5. The bearing of the transmitter from the receiver is 347°, whereas the magnetic north pole has a bearing of 16°. The altitude of both sites is about 3,500 feet, and they are within line-of-sight of each other.

The transmitter feeding the low-frequency antenna is a supersonic generator capable of delivering 800 watts in the frequency range of 14 to 70 kc/s. Since there is no ground wave in the direction of the receiver, the field strength as measured is due entirely to the wave reflected from the ionosphere. Although there is the distinct advantage in not having to separate the ground wave from the received signal, the fact that there is no ground wave means that some other method must be used to obtain a reference signal for the phase measurements. This reference is supplied by use of a 50-watt, very-high-frequency transmitter which is in line-of-sight of the receiver.

A crystal oscillator provides a stable frequency source for the low-frequency transmitter. It is also the reference for the modulation of the very-high-frequency transmitter. Since the modulating frequency is limited to less than 3,000 cycles per second because of the design of the equipment, the 50-kc/s oscillator output is divided by 31. A 1,612-c/s signal is sent to the receiving site as the reference signal. The division is accomplished by the use of a scaling circuit employing the proper feedback between stages in order to realize the factor of 31.

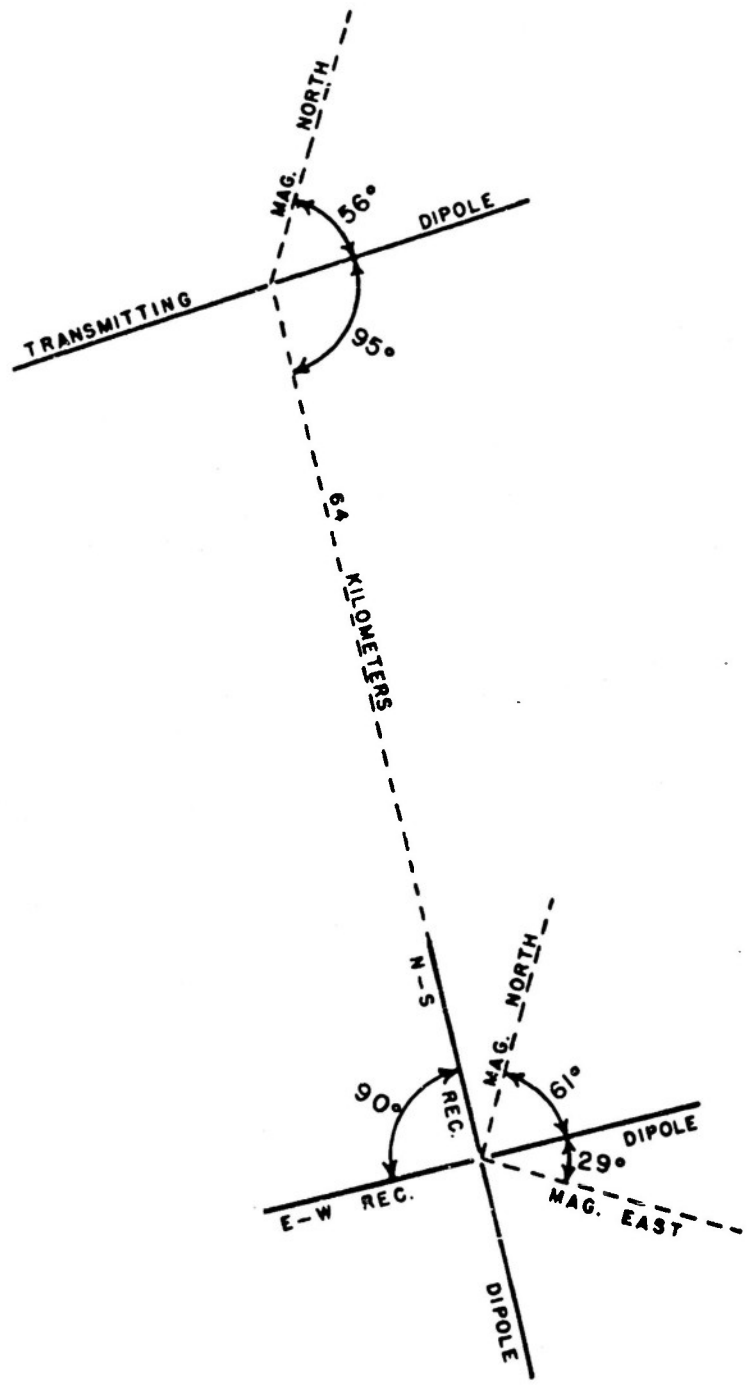

Figure 5. Geometry of the Transmitting and Receiving Antennae

The 50-kc/s receiving antennae consist of crossed dipoles 100 feet in length. By switching the receiver from one antenna to the other, it is possible to determine the polarization of the received wave. The receiving dipoles have essentially the same pattern as the transmitting antenna but have a high impedance. A 50-kc/s pre-amplifier is used to convert the double-ended signal from the antennae into a single-ended signal for use in the receiver. The receiver is a double-conversion superheterodyne using the twenty-fifth and the seventh harmonics of the 1,612-c/s reference signal as local oscillator frequencies. These frequencies were chosen so that the second intermediate frequency would be exactly 1,612 c/s. The received signal is thus reduced in frequency to equal that of the reference signal. A direct comparison of phase is possible by means of a phase meter.

Atmospheric noise was one of the main considerations in the design of the entire system. The 1,612-c/s intermediate frequency made a very narrow bandwidth of 30 c/s easy to realize. The overall system required the bandwidth to be of this order of magnitude, since the phase meter would not function properly for signal-to-noise ratios which were too low. The noise bandwidth at the output of the phase meter is also 30 c/s; for recording purposes, additional filtering to limit the bandwidth of the system to 1 c/s is employed. For a reasonable signal-to-noise ratio, the resolution of the phase-measuring system is equivalent to a change of 0.05 km in virtual height. This resolution is much superior to that of the conventional pulse techniques.

The amplitude of the reflected wave is recorded by using a Navy AN/URM-6 field-strength meter. The bandwidth of this receiver at 50 kc/s is 350 c/s. The recorded output is the resultant of signal plus noise. By automatically turning the low-frequency transmitter off for 45 seconds of each 5-minute interval, a record of the atmospheric noise level is obtained.

In Section III, the electronic components of the transmitting and receiving system are described. Figures 6 through 8 are photographs showing the transmitting and receiving equipment.

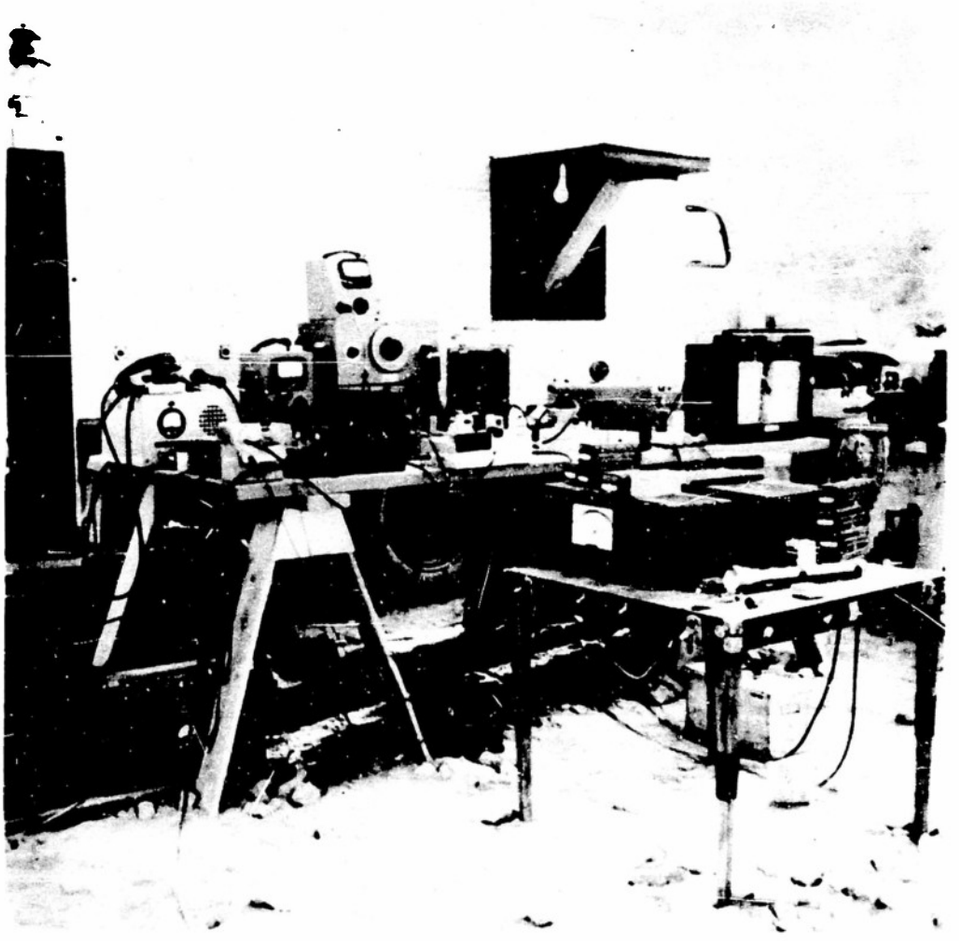

Figure 6. The Receiving Equipment

Figure 7. The Receiving Equipment

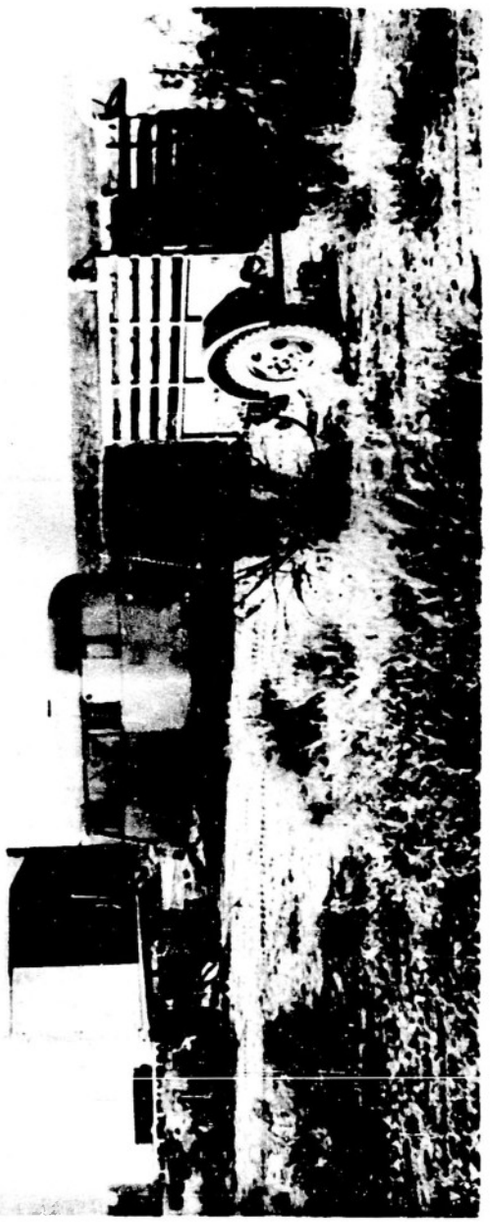

Figure 8. The Transmitting Station

III. THE TRANSMITTING AND RECEIVING EQUIPMENT

A. The Transmitting System

The transmitting equipment is shown in the block diagram of Figure 9. A 100-kc/s crystal controls the frequencies of the entire system. The 100 kc/s is divided first by 2 in order to obtain the standard 50 kc/s of the transmitted wave. The 50 kc/s in turn is divided by a factor of 31 in order to obtain a frequency which can be used to modulate the VHF (30.54-mc/s) line-of-sight communication link. The VHF transmitter, an AN/FRC-6, is capable of putting out over 50 watts, whereas the low-frequency transmitter puts out over 600 watts.

An appreciable amount of power was required to operate the equipment at the transmitting site. This power was furnished by a trailer-mounted, motor-generator set with a rating of 7.5 kw which was ample.

1. Low-Frequency Power Output and Driver Stages

The combined unit including the high-voltage power supply was built by the Herrnfeld Engineering Company (Los Angeles) under specifications for a supersonic power oscillator. The unit has been modified slightly to conform to the circuit diagram of Figures 10 and 11. The maximum continuous power output is a little over 600 watts, and it is possible over short periods of time to increase the power output to about 800 watts. The output impedance was approximately 100 ohms and could be changed to 400 or 1,600 ohms by making proper changes at the terminals of the output transformer. As seen in the circuit diagrams the power output stage consists of two 250TH Eimac tubes operating in push-pull and driven by two 6L6 tubes also in push-pull. The oscillator stage incorporated in the original transmitter was not suitable for our purposes and changes were made to allow either a Hewlett-Packard oscillator or the crystal oscillator to control the frequency from 15 to 100 kc/s. One of the features of the transmitter was a relay operated by a timing motor which automatically removed the signal about 45 seconds out of every 5 minutes.

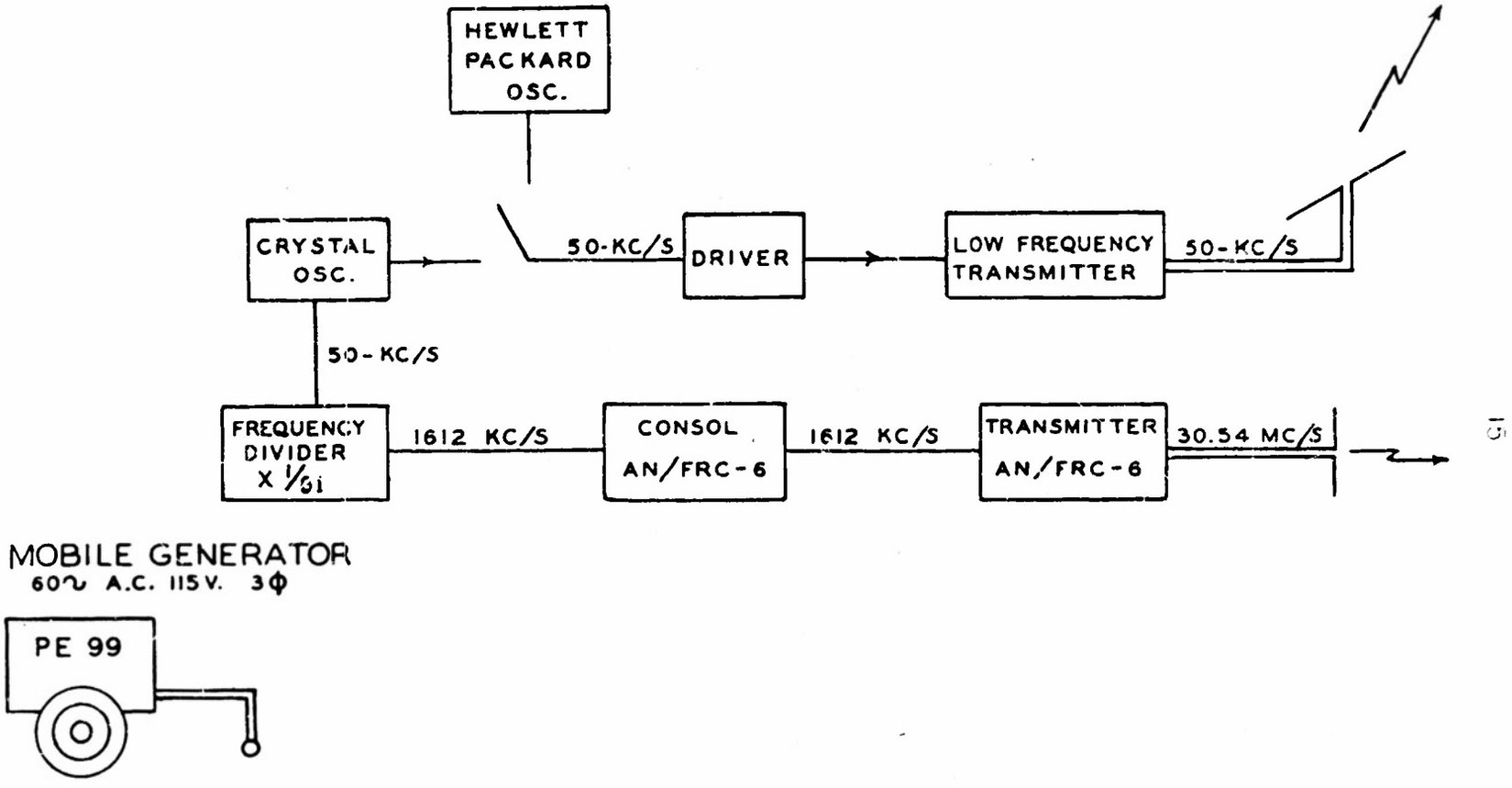

FIGURE 9.

BLOCK DIAGRAM OF TRANSMITTING STATION.

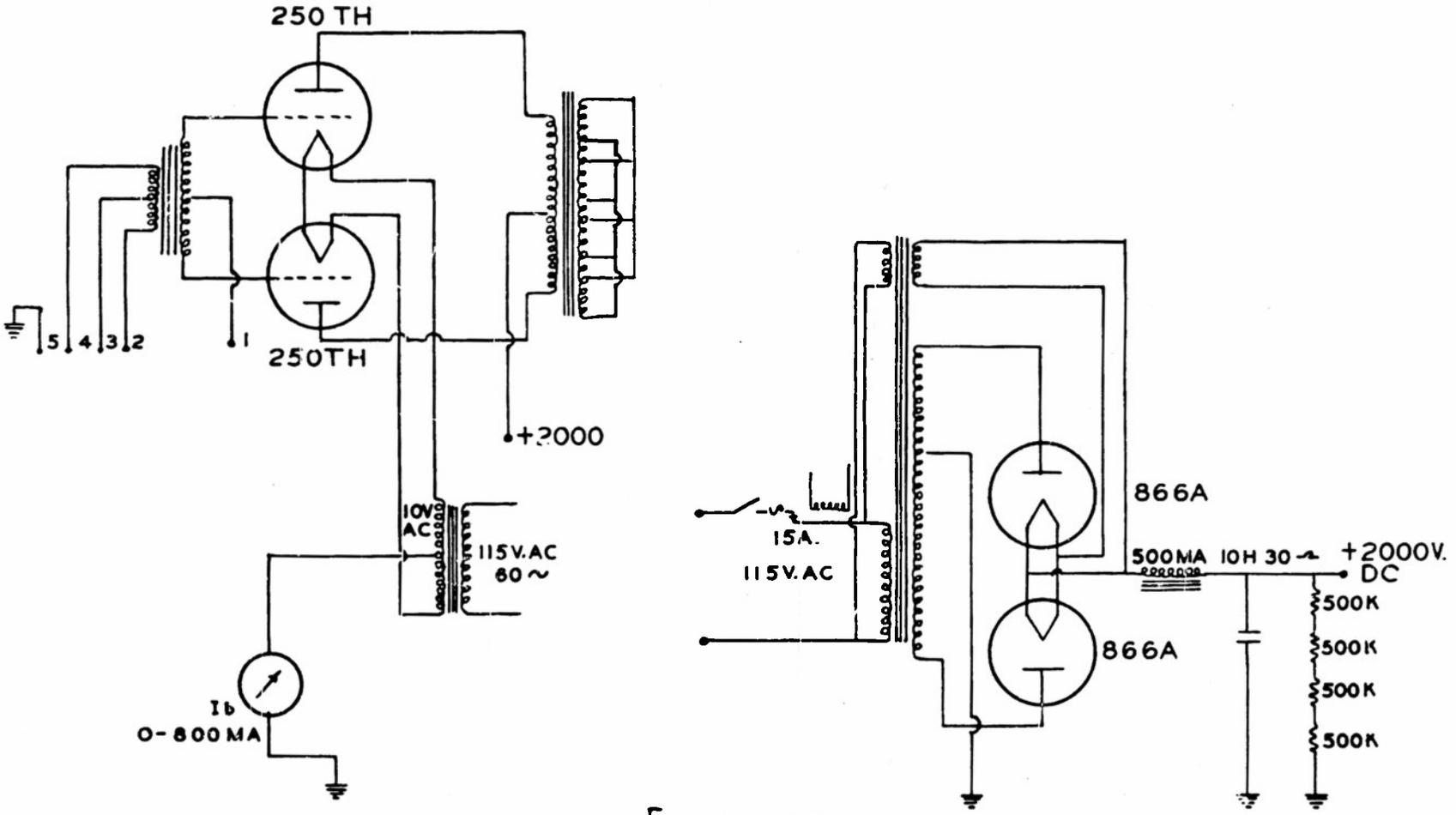

FIGURE 10

50-KC/S TRANSMITTER OUTPUT STAGE AND HIGH VOLTAGE POWER SUPPLY.

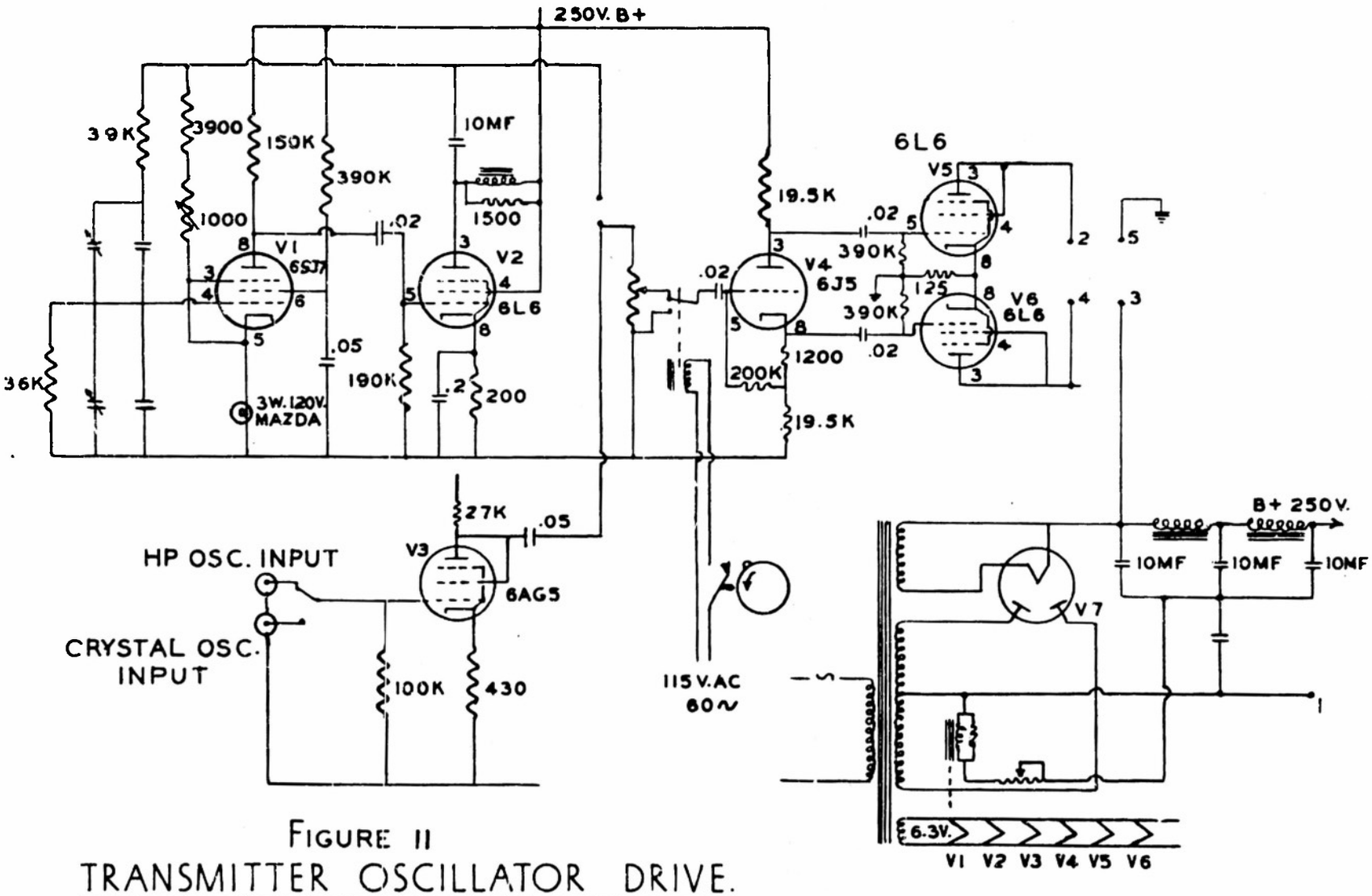

FIGURE 11

TRANSMITTER OSCILLATOR DRIVE.

2. Stable Frequency Source

The Federal Communications Commission in granting the project a license to operate the station specified that the frequency must be held to a tolerance of 0.01 per cent. The requirements of the phase-measuring system are a little more stringent in that the frequency must be held to 1 part in 500,000. The over-all system has a BW of about 1 c/s; thus any slight change in frequency results in an indication of phase change. These phase changes must be kept below about 5^{o} since this is the estimated accuracy of the phase-measuring equipment. Since crystals operating below 80 kc/s were not readily available, it was necessary to take the output of a 100-kc/s crystal oscillator and divide it by 2 in order to supply a stable 50-kc/s signal. The circuit diagram of the oscillator and scaler is shown in Figure 12. The output of the oscillator stage is a sawtooth wave with more than enough amplitude to trigger the scaler, which is a bistable multivibrator. The multivibrator triggers only on receiving a negative pulse from the preceding stage; therefore it goes through only 1 cycle for every two of the crystal oscillator.

The output of the frequency divider is a square wave with a period of 20μ sec. The transmitter on the other hand, requires a 50-kc/s sine wave and a voltage level up to about 30 volts. The 50-kc/s filter-amplifier (Fig.13) filters out all but the fundamental of the square wave and is capable of putting out 50 volts undistorted. The filter section is of interest in that it (or a slight variation) is used many times in the system. The cathode followers are used to isolate the filter from the rest of the circuit. L_1 is a 5-mh toroid with a Q of about 100 at 50 kc/s. The tuned circuit consisting of L_1 and C_1, therefore, has a resonant impedance of 0.15 megohm. R_1 and the tuned circuit form a voltage divider network which gives a maximum output at the resonant frequency. If R_p be designated as the impedance and Q_p, the Q of the tuned circuit at resonance, then the Q of the filter is given by

$$Q = Q_p R_1/(R_1 + R_p) \qquad (1)$$

If it is necessary to have a high Q, then R_1 must be made much larger than R_p, but then a sacrifice must be made in voltage output since there will be a loss in gain of $R_1/(R_1 + R_p)$. In the case of the 50-kc/s filter it was not necessary to have a high Q; therefor R_1 was put equal to R_p, giving a Q of $Q_p/2$.

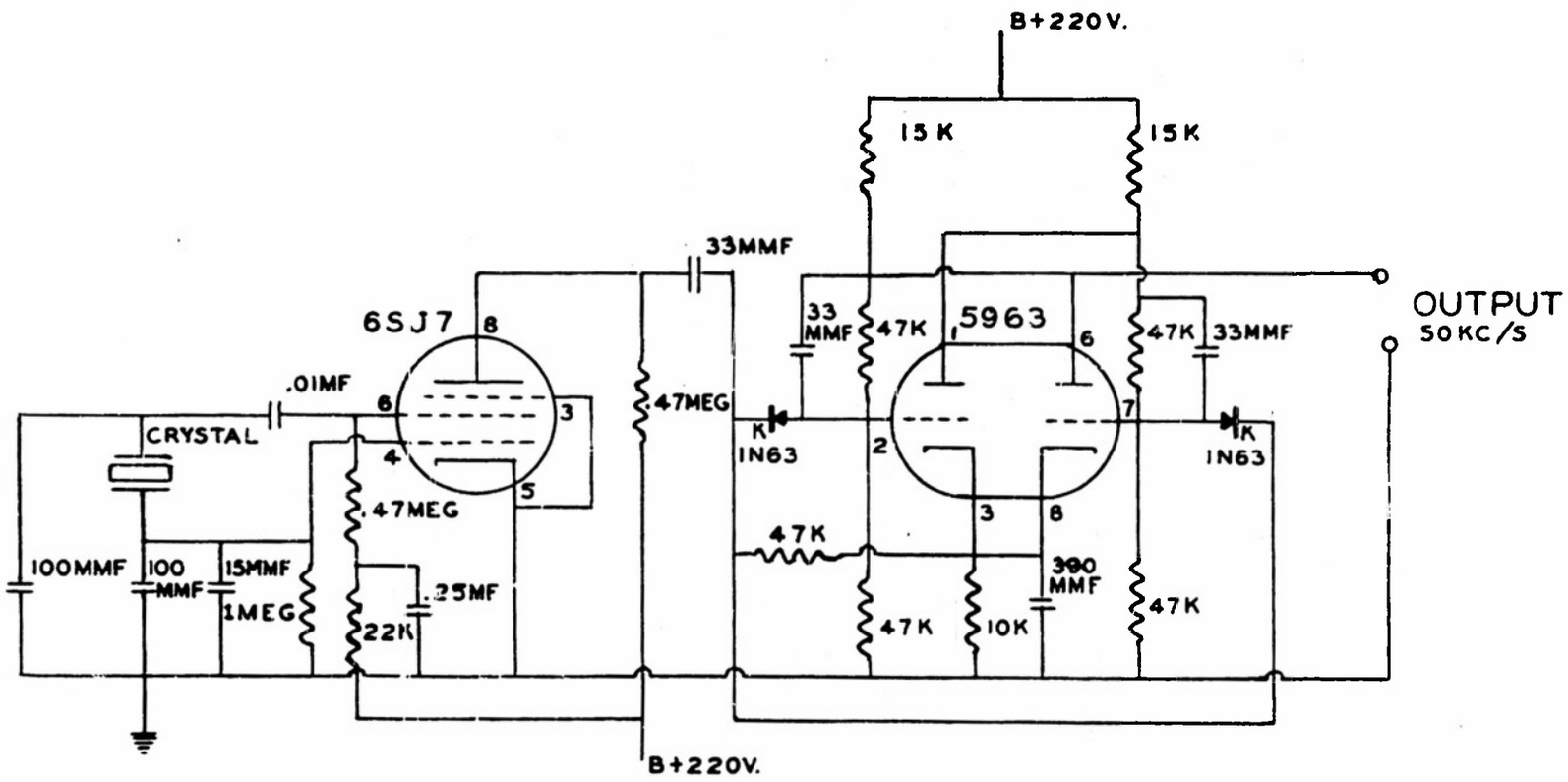

FIGURE 12

100-KC/S CRYSTAL OSCILLATOR AND SCALER CIRCUIT.

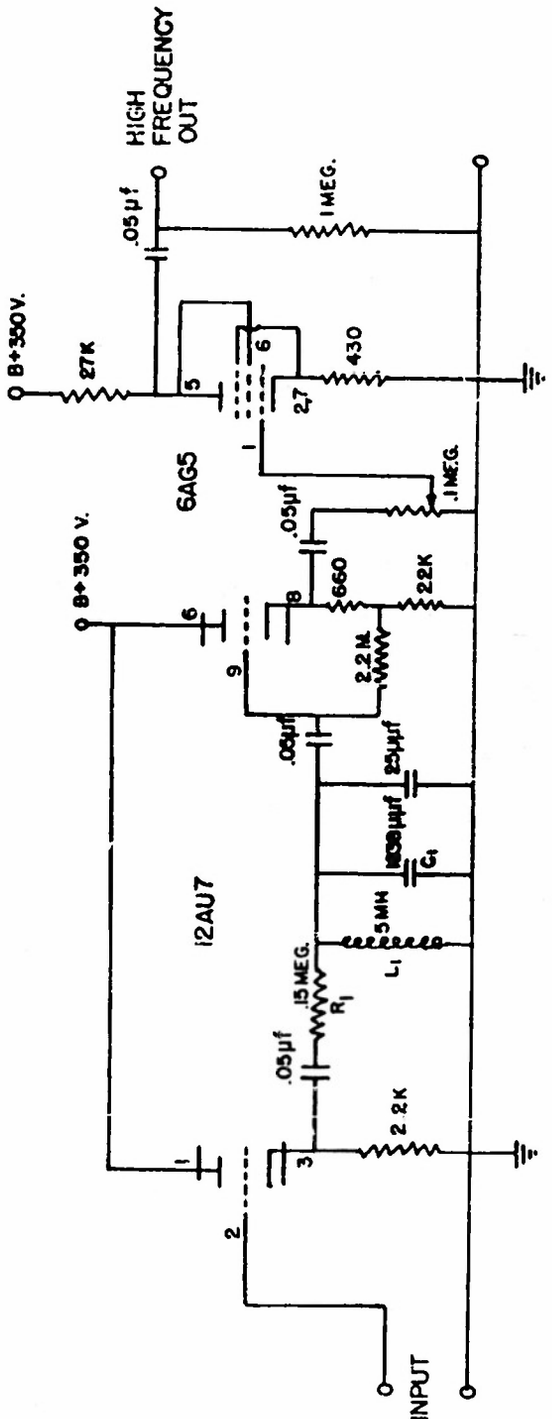

FIGURE 13 50KC/S FILTER

The amplifier stage is operated from a high B+ voltage in order to obtain the 50-volt output. The cathode resistor is left unbypassed to help keep the distortion down.

3. Frequency Divider of 50 kc/s to 1,612 c/s

It is necessary to derive a frequency in the range 400 to 3,000 c/s which is directly related in phase to the 50 kc/s. This signal will be used to modulate the FM transmitter in the line-of-sight communication link. If 50 kc/s is divided by 31, the resulting frequency is 1,612 c/s. The factor 31 is chosen because (1) it is an odd number, (2) it is simple to realize, and (3) it falls in this frequency range. The odd number is necessary since the square wave which will eventually be formed must contain the thirty-first harmonic. The General Electric Company makes a binary scalar (Fig. 14) which will operate at 50 kc/s; these scalars are used in the dividing circuit. They function exactly as the scalar shown in Figure 12 but cannot be operated at as high a frequency. The scalar by nature divides frequency by 2; thus one unit divides by 2, two units divide by 4, three by 8, four by 16, five by 32, etc. Feedback properly employed in the scalar circuits can produce division by any number required. In determining how to divide by a given number, each scalar is given a number in the binary system as shown in Figure 15a. One cycle of this system is defined as complete when the last scalar has been cleared, i.e., when it has put out a negative pulse. This negative pulse can be fed back to any one scalar or to all of the preceding scalars. Thus when the following cycle starts, a number which has been determined by the feedback is already set into the system. In Figure 15a the input frequency would be divided by 32 without feedback, but with the feedback the number 12 is set in at the end of each cycle, and the circuit divides by 20. Inasmuch as 1+2+4+8=15, it is possible to count down by 17 to 32 with five scalars. To divide by a factor of 9 to 16, only four scalars are needed, etc.

For any division other than by a power of 2, the output of the scalar network is not a symmetrical square wave. The positive part remains the same length for all divisions between 32 and 17, for example, and the negative part diminishes in length. Assuming that the negative part can be divided into 16 parts for division by 32, it is found that the number of one-sixteenths subtracted from the length of the negative part is exactly equal to the number fed back (Fig. 15b). It may not be suitable to have the waveform shown in Figure 15b for division by 20.

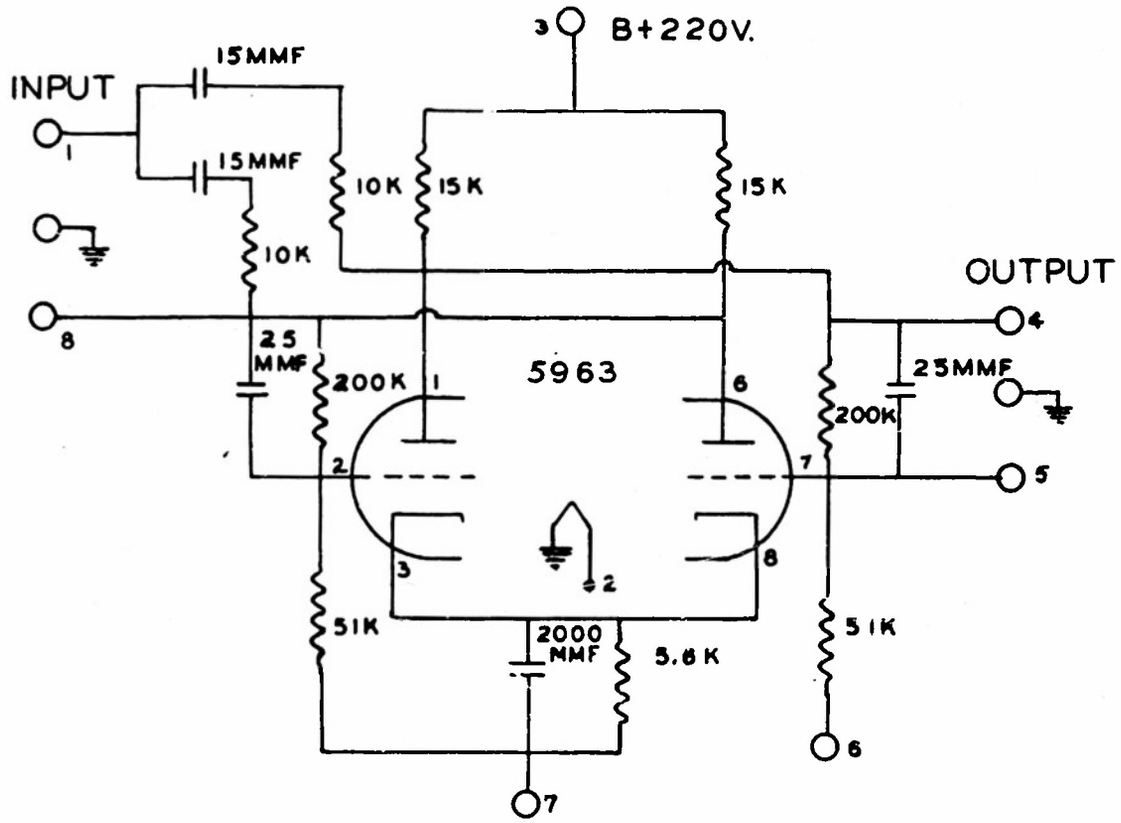

FIGURE 14

G.E. BINARY SCALER.

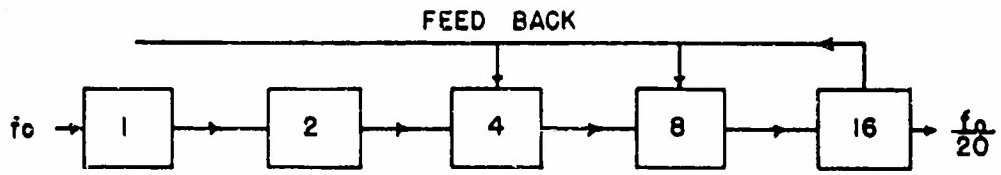

FIGURE 15a BLOCK DIAGRAM FOR DIVISION BY 20

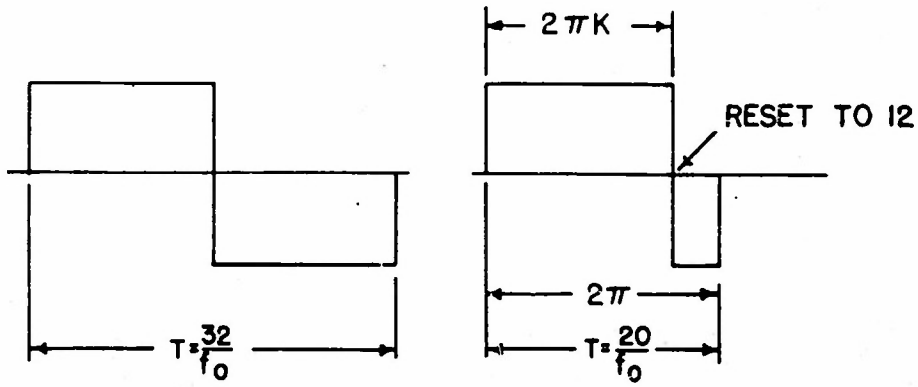

FIGURE 15b WAVE FORM FOR DIVISION BY 20

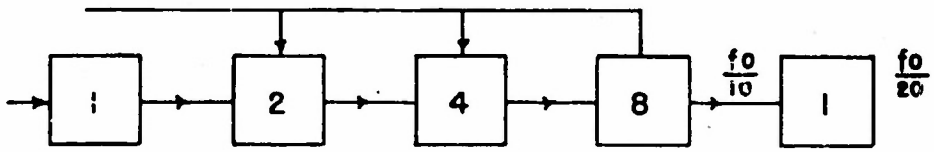

FIGURE 15c ALTERNATE DIAGRAM FOR DIVISION BY 20

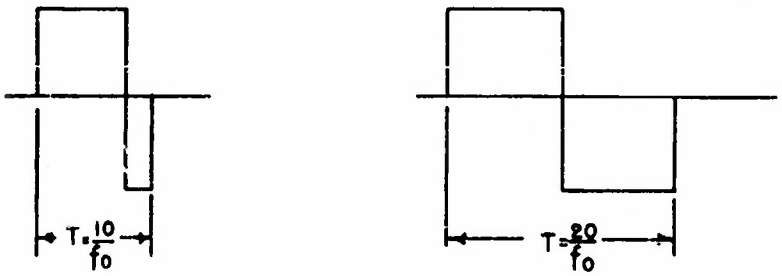

FIGURE 15d WAVE FORM OF ALTERNATE METHOD

Nothing can be done about the waveform unless the divisor is even, as it is in this case. Then the division can be done in two steps in order to obtain a symmetrical square wave (Figs. 15c and d).

In dividing by 31 (Fig. 16) the output of the five scalars will not be quite symmetrical. It will not matter, however, since only the first harmonic will be filtered out. The 1,612-c/s filter is designed exactly as the 50-kc/s filter with the appropriate changes in the L_1 and C_1 (Fig. 13).

4. VHF Frequency-Modulated Transmitter

The location of the receiving site was chosen so that it was line of sight from the transmitter. The U. S. Navy assigned to the project two AN/FRC-6 FM transmitter-receiver units. These units were designed to operate in the frequency range 30 to 40 mc/s with a power output of not less than 50 watts.

Filters in the receiving circuit limit the response to 3,000 c/s. This fact, of course, puts a limit on the frequency which is sent to the receiver for reference signal. A block diagram of the transmitter is shown in Figure 17. The actual type of modulation is phase, but proper filtering, together with the two quadruplers and the one doubler, convert phase modulation to frequency modulation. A console is a part of the AN/FRC-6 which can be used to control both the transmitter and the receiver. It was in the console that the modulating frequency was inserted (Ref. 1).

B. The Receiving System

The block diagram of Figure 18 shows the function of the receiving station. The 50-kc/s signal is received by two receivers, one of which provides the phase measurement, and the other, the amplitude measurement. The AN/URM-6 Stoddart receiver on loan from the Navy Electronic Laboratory (San Diego) was designed to be a field-strength meter; thus it was complete in itself. On the other hand, the phase-measuring equipment had to be completely designed and built, except for VHF frequency-modulated receiver and the phase meter. By means of the superheterodyning principle the 50-kc/s signal was reduced in frequency twice. The output of the receiver was then compared with the reference signal in the phase meter. In turn the output of the phase meter was recorded.

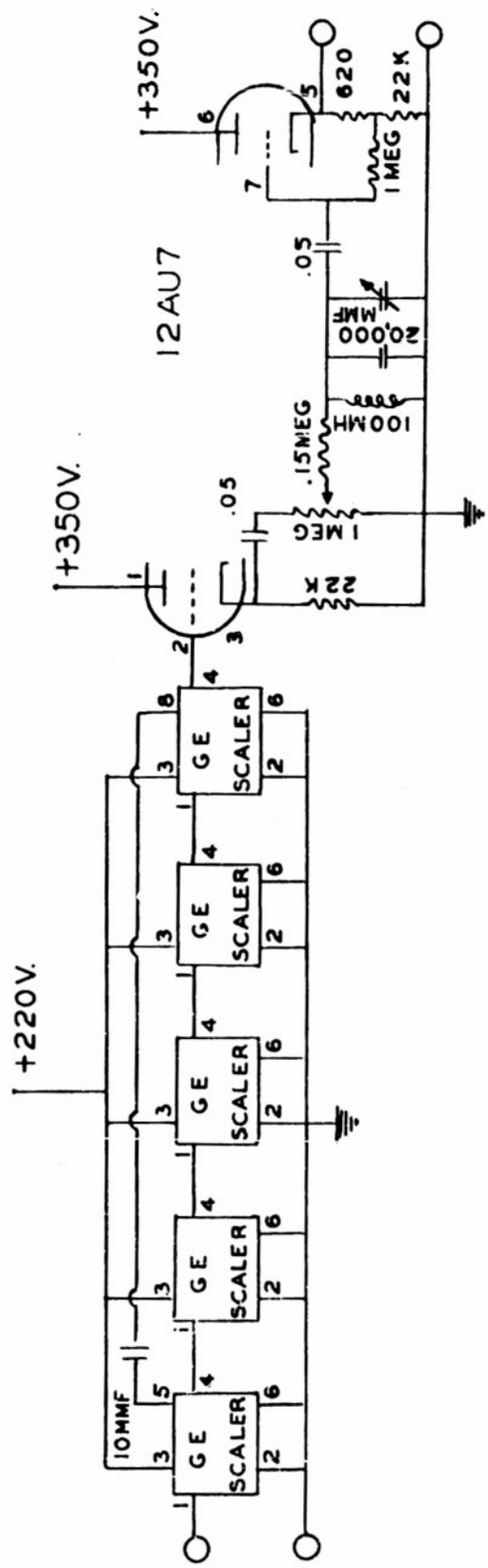

FIGURE 16

FREQUENCY DIVIDING CIRCUIT.

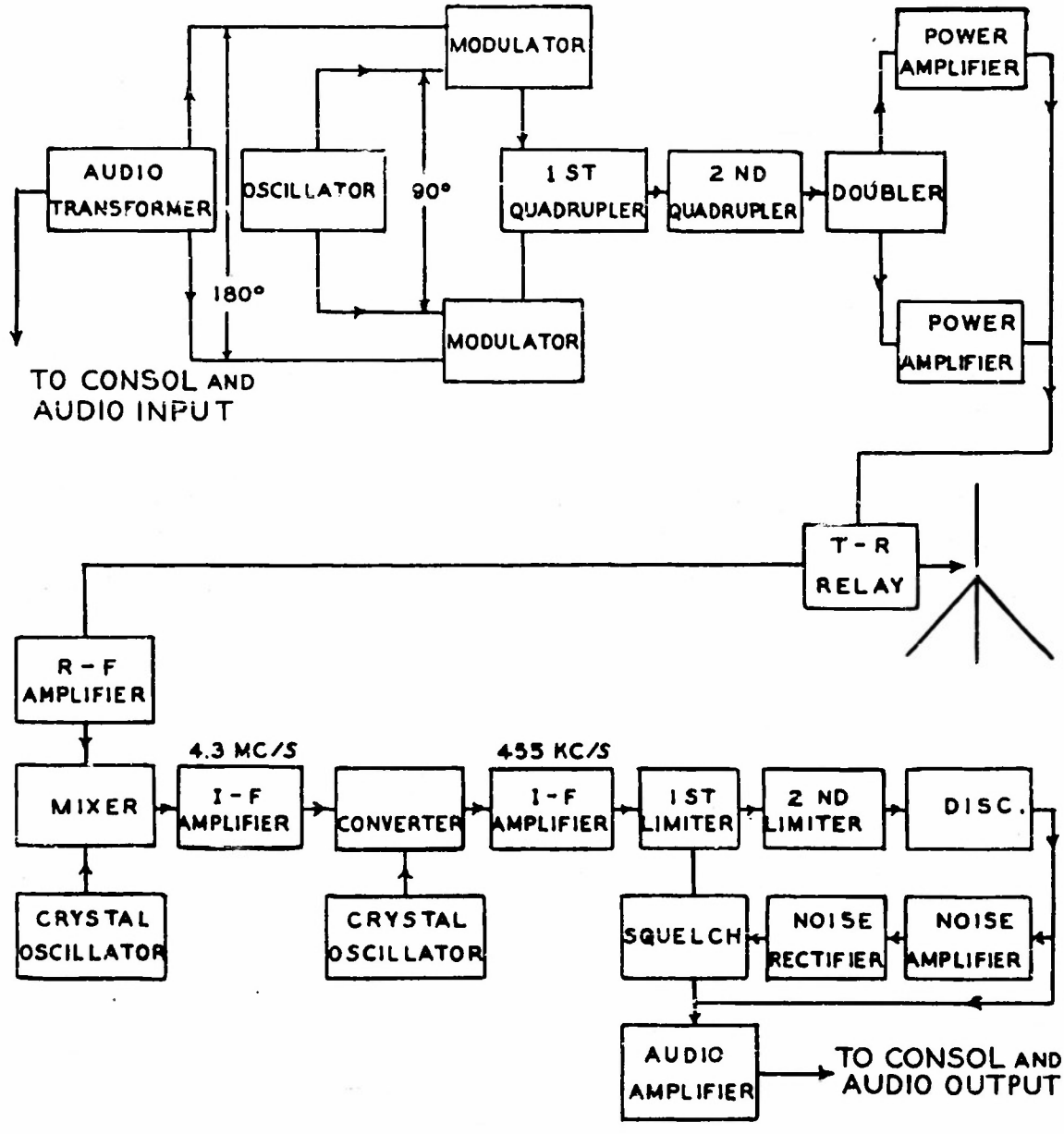

FIGURE 17

BLOCK DIAGRAM OF AN/FRC-6
30-Mc/s FM TRANSMITTER.

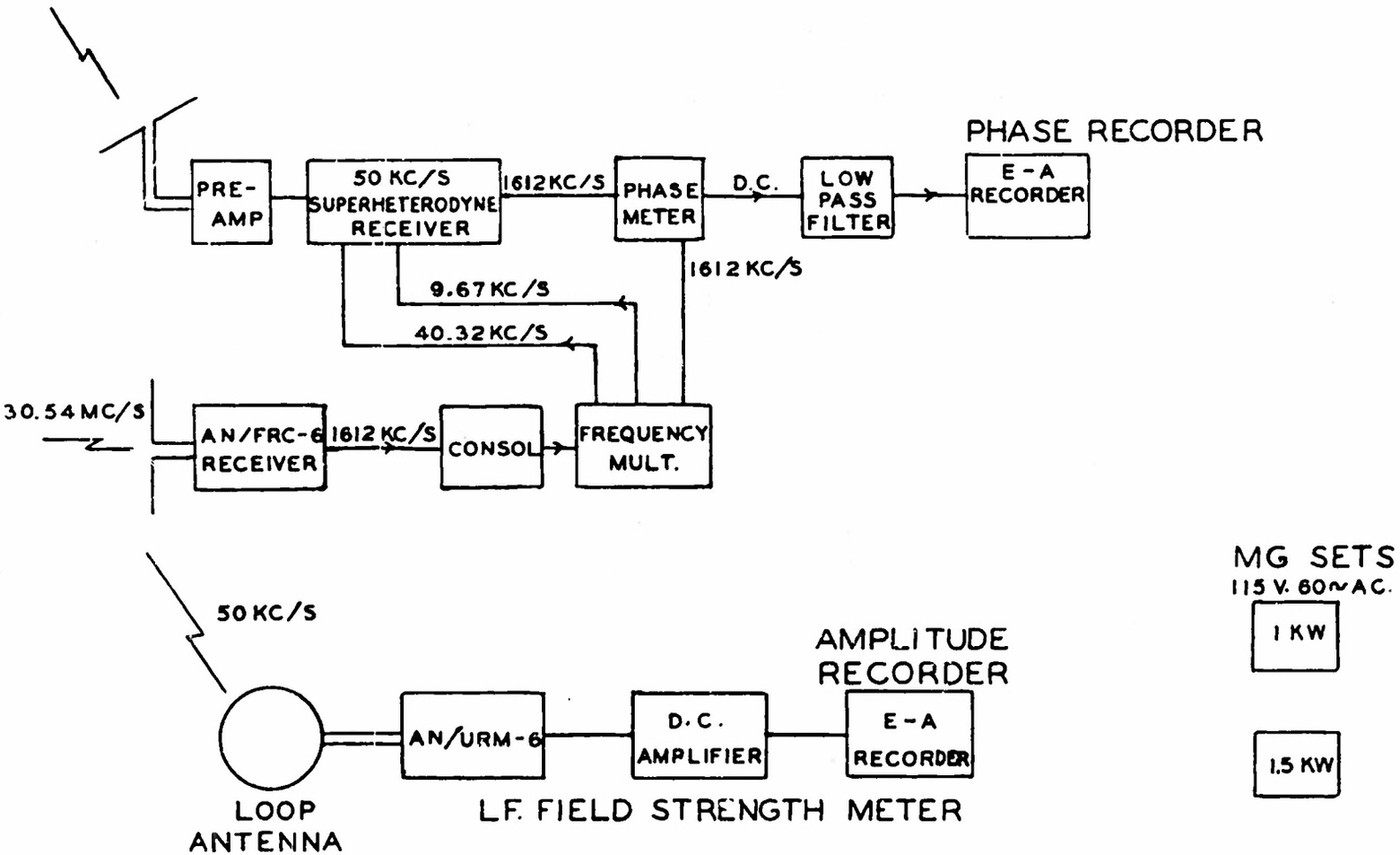

FIGURE 18

BLOCK DIAGRAM OF RECEIVING STATION.

1. VHF Frequency-Modulated Receiver

The AN/FRC-6 was used as a means of communication when the measurements were not being taken. The antenna used is described (Ref. 2) as an elevated, modified, ground-plane, wide-band antenna. The ground plane is at an angle of 143° with respect to the vertical. This feature helps to make the antenna match a greater range of frequencies and also "squashes" the radiation pattern down. It is estimated that the field strength at the receiver 40 miles away from, but line of sight to, the transmitting site was 1,500 μ volts/meter. With this field strength the S/N ratio should have been, and was, excellent; it was measured at one time to be 30/1. As long as the S/N ratio is larger than 1, there is no doubt concerning the desirability of the FM system over the AM.

Goldman (Ref. 3) derives the equation for the noise reduction of an FM system over that of an AM system. The reduction factor r is given by

$$r_1 = \sqrt{3}\,\Delta f / BW_a \qquad (2)$$

for random noise and by

$$r_2 = 2.8\,\Delta f / BW_a \qquad (3)$$

for impulse noise. Here BW_a is the audio passband, and Δf is the maximum frequency deviation. The noise-reduction factor is at least 8 for the present system.

The block diagram of the FM receiver is shown in Figure 17. It is a double-conversion receiver with a first IF frequency of 4.3 mc/s and a second IF frequency of 455 kc/s. The local oscillators are crystal-controlled. This factor is just as important as having the initial carrier frequency crystal-controlled, since drift in the local oscillator would appear as a drift in the carrier frequency. The output of the receiver during the experimental test is the 1,612 c/s originating at the transmitter. This frequency is fed into the console control unit and thence into the frequency-multiplying circuit.

2. Frequency Multiplier

The function of the frequency multiplier (circuit diagram in Fig. 19) is to generate from the 1,612 c/s the 50 kc/s and the two local oscillator frequencies which are the twenty-fifth and the seventh harmonics of 1,612 c/s. This function is accomplished by clipping the input sine wave and obtaining a square wave whose voltage can be described by

$$v = \frac{4}{\pi} E(\cos x - \tfrac{1}{3}\cos 3x + \tfrac{1}{5}\cos 5x - \tfrac{1}{7}\cos 7x + \cdots) \qquad (4)$$

which is seen to contain all the wanted odd harmonics of the fundamental frequency. Some care must be taken in designing the squaring circuit to make sure that the resulting waveform is symmetrical. Such an unsymmetrical waveform is shown in Figure 15b. The voltage v' of this waveform can be expanded into

$$v' = \frac{4}{\pi} E(\tfrac{2k-1}{4}\pi + \sin k\pi \cos x + \tfrac{1}{2}\sin 2\pi k \cos 2x + \cdots) \qquad (5)$$

which reverts to Equation (4) when $k=\frac{1}{2}$. In many squaring circuits the k of Equation (5) is actually a function of the voltage input. As k changes, one finds that the harmonic content changes. For example, if one wishes to extract the thirty-first harmonic of Equation (5) but k has a value of 15/31 or 16/32, there will be no thirty-first harmonic present to extract. Thus for a change in k of only 3.2 per cent the harmonic content goes from a maximum to zero. A circuit was actually built such that k was so sensitive to the changes of input voltage that it had to be discarded.

The block diagram of the multiplier is shown in Figure 20. Even with the very good S/N ratio obtained from the FM receiver, there remained with the reference signal sufficient noise to upset the desired operation of the multiplier. Whereas the BW of the receiver was about 3,000 c/s, the bankwidth of the filter was about 30 c/s; therefore the S/N ratio was increased by a factor of 10 to a value of 300. The filter was followed by an amplifier whose function was to increase the voltage to above 50 volts rms. A clipping reference voltage of $1\frac{1}{2}$ volts working against the 50-volt input produces a well-shaped square wave. The cathode follower output makes available an isolated 1,612-c/s source

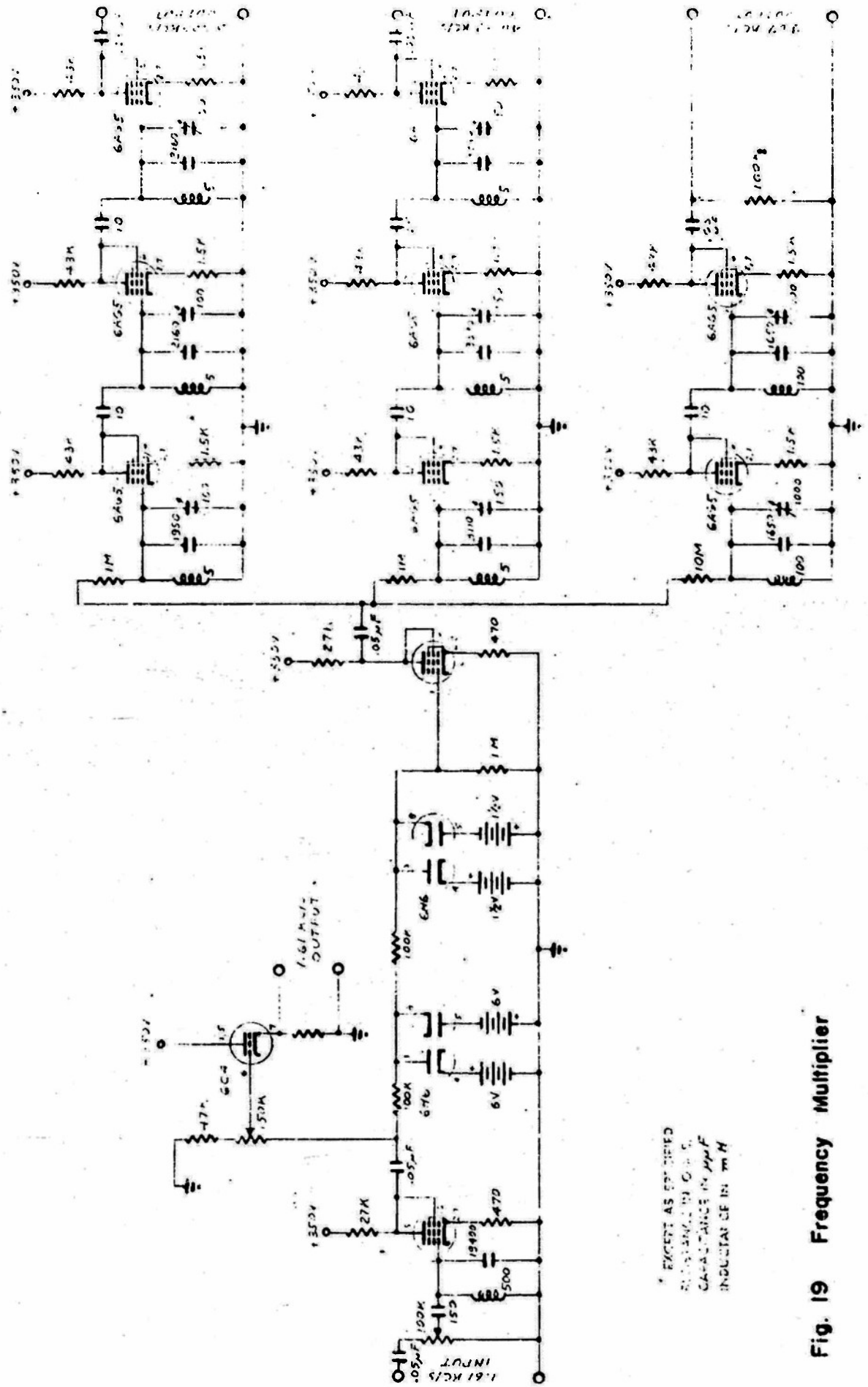

Fig. 19 Frequency Multiplier

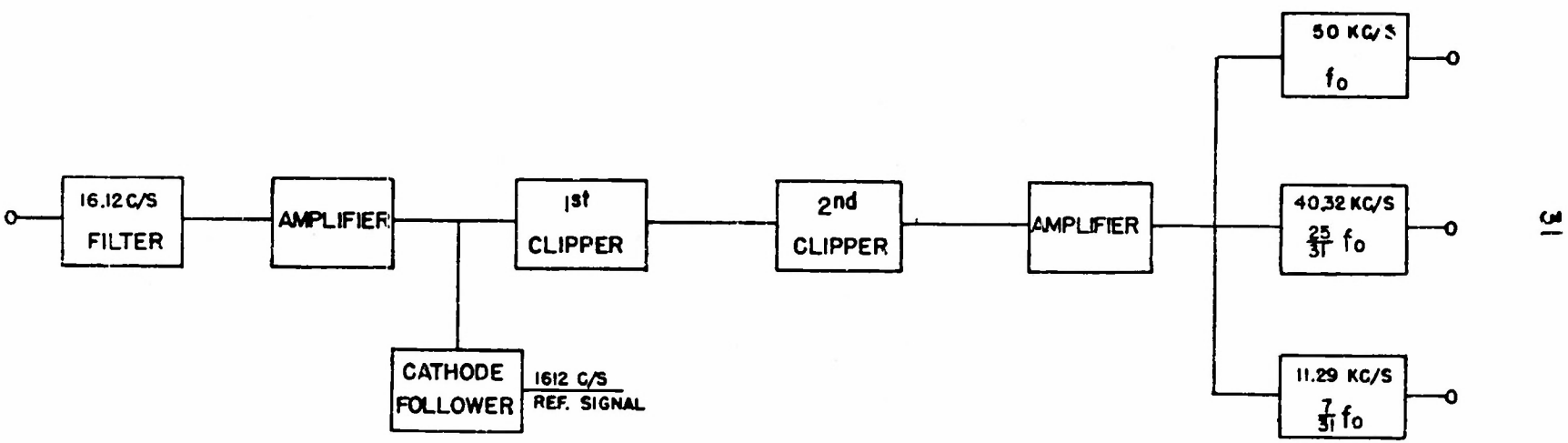

FIGURE 20 BLOCK DIAGRAM OF MULTIPLIER

for the reference signal to be used with the phase meter. The voltage output is monitored in order to assure the operators that the linear limits of the amplifier are not exceeded. The clipping takes place in two stages. It was found that, if clipping was done in one stage, the resultant waveform was not suitable. Therefore the clipping was done first at the 6-volt level and then at the $1\frac{1}{2}$-volt level.

It is of interest to discuss the filtering necessary to obtain, for example, the thirty-first harmonic. There are three filtering sections similar to the one described in Section III-A-3. The envelope of the waveform at the output of the first filter section is shown in Figure 21. One would expect this waveform if a tuned circuit received a burst of energy every 1/3,200 second. The Q of the tuned circuit determines the rate of decay. This waveform can also be regarded as an amplitude-modulated wave where the carrier is the 50 kc/s and the side bands are frequencies separated from the carrier by all the harmonics of 1,612 c/s. The remaining filtering in the network must be sufficient to eliminate all the side bands. The specifications for complete filtering are thus no different from those requiring that the filter separate the thirty-first harmonic from the twenty-ninth and thirty-third harmonics. However, this discussion gives an insight into the type of waveform to be expected from incomplete filtering.

It was necessary to use three stages of filtering for the twenty-fifth and the thirty-first harmonics, but only two stages were needed to extract the seventh harmonic. The voltage output of the seventh and twenty-fifth harmonics was fed directly into the superheterodyne receiver. The 50-kc/s output was used to tune up the superheterodyne receiver. The authors would like to point out how vitally important this was. The superheterodyne receiver has such an extremely narrow band that lining it up would have been virtually impossible without having the exact input frequency available. The 50-kc/s filtering section must be entirely incapacitated to avoid feeding this signal back into the antenna during periods of operation.

3. The 50-kc/s Receiving Antennae

The receiving-antenna system was a problem in itself. The two types of antennae having the desired characteristics are the loop and the dipole since each can be used to discriminate between polarizations of a down-coming wave. The field pattern of the loop is well known, and the theory of the dipole is discussed in Section IV. The loop antenna was

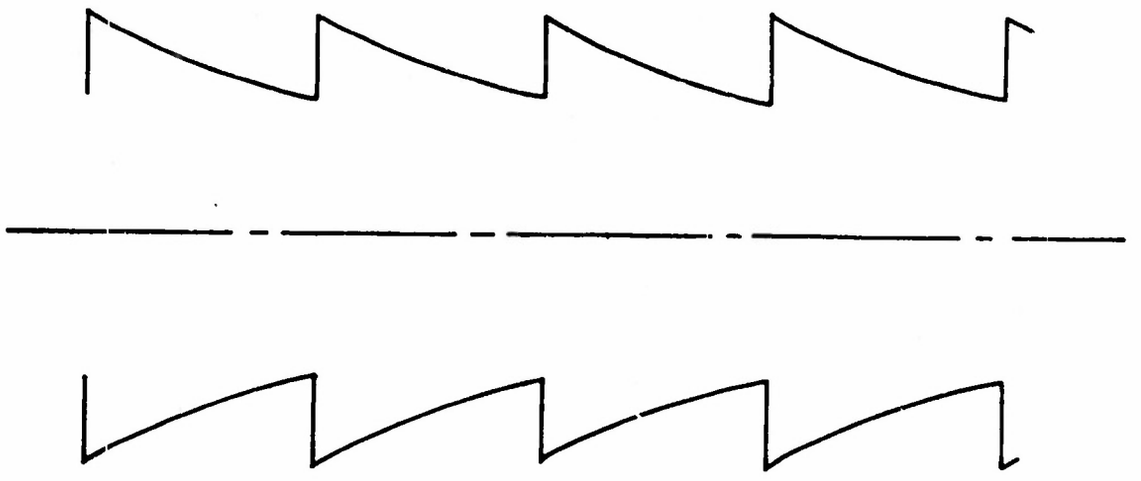

FIGURE 21
ENVELOPE OF FILTERED SQUARE-WAVE

used with the Stoddart receiver for field-strength measurements, and the dipole antenna was used with the phase-measuring receiver.

Consider a dipole lying on the plane earth. For all practical purposes it has two separate fields (Section IV). One is that which can be calculated by merely considering reflection from the plane earth; the other is that which gives rise to the ground wave. The field pattern in the plane normal to the length of the dipole is shown in Figure 3, and the pattern in the ground plane is shown in Figure 4.

The pattern of Figure 3 has maximum sensitivity in the vertical direction and is responsible for receiving the reflected wave. The pattern of Figure 4 has the shape of a quadrupole field and is responsible for picking up the vertically polarized atmospheric noise which comes in as a ground wave or at large angles of incidence. Noise actually comes in from all directions but is more concentrated near the horizon. The over-all effect of the dipole field pattern is very similar to that of the loop antenna field. However, the dipole tends to emphasize the directivity toward the vertical and is somewhat superior to the loop antenna for over-all S/N ratio.

The dipole and the loop are double-ended antennas which must be perfectly balanced if they are to have the theoretical characteristics. This balance is extremely critical for optimum operation of the dipole. The balance is a function of the length of the antenna and the distributed capacity to ground over the length of the dipole. It is also dependent upon the input stage of the receiver.

The receiving dipole used was about 150 feet long; at 50 kc/s it is still an elementary dipole having a very highly capacitive reactance which is easily unbalanced. Two such antennas were placed at a right angle to each other so that one was along the line of sight to the receiver. Thus the relative polarization of the down-coming wave can be determined. In the case where the receiving site is at a right angle to the transmitting antenna, there is no interference from the 50-kc/s ground wave.

4. Receiver Pre-Amplifier

Almost all receivers designed for low and very low frequencies are single-ended, whereas the antennae which the authors used are double-ended. A pre-amplifier was built which consists of two double-ended to single-ended converters, one for the dipole and one for two

vertical rod antennae.* The signal output of the two input converters can be subtracted in a third differential amplifier. As can be seen in Figure 22, the pre-amplifier consists of three identical amplifier sections.

The differential amplifier actually subtracts the two voltages which appear at the grids of the two sections of the tube. One section operates as a cathode follower so that the cathode potential follows the grid voltage. The second section then amplifies the difference between the second grid and the cathode, this difference is the same as that between the second grid and the first grid. If these voltages are alike but 180° out of phase, the gain of the differential amplifier is approximately twice the gain of the amplifier stage.

The pre-amplifier was designed to operate in the field on batteries so that it could be placed at the antenna terminals. It serves to isolate the antenna from the rest of the system, has a gain of 40 db, and can be tuned from 15 to 100 kc/s with proper selection of toroids. The pre-amplifier has a Q of 50; thus at 50 kc/s it has an over-all bandwidth of about 1,000 c/s.

5. Low-Frequency Double Superheterodyne Receiver

The importance of the receiver should not be underestimated, and its characteristics should be understood thoroughly. There are several factors which limit the usefulness of a receiver; for example, (1) the noise figure of the input stages, (2) the nature of the noise that enters the receiver, (3) the limitation of gain with a specified bandwidth, (4) limitations which involve the possibility of oscillation with a high gain, and (5) temperature stability required on L, C, and R components as well as on electron tubes, crystals, etc.

The noise figure of a receiver is a figure of merit. It is the ratio of the total noise power in the input stages per unit bandwidth to the noise power of the resistance in the input network. The noise figure of the receiver is largely a function of the tube noise of the input stage; thus it is necessary to minimize this noise. Low plate voltage and plate current are the usual criteria in the design. If the gain of the first stage

---

* The vertical antennae can be oriented in such a manner as to cancel out an interfering ground-wave signal. However, it was not necessary to use the vertical antennae in making the 50-kc/s measurements.

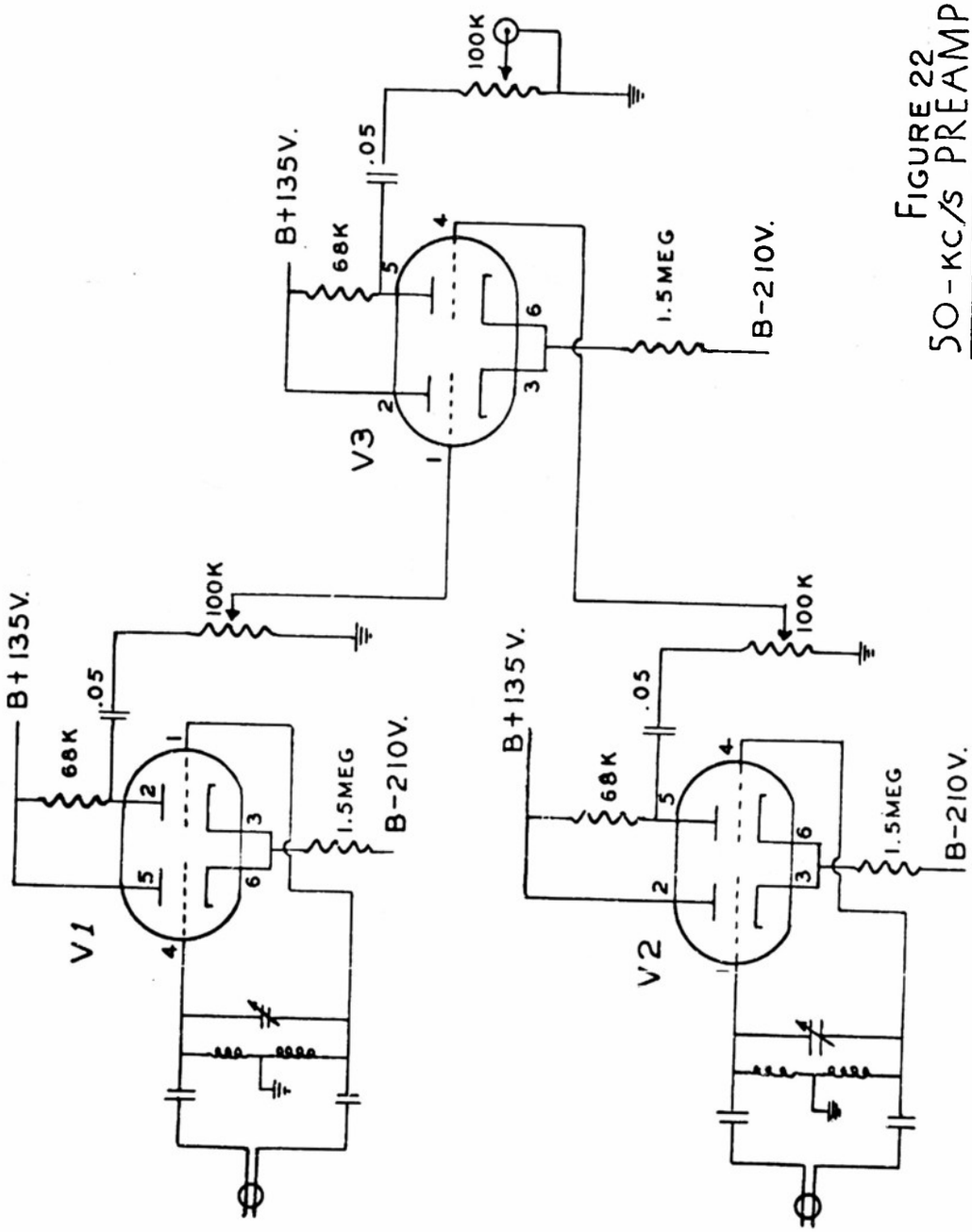

FIGURE 22
50-KC/S PREAMPLIFIER.

is sufficient, the noise contributed by the second is negligible. The noise voltage referred to the grid of the first stage for a BW of 100 c/s may be as high as 10 μ volts, but a properly designed input stage should have less than 1 μ volts of tube noise. In some receivers it is extremely important that the noise figures be kept as close to optimum as possible. For our purpose we find that, by lengthening the receiving antenna, the atmospheric noise overrides the receiver noise of a moderately well-designed first stage and thus becomes the limiting factor of the receiver.

Noise is the one factor that has been considered a necessary evil throughout the entire system. Essentially it is the one limitation that made the work on this project so very difficult. Noise forced the experimenters to maximize the power output of the transmitter and to limit the bandwidth of the receiving equipment to as small a value as possible. Noise in the low- and very-low frequency range is due largely to thunderstorms taking place all over the earth. The spectrum of a storm has a maximum value near 10 kc/s. This noise has the characteristics of random noise with superimposed bursts occurring at rather close intervals. The noise level at any one time is dependent upon the number of thunderstorms going on in the world, the closest ones naturally having the greatest effect. Let us point out that the magnitude of disturbance at the output of the receiver is in proportion to $(BW)^{\frac{1}{2}}$ for random noise and to BW for impulse noise. Also for impulse noise the length of the disturbance at the output of the receiver is proportional to Q. Here we have the equivalent of two opposing requirements. In order to reduce the magnitude of the impulse noise, the BW must be reduced; as a result the Q of the receiver must increase. But as Q increases, the duration of the disturbance due to pulses increases.

The atmospheric noise is considered as being composed of background noise whose average value is relatively constant and the impulse noise which occurs intermittently and has peak amplitude several times the amplitude of background noise. In order to function the receiver must first be able to detect the signal in the presence of the background noise. The signal we are trying to receive has a fixed frequency; thus its spectrum is a delta function at 50 kc/s. The spectrum of the noise may be considered uniformly distributed over the frequency range near 50 kc/s. It is found that, with a bandwidth of 350 c/s at 50 kc/s, the field strength of the noise picked up varies from 5 μ volts/meter or less in the winter daytime to about 30 μ volts/meter in the summer nighttime. The question now arises as to what must be the field strength of the signal in order that the signal can be picked out of the noise. It is possible to detect the presence of a signal in the noise with S/N ratios down to -6db. Whether or not a signal exists cannot be determined if

the field strength is less than half the magnitude of the atmospheric noise.

In general, if the spectra of the signal and of the noise are known, it is possible to design an optimum filter for the signal. This design would involve specifying a frequency response which (1) attenuates in that portion of the band where the S/N ratio is poor and (2) amplifies in the portion where the S/N ratio is good. For a complicated signal this is a complicated procedure. However, if there is signal power at only one frequency, the optimum filter is easily specified; namely, it must have infinite attenuation at all frequencies except 50 kc/s. This specification is not physically possible, but the filter should have a narrow enough band to obtain a reasonable S/N ratio. The 50-kc/s signal strength has no lower limit and may be as high at 85 μ volts/meter under optimum conditions. Therefore the receiver should be designed with as narrow a band as practical. For example, it is assumed that a receiver has a bandwidth of 360 c/s. To increase the S/N ratio by a factor of 6, the BW would have to be reduced to 10 c/s. To obtain the corresponding increase in S/N ratio by increasing the power transmitted would require 36 times the power. It is much simpler and less costly to improve the receiver than to increase the power output of the transmitter.

The block diagram of Figure 23 shows the special-purpose receiver that was designed and built to operate at 50 kc/s. The receiver has two stages of superheterodyne in order to attain a final bandwidth of almost 30 c/s at the 1,612.9 c/s second IF frequency. The 50-kc/s input is mixed with 40,322.6 c/s, which is the twenty-fifth harmonic of the 1,612.9 c/s transmitted over the FM link. The resulting first IF frequency is 9,677.4 c/s. This frequency in turn is mixed with 11,290.3 c/s, which is the seventh harmonic of the 1,612.9 c/s; the resulting IF frequency is 1,612.9 c/s, which we note is the same frequency (as it must be) as that modulating the FM transmitter.

The converter can be considered as a device which multiplies its two input signals. Thus if f_o is the carrier frequency and f_1 is equivalent to the local oscillator frequency, their product is

$$\sin(2\pi f_o + \phi) \sin(2\pi f_1 + \alpha) \tag{6}$$

It contains two frequency components, one the sum of f_o and f_1 and the other their difference. A filter is used to separate out the difference of the two frequencies. In this process the particular phase of each voltage is carried along, and since we desire to measure phase, this characteristic is very important. If f_o and f_1 are derived from independent sources, then as the source frequency varies, the measured phase varies also. It

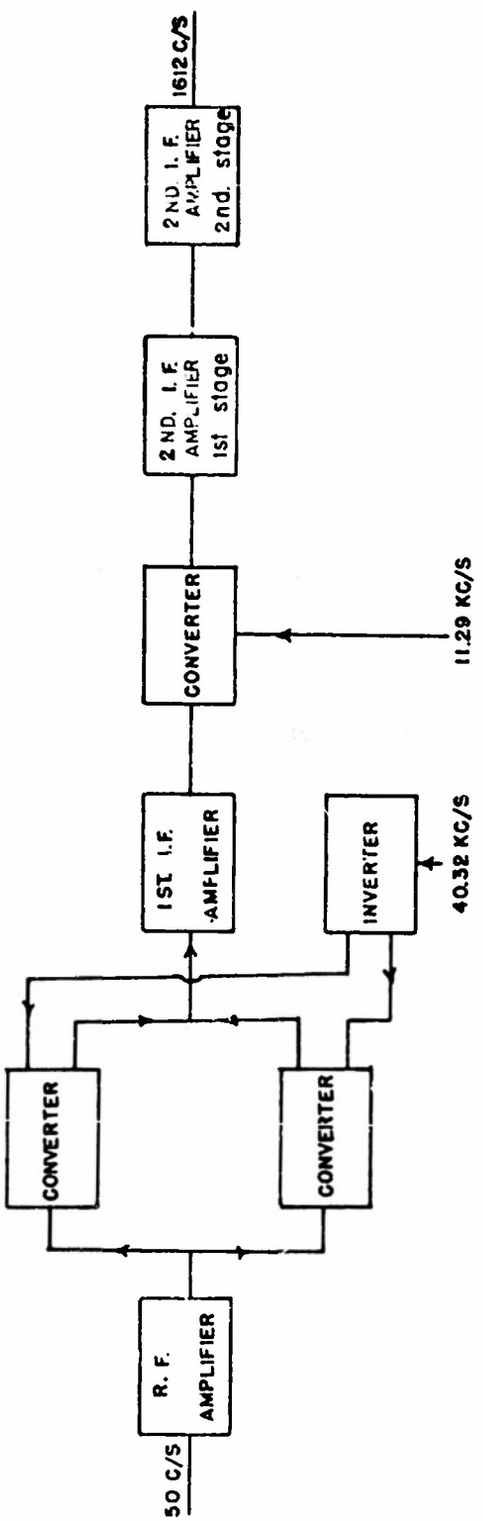

FIGURE 23 BLOCK DIAGRAM 50KC/S RECEIVER

is desired that f_0 and f_1 be derived from the same source, and for this reason it was necessary to transmit the reference signal to the receiving site in such a way that the frequency relationships could be determined.

One might ask why there are two stages of IF instead of one. In answer let us explain why a straight amplifier at 50 kc/s was not used. If a straight amplifier were used, then at some point in the receiver the voltage level would be such that it would be almost impossible, without using very special shielding techniques, to prevent some of the signal from feeding back into the antenna. Also the reference signal for the phase measurement would be present at high level, and care would have to be taken to assure that it did not feed back into the antenna and appear as a signal at the output of the receiver. If the local oscillator frequency is chosen too close to the carrier, the input circuit may become overloaded by this voltage, and the converter may not function properly. The authors used as the criterion that each IF frequency should be not less than one-tenth the previous IF or carrier frequency as the case might be.

The superheterodyne has other advantages, the main one being the virtual impossibility that it may oscillate since the amplification is accomplished in steps at the various frequencies. One characteristic of the frequency chosen that could cause trouble is that the second IF frequency and the reference signal are the same and could interfere with one another. However, not much gain is required in the receiver at 1,600 c/s, and the input to the 1,600 c/s amplifier is well shielded. In the frequency range of 1,000 to 200,000 c/s it is quite easy to obtain toroids for use in tuned circuits which have Q values of over 100. Since the bandwidth of a circuit tuned to frequency f is f/Q, a bandwidth of 30 c/s is easier to obtain at 1,600 c/s, where the effective Q need be only 50, than at 50 kc/s, where the effective Q would have to be 1,600.

The circuit of the superheterodyne receiver (Fig. 24) is straightforward save for the first mixer section. The converter operates in a push-pull fashion. The signal grids are driven in phase with one another, and the local oscillator grids are driven 180° out of phase. The output is thus double-ended, and this output in turn is converted to single-ended by a differential amplifier.

6. Phase-Measuring Equipment

The output of the receiver is 1,612 c/s, and the output of the FM transmitter is likewise 1,612 c/s. Since the phase of the receiver output varies exactly as the phase of the reflected wave, it is only necessary

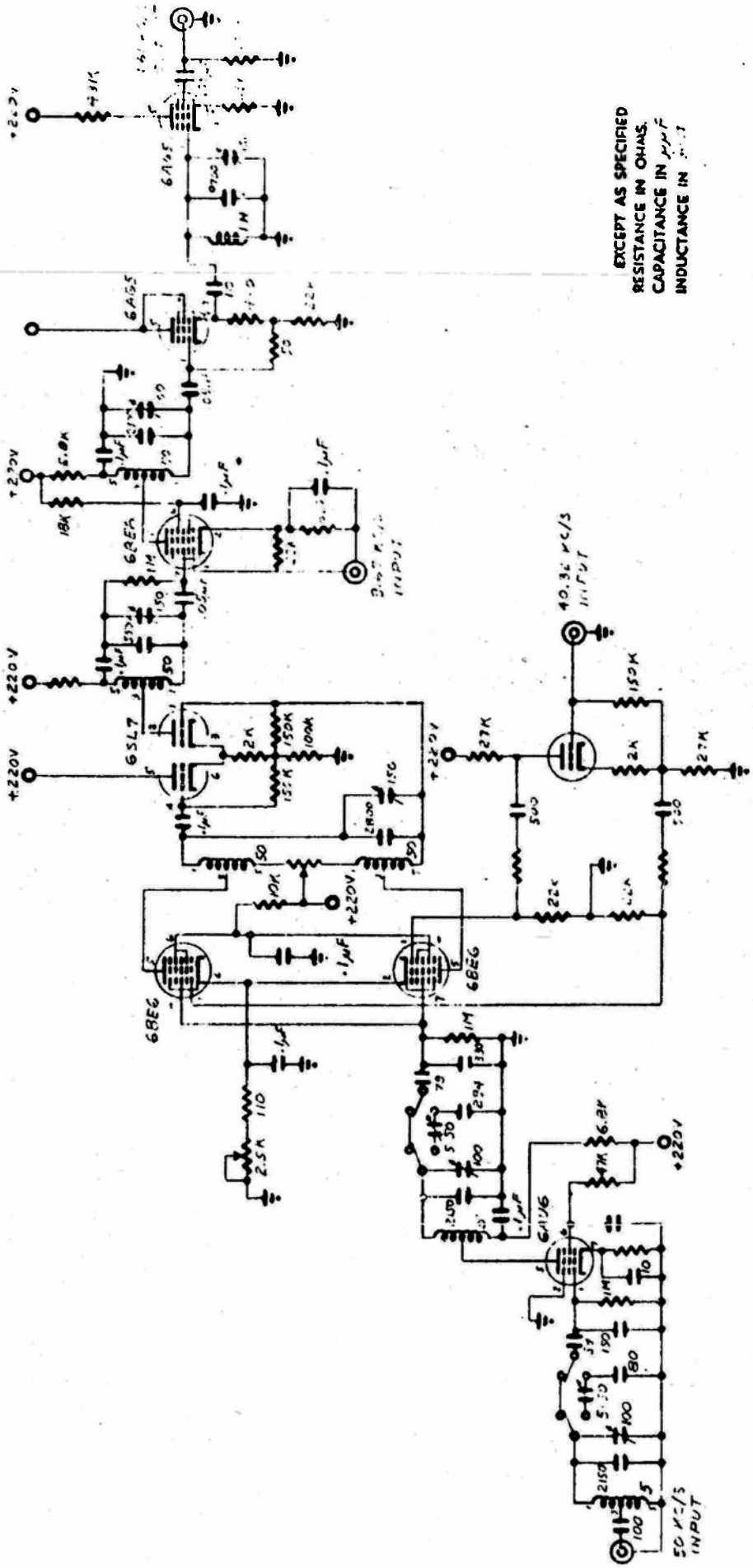

Fig. 24 Superheterodyne Receiver

to compare the two signals and record the changes in phase angles between them. This comparison was made by using a phase meter (Type 320) made by Technology Instrument Corporation (Ref. 4). The inputs to the phase meter are labeled A and B. If the receiver output is put into A, the meter reads directly the number of degrees by which the receiver output leads the reference signal. Electronically the meter measures the time difference between the zero crossings of the signal A and the zero crossings of signal B, this difference being proportional to the phase difference. Signal A consists of the 1,612-c/s signal plus noise. The position of the zero crossings varies at a rate of 30 c/s (the BW of the receiver), and the amplitude in degrees of this variation depends on the S/N ratio of the receiver output. The output of the phase meter can be, and is, filtered. But this filtering is good only so long as the phase meter does not become confused when operating near 0 or 360°; at that time the noise causes large fluctuations in phase, and control is lost. There is a saving factor in that the phase meter can be switched so that 180° is added to the reference signal. This switching helps as long as the S/N ratio is not too poor coming out of the superheterodyne receiver.

The problems involved in filtering the phase meter output is not the conventional type. As long as the noise does not cause the phase meter to read 0° at one instant and -360° the next, filtering can be done by the conventional techniques, and very narrow bandwidth can be obtained. However, the S/N ratio determines how near to 0 or 360° the meter may be operated properly, and there will be values of S/N that will prevent use of the phase meter entirely. Under these conditions the receiver-output S/N ratio must be further improved.

The output of the phase meter provides for the use of a recorder. The recorder was an Esterline-Angus, 5-mil movement with a nominal 400-ohm impedance. The recorded circuit (Fig. 25) included a filter having a transfer function of $0.445/(1+jf\ 0.755)$, which had a bandwidth of about 1.3 c/s.

7. Amplitude-Measuring Equipment

Through the Navy the project was able to obtain the use of the Stoddart receiver (AN/URM-6) whose frequency range is 15 to 250 kc/s covered in four bands. The receiver was designed to be a field-strength meter as well as a communications receiver. The AN/URM-6 is a superheterodyne receiver with a bandwidth of 80 c/s at 16 kc/s, 100 c/s at 20 kc/s, and 350 c/s at 50 kc/s. The field-strength of the 50-kc/s signal was measured by the use of a calibrated loop antenna at the input of the receiver and recorded on an Esterline-Angus recorder.

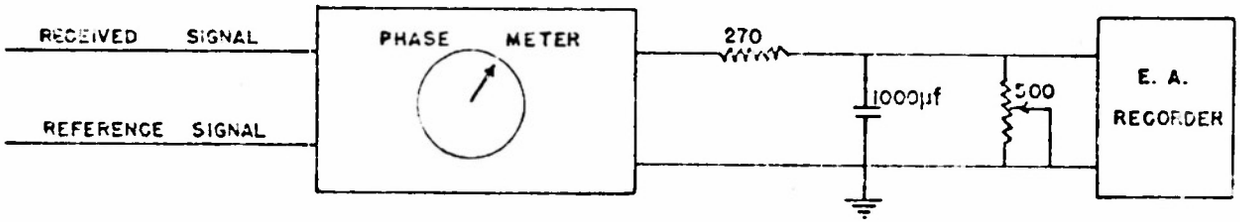

FIGURE 25 PHASE RECORDING CIRCUIT

IV. THE LOW-FREQUENCY TRANSMITTING ANTENNA

In order to investigate the D- and E-regions of the ionosphere, it was necessary to design a transmitting antenna for use in the frequency range of 14 to 75 kc/s. Conventional antenna systems were found to be undesirable because of the excessive cost, which amounts to one million dollars, on the average, for each 10 per cent of efficiency achieved. The cost of low-frequency antenna systems is high because they usually require tall towers, extensive ground systems, and either high-voltage tuning capacitors or large tuning coils. Tuning coils or tuning capacitors can be eliminated by using a resonant antenna such as a half-wave linear dipole, and it was with the idea of using a resonant antenna that an investigation of ground antennae was started. A ground antenna is, in this case, a half-wave linear dipole (or resonant loop) a full wavelength in circumference, placed directly on the ground or a very small fraction of a wavelength above the ground. A half-wave linear dipole at 14 kc/s would be 10.7 km (35,000 feet) long. The greater part of the material in this section deals directly with the dipole antenna; however, the theory is readily extended to the loop antenna.

A. Sommerfeld's Integral Equations

In order to determine whether or not it is practical to use such a ground antenna, we refer to the work of Sommerfeld (Refs. 5,6), who treated the problem of a horizontal Hertz dipole (Ref. 7) over an arbitrary plane earth. Sommerfeld has derived rigorous integral equations for the Hertz vector of such a dipole antenna. For completeness, his derivation is briefly outlined here.

The Hertz vector Π for the Hertz dipole of Figure 26, which is located at (0,0,h), is

$$\vec{\Pi} = \vec{i}\,\Pi_x = \frac{\vec{i}\, I\ell\, e^{j(kR-\omega t)}}{4\pi\omega\epsilon R} \tag{7}$$

where k is the wave number $\sqrt{\omega^2\mu\epsilon - j\sigma\mu\omega}$ of the medium of capacitivity ϵ, magnetic permeability μ, and conductivity σ; j is the usual imaginary notation, and

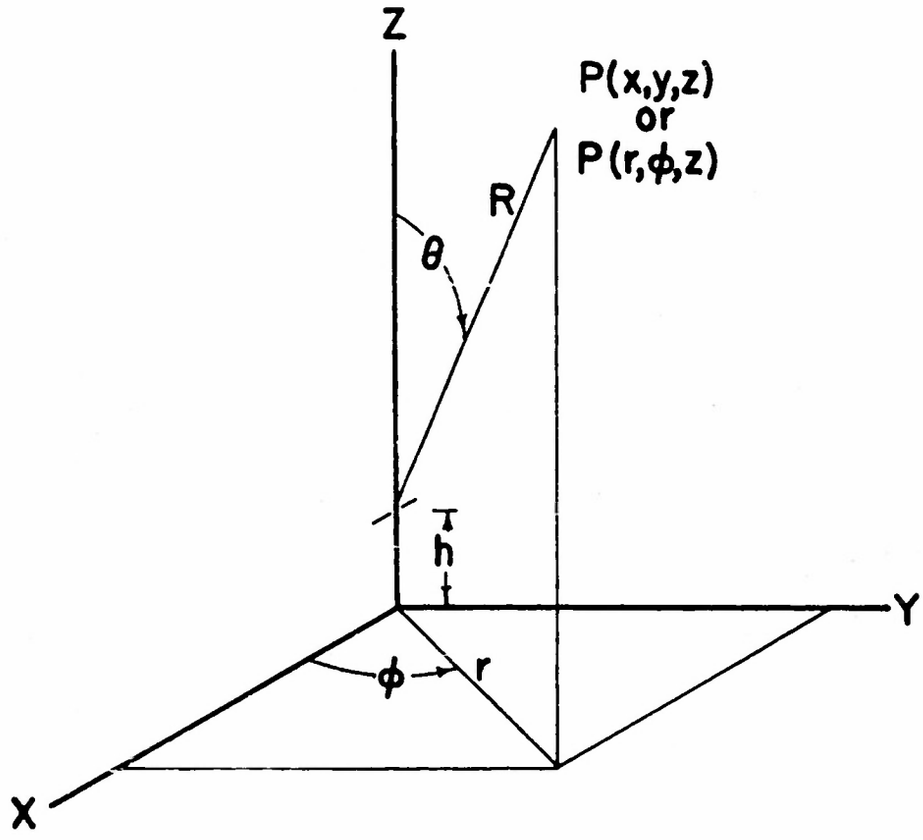

Figure 26.
Hertz dipole in free space

$$R^2 = x^2 + y^2 + (z-h)^2 = r^2 + (z-h)^2$$

The electric current in the dipole is $i = I \cos \omega t$ amperes. The Hertz vector satisfies the wave equation

$$\nabla^2 \vec{\Pi} = \mu\epsilon \frac{\partial^2 \vec{\Pi}}{\partial t^2} + \mu\sigma \frac{\partial \vec{\Pi}}{\partial t} \tag{8a}$$

as do the electromagnetic-field components. First of all, the time dependence can be removed, and the wave equation becomes

$$\nabla^2 \vec{\Pi} = -(\omega^2 \epsilon\mu + j\sigma\mu\omega)\vec{\Pi} = -k^2 \vec{\Pi} \tag{8b}$$

If the dipole is oriented in the x direction, the Hertz vector, at any point in space, has an x component only. In the plane $z = 0$, the magnitude of the Hertz vector is a function of r only.

The electric and magnetic intensity vectors $\vec{E}$ and $\vec{H}$ of the radiation field can be obtained from $\vec{\Pi}$ as follows:

$$\vec{E} = k^2 \vec{\Pi} + \nabla(\nabla \cdot \vec{\Pi}) \tag{9}$$

$$\vec{H} = \frac{k^2}{j\omega\mu} \nabla \times \vec{\Pi} \tag{10}$$

Equations 9 and 10 may be derived from Maxwell's equations.

The horizontal dipole above an arbitrary plane earth, at $z = 0$, may be represented by the total Hertz vector $\vec{\Pi}_1$: $\vec{\Pi}_1$ is made up of a primary excitation $\vec{\Pi}_{prim}$ due to the dipole only and a secondary excitation $\vec{\Pi}_{sec}$ due to the perturbation effect of the plane earth. The Hertz vector in the earth $\vec{\Pi}_2$ is completely determined by the boundary conditions imposed upon $\vec{\Pi}_1$ by $\vec{E}$ and $\vec{H}$. These boundary conditions for the two components of $\vec{\Pi}$ (Π_x and Π_z) are

$$\Pi_{x_1} = n^2 \Pi_{x_2} \tag{11}$$

$$\frac{\partial \Pi_{x_1}}{\partial z} = n^2 \frac{\partial \Pi_{x_2}}{\partial z} \tag{12}$$

$$\Pi_{z_1} = n^2 \Pi_{z_2} \tag{13}$$

$$\frac{\partial \Pi_{z_1}}{\partial z} - \frac{\partial \Pi_{z_2}}{\partial z} = \frac{\partial \Pi_{x_2}}{\partial x} - \frac{\partial \Pi_{x_1}}{\partial x} \tag{14}$$

where $n^2 = k_2^2/k_1^2$. The constants for the earth are ϵ_2 , μ_2 , σ_2 ; and the constants for air are $\epsilon_1 = \epsilon_v$, $\mu_1 = \mu_v$, $\sigma_1 = 0$.

In order to apply these boundary conditions, Equation 7 must be put in the form of a superposition of eigenfunctions. By making use of the Fourier-Bessel integral theorem, Equation 7 may be written in cylindrical coordinates as follows:

$$\vec{\Pi} = \vec{\Pi}_{prim} = \frac{\vec{i}\, Il}{4\pi\omega\epsilon_v} \frac{e^{jkR}}{R}$$

$$= \frac{\vec{i}\, Il}{4\pi\omega\epsilon_v} \int_0^\infty J_0(\lambda r) e^{-a(z-h)} \frac{\lambda d\lambda}{a} \tag{15}$$

where λ , the eigenvalue of the eigenfunction, has a continuous spectrum $0 \le \lambda \le \infty$ and $a = \sqrt{\lambda^2 - k_n^2}$.

Sommerfeld's integral equations for Π_1 and Π_2 may now be written for the horizontal dipole at a height h above an arbitrary earth (Figure 27).

$$\Pi_{x_1} = \frac{Il}{4\pi\omega\epsilon_1} \int_0^\infty J_0(\lambda r) \frac{\lambda}{a_1} \left[e^{-a_1(z-h)} - e^{-a_1(z+h)} \left(1 - \frac{2a_1}{a_1 + a_2} \right) \right] d\lambda$$

$$= \frac{Il}{4\pi\omega\epsilon_1} \left[\frac{e^{jk_1R}}{R} - \frac{e^{jk_1R'}}{R'} + 2\int_0^\infty J_0(\lambda r) e^{-a_1(z+h)} \frac{\lambda d\lambda}{a_1 + a_2} \right] \tag{16}$$

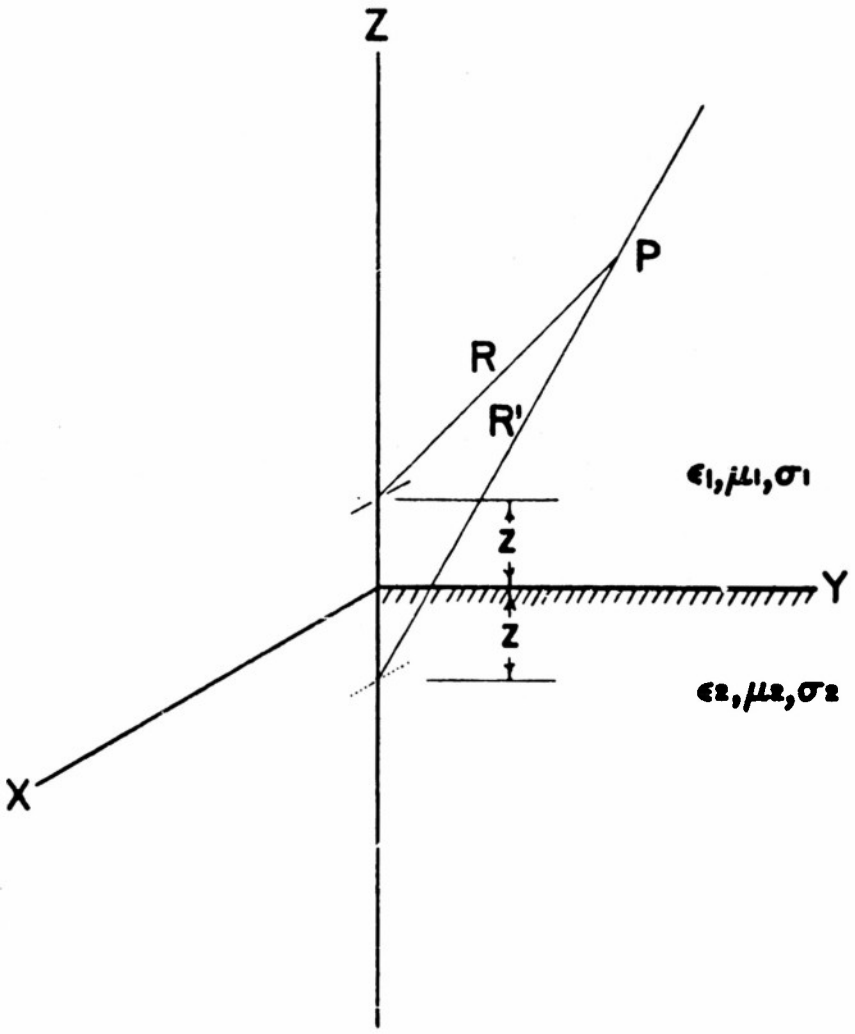

Figure 27 .

Hertz dipole over a plane earth

$$\Pi_{x_2} = \frac{I\ell}{4\pi\omega\epsilon_1} \frac{2}{n^2} \int_0^\infty J_0(\lambda r) e^{a_2 z - a_1 h} \frac{\lambda d\lambda}{a_1 + a_2} \tag{17}$$

$$\Pi_{z_1} = \frac{I\ell}{4\pi\omega\epsilon_1} \frac{2\cos\phi}{k_1^2} \frac{\partial}{\partial r} \int_0^\infty J_0(\lambda r) e^{-a_1(z+h)} \frac{a_1 - a_2}{n^2 a_1 + a_2} \lambda d\lambda$$

$$= \frac{-I\ell}{4\pi\omega\epsilon_1} \frac{2\cos\phi}{k_1^2} \int_0^\infty J_1(\lambda r) e^{-a_1(z+h)} \frac{a_1 - a_2}{n^2 a_1 + a_2} \lambda^2 d\lambda \tag{18}$$

$$\Pi_{z_2} = \frac{I\ell}{4\pi\omega\epsilon_1} \frac{2\cos\phi}{k_2^2} \frac{\partial}{\partial r} \int_0^\infty J_0(\lambda r) e^{a_2 z - a_1 h} \frac{a_1 - a_2}{n^2 a_1 + a_2} \lambda d\lambda$$

$$= \frac{-I\ell}{4\pi\omega\epsilon_1} \frac{2\cos\phi}{k_2^2} \int_0^\infty J_1(\lambda r) e^{a_2 z - a_1 h} \frac{a_1 - a_2}{n^2 a_1 + a_2} \lambda^2 d\lambda \tag{19}$$

where $R^2 = x^2 + y^2 + (z-h)^2$ and $R'^2 = x^2 + y^2 + (z+h)^2$.

It is believed that Equations 16 through 19 are valid for the radiation field; however, the techniques that various people have used on these equations in order to find Poynting's vector or the electric and magnetic field strengths invariably involve approximations which are not valid for all values of k_2. It can be seen that the evaluation of these integrals involves integration of an equation having a Riemann surface

of four sheets with branch points at $\lambda = k_1$ and $\lambda = k_2$. Care must be taken that the path of integration lies in the proper sheet. Equations 18 and 19 have an additional complexity of a pole at $\lambda = p$, where $1/p^2 = (1/k_1^2) + (1/k_2^2)$ because of the fact that $n^2 a_1 + a_2$ is zero for $\lambda = p$. The significance which Sommerfeld places upon the solution obtained by integration around this pole is discussed in Section IV-D.

The appearance of a component of the Hertz vector in the z direction is worth noting, because the primary excitation had no such component. The Π_z values of Equations 18 and 19 are brought about by the perturbation effect of the plane earth, and we see from Equation 9 that a vertically polarized wave results. This wave has a maximum value in the $\pm$ x direction and a zero value in the $\pm$ y direction. This property will be extremely important in the consideration of the antenna as an instrument for ionospheric research.

In Equation 16, we can see that the solution for Π_x is the sum of the solutions of two dipoles, one at $z = h$ and another at $z = -h$, plus the expression

$$\frac{I\ell}{4\pi\omega\epsilon_1} \; 2\int_0^\infty J_0(\lambda r) e^{-a_1(z+h)} \frac{\lambda d\lambda}{a_1 + a_2}$$

We know from physical reasoning that for $k_2 = k_1$ this term must be equal to

$$\frac{I\ell}{4\pi\omega\epsilon_1} \; \frac{e^{jk_1R'}}{R'}$$

and that for $k_2 = \infty$ the term must equal zero. Furthermore, for finite current I and with $k_2 = \infty$, Π_{x2}, Π_{z1}, and Π_{z2} must also be zero. In addition, Π_{z1} and Π_{z2} are, of course, zero for $k_2 = k_1$.

B. Ground Losses

It is interesting to note that the determination of power output from Equations 16 through 19 is not unduly complicated. We shall not go through the development, which is available in References 5 and 6, but shall merely write the expression for radiation resistance

$$R_{rad} = \frac{k_1^2 \ell^2}{4\pi} \sqrt{\frac{\mu_v}{\epsilon_v}} \left(\frac{2}{3} - \frac{\sin\zeta}{\zeta} + \frac{\sin\zeta - \zeta\cos\zeta}{\zeta^3} + L \right) \qquad (20)$$

where

$$L = \frac{1}{k_1^3} \mathcal{R}_e \left[j \int_0^\infty e^{-2a_1 h} \frac{2a_1 a_2 - \lambda^2}{n^2 a_1 + a_2} \lambda \, d\lambda \right] \tag{21}$$

and $\zeta = 2 k_1 h$. Thus R_{rad} is a function of the height h above the ground. L vanishes for $k_2 = \infty$. This special case is plotted in Figure 28. The scale is changed so that the resistance of the antenna for infinite height is 70 ohms. If one wishes to evaluate L for finite values of k_2, again approximations must be made which will not be valid in general. The solution assumes an infinitesimal source, and at this source the fields must, of necessity, by infinite. Thus it seems plausible that, if h is allowed to approach zero, and if σ_1 is not zero, the radiation resistance R_{rad} goes toward an infinite value. It follows that an infinite field causes infinite loss for a finite current in the antenna. This physical reasoning agrees with the result which Sommerfeld obtained on evaluating L for a partially conductive earth. It is important to note that, although the total resistance is infinite, this fact is due entirely to absorption in the ground, and only a finite amount of the loss is radiated into the air for a finite driving current. Therefore the efficiency of the dipole would be zero.

If we consider an actual antenna, we find that because of the finite dimensions of a physical antenna infinite fields do not exist. The fields are high enough, however, to cause considerable losses if the antenna is actually laid on the ground. We are able to reduce the losses to a reasonable value by raising the antenna several feet above the ground. At low frequencies, it is apparent that the actual height above the ground is the determining factor for reducing losses, not the ratio h/λ

C. The Reflection Method

For in ionospheric-research antenna, one would be most interested in the field-strength pattern in two planes (the x-z plane and the y-z plane) for all angles of θ (Figure 27), for in these two planes the wave incident on the ionosphere is polarized either in the plane of incidence or normal to the plane of incidence. We can obtain this field pattern by developing a reflection method whose validity has been checked by experiment. In this method, we assume that the fields radiated directly from the antenna are related to the current flowing in the antenna and are independent of the presence of the earth. In order to find the field at a point P (Figure 29) due to a dipole an arbitrary distance h above the plane earth, the wave leaving the antenna at an angle θ is added to the reflected wave

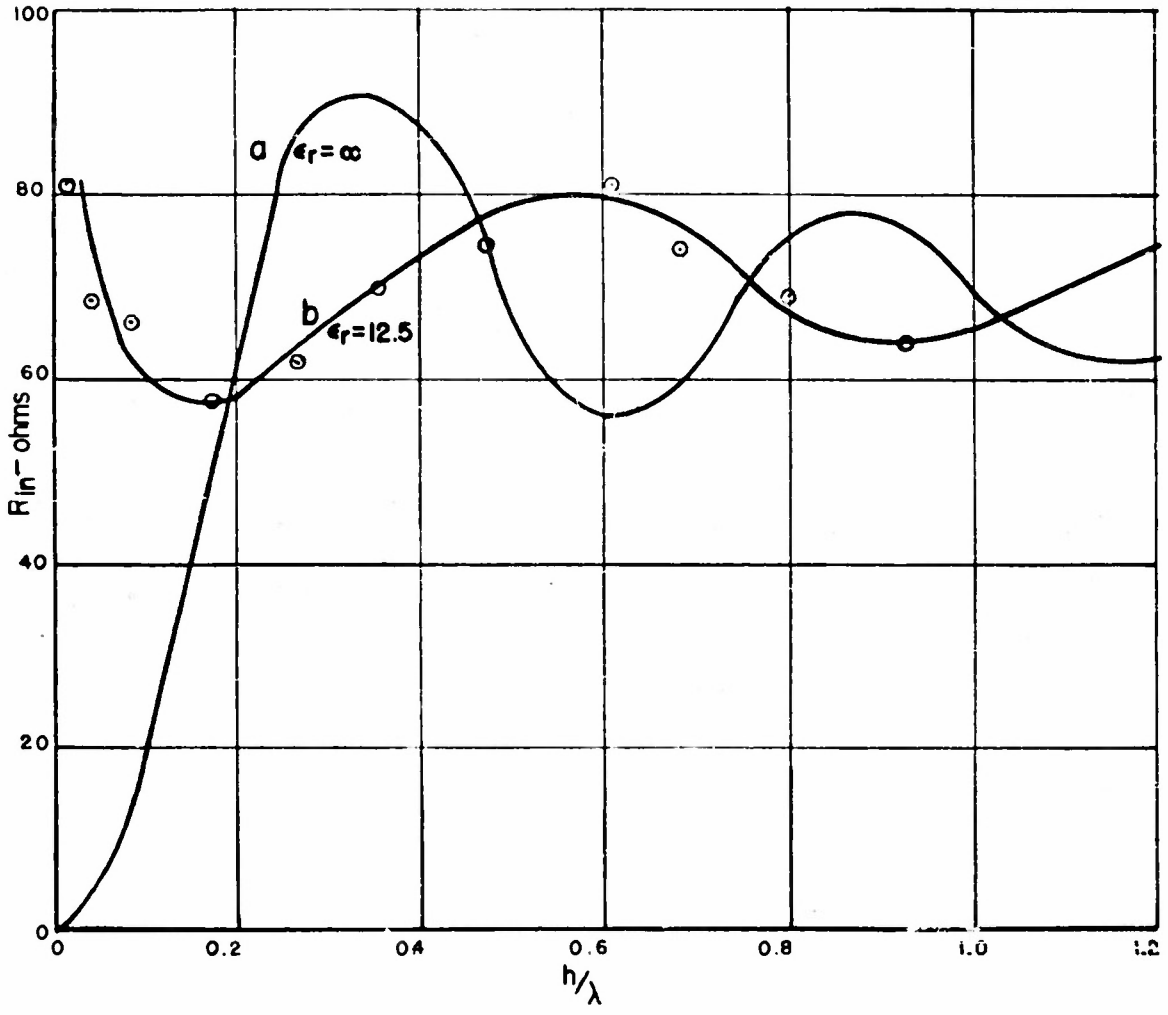

Figure 28

Input resistance of a half wave dipole above a plane earth. a) Calculated for $\epsilon_r = \infty$ b) Experimental for $\epsilon_r = 12.5$

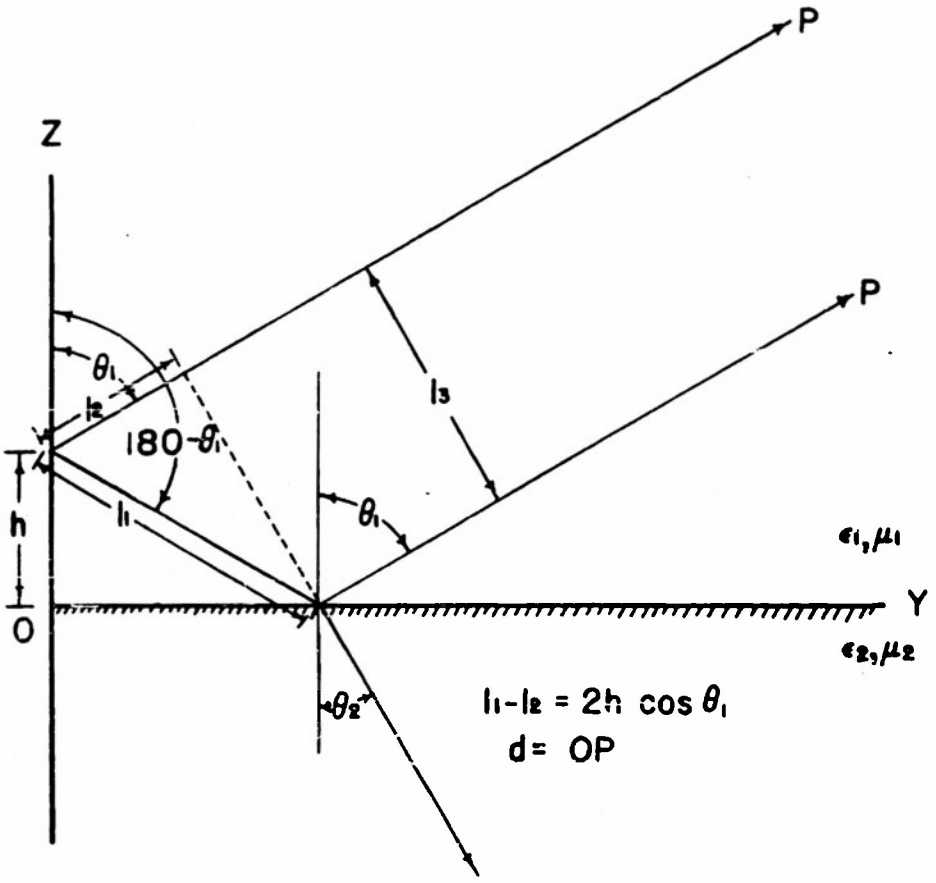

Figure 29

Geometry of the reflection method

which left the antenna at an angle $180^\circ - \theta$. For this condition to be valid, ℓ_3/d must be much less than 1. A complex dielectric constant introduces a change in the phase of the reflected wave. However, this change need not be considered here, and the earth is assumed to be a perfect dielectric.

The reflection coefficient for an electromagnetic wave polarized perpendicular to the plane of incidence is

$$\rho_{\perp} = \frac{\cos\theta_1 - \sqrt{n^2 - \sin^2\theta_1}}{\cos\theta_1 + \sqrt{n^2 - \sin^2\theta_1}} = \frac{E_3}{E_1} \tag{22}$$

and for the wave polarized in the plane of incidence, it is

$$\rho_{\parallel} = \frac{\epsilon_2 \cos\theta_1 - \epsilon_1 \sqrt{n^2 - \sin^2\theta_1}}{\epsilon_2 \cos\theta_1 + \epsilon_1 \sqrt{n^2 - \sin^2\theta_1}} = \frac{E_3}{E_1} \tag{23}$$

$$\mu_1 = \mu_2 = \mu_v$$

Since the reflected wave travels a path which is longer by an amount $\ell = \ell_1 - \ell_2 = 2h \cos\theta_1$ (Figure 29), it is delayed in phase by an angle

$$\delta = \frac{2h\cos\theta_1\, 360^\circ}{\lambda} \tag{24}$$

Thus, if the reflected field intensity is E_3, the total field at point P is

$$E_P = E_1 + E_3 e^{-j\delta} = E_1\left(1 + \rho e^{-j\delta}\right) \tag{25}$$

In the y-z plane, for $h=0$, Equation 25 becomes

$$E_P = \frac{2E_1 \cos\theta_1}{\cos\theta_1 + \sqrt{n^2 - \sin^2\theta_1}} \tag{26}$$

Note that, when h is equal to zero, the field has the same maximum value below the antenna as above. In the dielectric, the entire pattern is confined to a cone of revolution whose central angle is

$$\beta = \sin^{-1}\frac{k_2}{k_1} = \sin^{-1}\sqrt{\epsilon_r} \tag{27}$$

where $\epsilon_r = \epsilon_2/\epsilon_1$

Figure 30 shows how the pattern, for $h = 0$, varies for different values of the relative capacitivity, and we can observe how the radiation resistance decreases with increasing relative capacitivity. As before, constant driving current is assumed. The pattern of the antenna has a maximum value in the $\theta = 0°$ direction and has decreased by only 10 per cent at $\theta = 30°$. Figure 31 is a plot of the normalized maximum field as a function of ϵ_r. The fact that there is zero field strength in the $\theta = 90°$ direction is useful, because the problem of separating ground wave from sky wave is eliminated in the y or $\phi = 90°$ direction. The ground wave in the x or $\phi = 0°$ direction is considered shortly.

It is possible to compare the results obtained by the reflection method for $h = 0$ with Sommerfeld's results at a point directly above the antenna, $\theta = 0$, and at a point off the side of the antenna, $\theta = \pi/2$ $\phi = \pi/2$. For the latter case, $\theta = \pi/2$, $\phi = \pi/2$, both methods give zero field strength. At $\theta = 0$, according to Equation 26 the field strength is $2\sqrt{\epsilon_1}/(\sqrt{\epsilon_1}+\sqrt{\epsilon_2})$ times the field strength of an equivalent dipole in free space. At $\theta = 0$, $r = 0$, Equation 16 for Π_x becomes

$$\Pi_x\Big|_{r=0} = \frac{I\ell}{4\pi\omega\epsilon_1}\left[\int_0^\infty e^{-\alpha_1(z+h)}\frac{2\lambda d\lambda}{\alpha_1+\alpha_2} + \frac{e^{jk_1(z-h)}}{z-h} - \frac{e^{jk_1(z+h)}}{z+h}\right] \tag{28}$$

The integral in this case can be evaluated for large values of z, and becomes

$$\Pi_x\Big|_{r=0} = \frac{I\ell}{4\pi\omega\epsilon_1}\left[\frac{e^{jk_1(z-h)}}{z-h} - \frac{e^{jk_1(z+h)}}{z+h} + \frac{2\sqrt{\epsilon_1}}{\sqrt{\epsilon_1}+\sqrt{\epsilon_2}}\,\frac{e^{jk_1(z+h)}}{(z+h)}\right] \tag{29}$$

For $h = 0$, Π_x is $2\sqrt{\epsilon_1}/(\sqrt{\epsilon_1}+\sqrt{\epsilon_2})$ times the free-space value; thus the two methods give the same result.

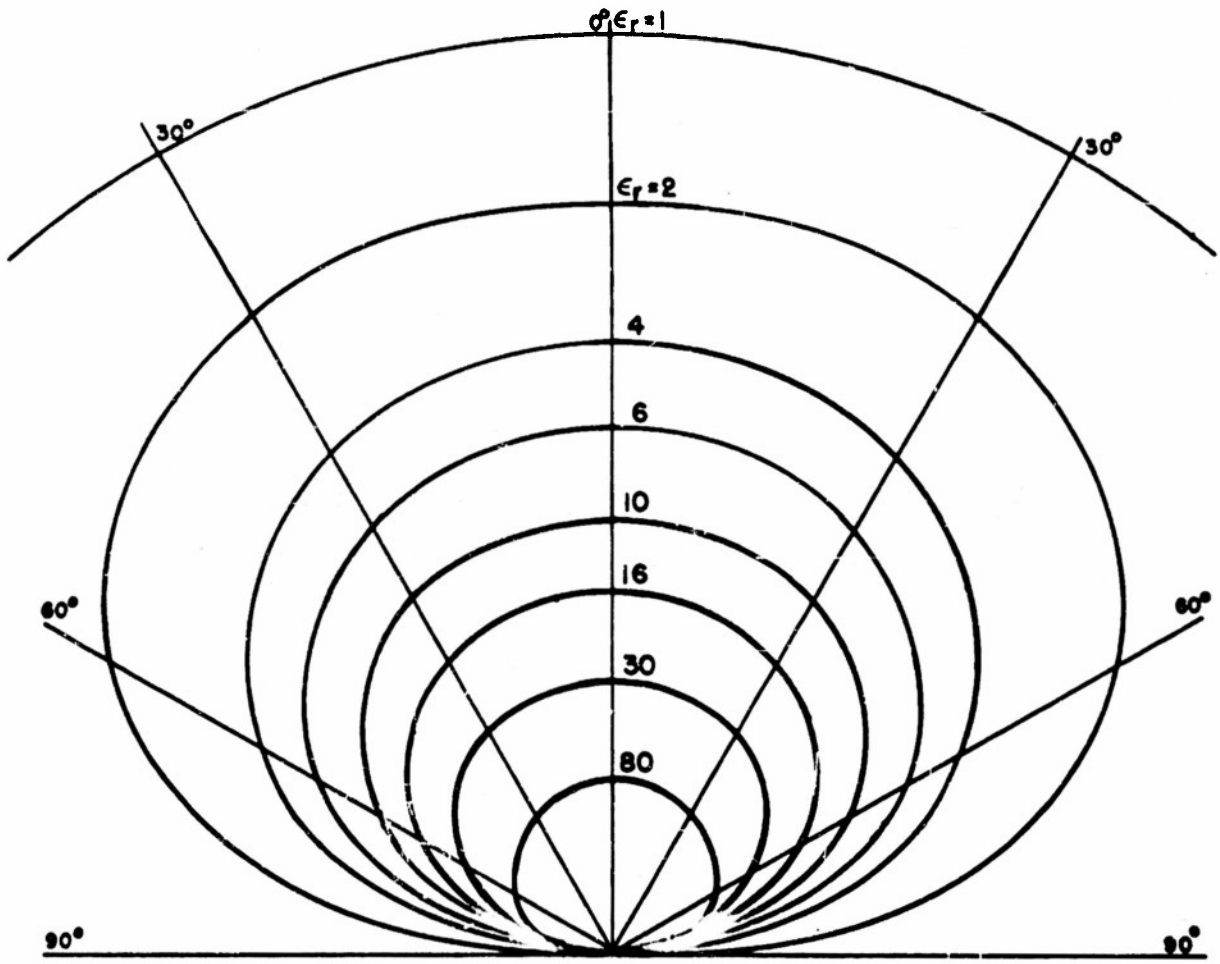

Figure 30.
Pattern in y,z plane of a dipole over a plane dielectric earth with h = 0.

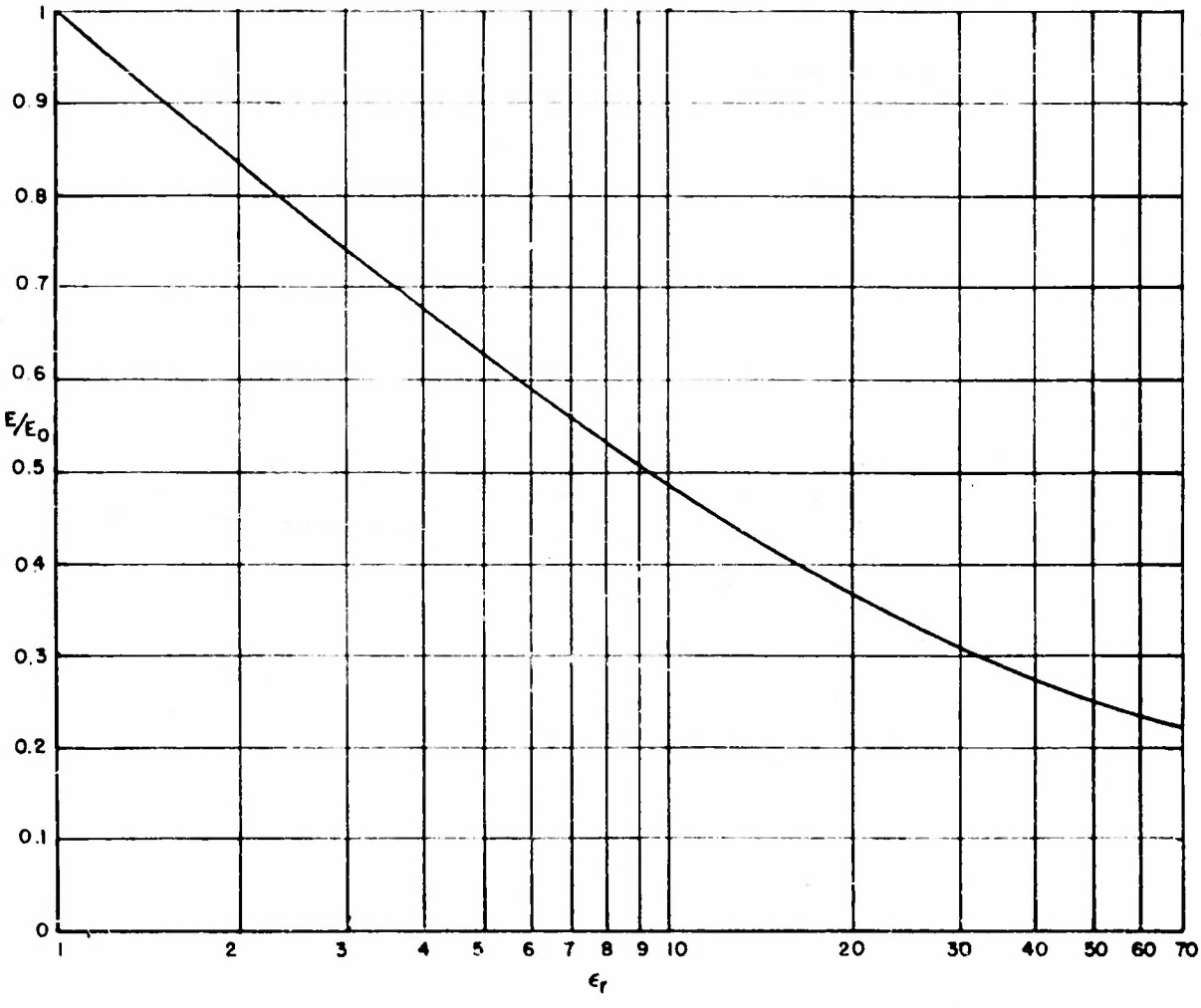

Figure 31.

Maximum field strength of a dipole over a plane dielectric earth ($h=0, \theta=0$) as a function of ϵ_r.

D. The Ground Wave

The radiation field of the horizontal dipole, over an abitrary earth, consists of a horizontally polarized sky wave and a vertically polarized ground wave. The reflection method does not give rise to a solution corresponding to a vertically polarized ground wave. For the case of a horizontal dipole at the surface of a perfect dielectric earth, the ground wave may be easily calculated from Sommerfeld's integral equation (Equation 18). This equation may be written in the form

$$\Pi_{z_1} = \frac{-I\ell}{4\pi\omega\epsilon_1} \frac{2\cos\phi}{k_1^2} \int_0^\infty J_1(\lambda r) e^{-a_1 z} \frac{(a_1 - a_2)}{n^2 a_1 + a_2} \lambda^2 d\lambda = P + Q \tag{30}$$

The integrand has branch points at $\lambda = k_1$ and $\lambda = k_2$ and a pole at $\lambda = p$, where p is given by the equation

$$n^2 \sqrt{p^2 - k_1^2} + \sqrt{p^2 - k_2^2} = 0 \tag{31a}$$

or

$$p^2 = k_1^2 k_2^2 / (k_1^2 + k_2^2) \tag{31b}$$

The term P of Equation 30 is the contribution of the pole to the value of the integral. Sommerfeld has shown that this portion of the solution for Π_{z1} gives rise to a ground wave. P may be calculated by applying the residue theorem of complex-variable theory. The integral of Equation 30 may be transformed into one involving the Hankel function H_1^1

$$\Pi_{z_1} = \frac{-I\ell}{4\pi\omega\epsilon_1} \frac{\cos\phi}{k_1^2} \int_{-\infty}^\infty H_1^1(\lambda r) e^{-a_1 z} \frac{a_1 - a_2}{n^2 a_1 + a_2} \lambda^2 d\lambda \tag{32}$$

The residue of the integrand at the pole $\lambda = p$ is

$$\mathcal{R}_{es} = \frac{-I\ell}{4\pi\omega\epsilon_1} \frac{\cos\phi}{K} H_1^1(pr) e^{-\sqrt{p^2 - k_1^2}\, z} p\left(\sqrt{p^2 - k_1^2} - \sqrt{p^2 - k_2^2}\right) \tag{33}$$

where $K = \frac{k_2^2}{\sqrt{p^2 - k_1^2}} + \frac{k_1^2}{\sqrt{p^2 - k_2^2}}$ Thus P is

$$P = j 2\pi \int_0^\infty \quad (34)$$

For large r, the asymptotic expression for the Hankel function may be used, and P becomes

$$P = -j \frac{I\ell}{2\omega\epsilon_1} \frac{\cos\phi}{K} p\left(\sqrt{p^2-k_1^2} - \sqrt{p^2-k_2^2}\right)\sqrt{\frac{2}{\pi p}}\, e^{j\left[pr - \frac{3\pi}{4}\right]} \frac{e^{-\sqrt{p^2-k_1^2}\, z}}{\sqrt{r}} \quad (35a)$$

The magnitude of P, at $\phi = 0$, $z = 0$, is

$$|P| = \frac{I\ell}{2\omega\epsilon_1}\sqrt{\frac{2p}{\pi}}\,\frac{\left(\sqrt{p^2-k_1^2} - \sqrt{p^2-k_2^2}\right)}{K}\,\frac{1}{\sqrt{r}} \quad (35b)$$

E. The Experimental Results

A half-wave antenna, at 197 mc/s, was used in order to investigate further the problem of a dipole over a dielectric earth. The field strength in the plane normal to the length of the antenna was measured, and the results are plotted in Figure 32. The pattern of the antenna agrees very well with the calculated values.

If the field strength above the antenna is found for the two heights of the antenna h which gives a maximum and a minimum value, it is possible to calculate the relative capacitivity ϵ_r. We have from Equation 25

$$E_{min} = \frac{2\sqrt{\epsilon_1}}{\sqrt{\epsilon_1} + \sqrt{\epsilon_2}} E_1 = \frac{2}{\sqrt{\epsilon_r} + 1} E_1 \quad (36)$$

$$E_{max} = \frac{2\sqrt{\epsilon_r}}{\sqrt{\epsilon_r} + 1} E_1 \quad (37)$$

The ratio of the two, E_{max}/E_{min}, is $\sqrt{\epsilon_r}$; ϵ_r was found to be 12.5.

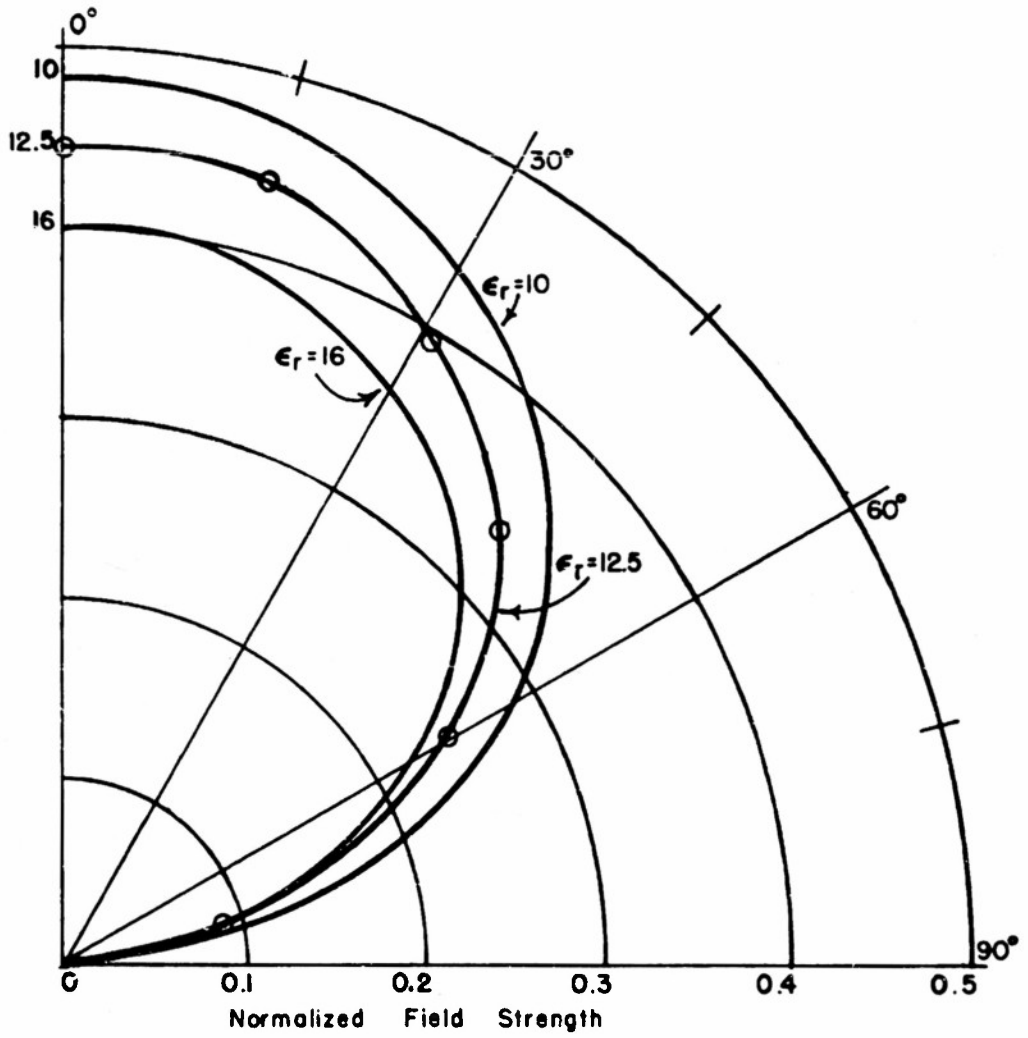

Figure 32.
Field pattern for a dipole over a plane earth h=o
(calculated results for ϵ_r = 16,10 and measured
values for ϵ_r = 12.5)

We have not yet tried to determine the losses in the earth when the ratio h/λ_v is small. The 200-mc/s experiment provided a measurement of input resistance as a function of height, and the results are plotted in Figure 28. Figure 28 shows fluctuations about 70 ohms for h greater than $\lambda/4$, but as h approaches zero, the input resistance increases instead of decreasing. This rise is attributed to higher field strengths in the dielectric that cause additional losses. With the antenna about 1.5 centimeters above the ground, the input resistance was found to be 80 ohms.

The resonant length of a half-wave dipole in this dielectric, at 197 mc/s, would be $\lambda_v/2\sqrt{\epsilon_r}$, or about $0.14\,\lambda_v$. As the antenna is brought near the earth, a change in the resonant length is observed; it is plotted in Figure 33. When the field strength from a dipole, whose length is shortened, is calculated, the correction factor λ'/λ_v must be used, where λ' is twice the actual length of the dipole, and λ_v is the wavelength in free space. The pattern of a half-wave dipole, with sinusoidal current distribution, changes only in magnitude with decreasing antenna length.

A 60-kc/s antenna, approximately 2,000 meters long, was built over dry granite with a relative capacitivity ϵ_r of about 6 or 7 and very low loss. This was a pilot model for the 16-kc/s antenna. The average height of the antenna above the earth was 1 meter, and the value of λ'/λ_v was 0.8. The input resistance of the dipole was 127 ohms, 39 ohms of which is attributed to copper losses. The remaining 88 ohms consists of radiation and absorption losses.

The maximum field of a half-wave dipole in free space is

$$E_{rms} = \frac{60\, I_{rms}}{d} \qquad \text{volts/meter} \qquad (38)$$

Therefore the field strength at a distance d directly above a ground dipole antenna is

$$E_{rms} = \frac{2}{1+\sqrt{\epsilon_r}} \frac{\lambda'}{\lambda_v} \frac{60\, I_{rms}}{d} \qquad \text{volts/meter} \qquad (39)$$

which we see depends upon the relative capacitivity and current. If we use $\epsilon_r = 6$ for our 60-kc/s antenna, we obtain

$$E_{rms} = 0.46 \frac{60\, I_{rms}}{d} \qquad \text{volts/meter} \qquad (40)$$

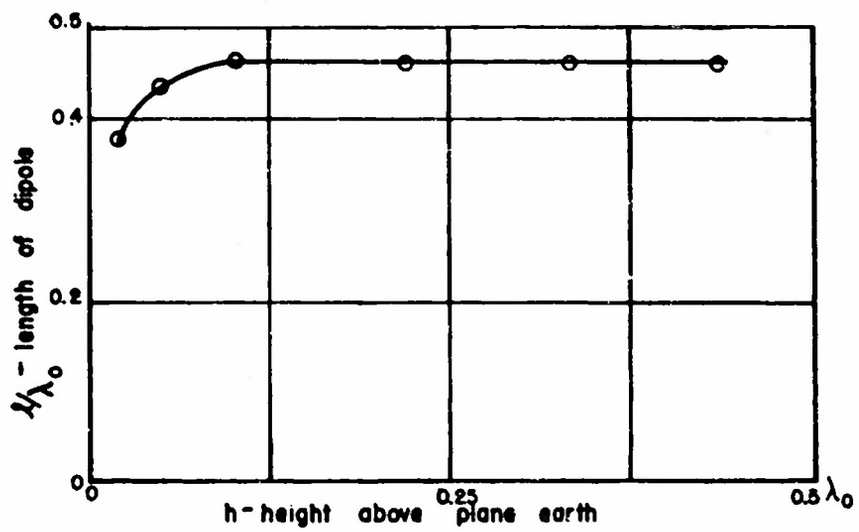

Figure 33.
The resonant length of a dipole as a function of height above the plane earth. $f_0 = 197$mc.

One can obtain the effective* efficiency from Equations 38 and 39

$$\mathcal{E}_{eff} = \left(\frac{2}{1+\sqrt{\epsilon_r}}\,\frac{\lambda'}{\lambda_v}\right)^2 \frac{72}{R} \times 100\% \qquad (41)$$

where R is the input resistance of the ground antenna. Neglecting the copper losses, the 60-kc/s antenna has an effective efficiency of 17 per cent.

In order to find the magnitude of signal that can be expected at the receiver site, let us assume that d in the reflection from the D-layer is 180 km and that the reflection coefficient is about 0.1. Equation 40 gives the result of 15 μ volts/meter for each ampere of current in the antenna.

A receiving site was set up about 55 km from the transmitter, in a direction normal to the transmitting antenna, and the sky-wave signal came in quite clearly. Except for the fact that the receiving antenna need not be resonant, its characteristics are identical with those of the transmitting antenna. It improves the signal-to-noise ratio by virtue of its discrimination against vertically polarized waves.

Experimentation was also carried out with a resonant loop. The radiated signal from this antenna was received at a distance of 160 km from the transmitting site. This antenna has zero field strength above it and a maximum field strength at low angles of elevation. With this antenna we found that, by raising the wire off the ground by about 1/2 meter, the resonant frequency is increased by a factor of 1.7, and the loss is reduced by a factor of 2. The loop antenna was abandoned temporarily in favor of the dipole which had the desired properties necessary for ionospheric measurements near vertical incidence. The cost of either antenna is small, a fact which was, of course, a prime factor in making it possible for the authors to carry on the ionospheric research program.

---

* The effective efficiency is defined as the ratio of the power required to set up a unity field strength at a height h_o over the earth to the power required to set up the same unity field strength at a distance h_o from a dipole in free space.

F. The 16-kc/s Transmitting Antenna

The 16-kc/s transmitting antenna was briefly described in Section II-B. The antenna was constructed in the Mojave Desert southwest of Randsburg, California (about 80 miles north of Pasadena). The altitude at the center of the antenna is 3,500 feet above sea level. The east end is at 3,700 feet, whereas the west end is at 3,200 feet. The terrain upon which the antenna is built is, on the whole, quite level.

The antenna consists of No. 10, No. 6, and No. 4 wire strung on poles placed 200 feet apart. The line was broken every 1,000 feet, or every fifth pole, and a switch was inserted in order to allow the antenna to be used at almost any frequency from 16 to 250 kc/s. Every fifth pole was independently guyed in four directions to protect the whole antenna from collapsing in case one section should fail. The poles were 4 x 6's of select structural and No. 1 common lumber 16 feet long. The average depth of the pole holes was 3 to $3\frac{1}{2}$ feet; thus the antenna wire everywhere was 10 to 11 feet above the ground. Light loading conditions were assumed in the structural design of the antenna, and since the altitude was slightly higher than 3,000 feet, additional safety factors were used. Figure 34 is a photograph showing an antenna pole being erected.

The original object in building the dipole was to provide a low-cost transmitting antenna which would require no tuning inductances but would, instead, present a resistive load to the transmitter. In this way the design of the transmitter was greatly simplified. As a half-wave dipole at low and very low frequencies. This antenna presented a resistive load. The current distribution in the dipole is sinusoidal with a wavelength λ_{eff}, which was approximately 94 per cent of the free-space wavelength λ.

The losses of the dipole are attributed to copper losses R_c, distributed ground losses R_g, and radiation losses R_r. The efficiency of the antenna is given by $R_r/(R_g + R_c + R_r)$, or R_r/R_o; therefore R_g and R_c should be made as small as possible. Unfortunately not much can be done about R_g; R_c can be reduced by using more copper in the antenna, especially if it is concentrated near the center.

The antenna consists mostly of No. 10 hard-drawn copper wire. The copper losses are found to be $(I^2 R_{ac}/4)\ \lambda_{eff}$ where I is the rms current at the center of the dipole. Therefore

$$R_c = R_{ac}\, \lambda_{eff}/4 \qquad (42)$$

Figure 34. Erecting an Antenna Pole

R_c is found to be 21 ohms at 50 kc/s and 40 ohms at 16 kc/s, whereas the measured value of R_o was 65 ohms at 50 kc/s and 82 ohms at 16 kc/s. Note that the difference in the input resistances at the two frequencies is just the difference in copper losses. It can be inferred that $R_g + R_r$ is not a function of frequency; this inference agrees with the theory.

The dipole can be used as an impedance transformer under limited conditions. The current and voltage are everywhere in phase. Thus if the dipole is fed at some point other than the center of the antenna, the input impedance remains resistive and increases to the value given by the empirical formula

$$R_{in_x} = R_o/\cos^2 \frac{2\pi x}{\lambda_{eff}} \tag{43}$$

Here λ_{eff} turns out to be a function of x because of the effect of the transmitter and the lead-in wires. As the feed point moves away from the center of the antenna λ_{eff} decreases.

At the experimental frequency 50 kc/s, the 65 ohm impedance of the dipole was transformed to 100 ohms to match the output impedance of the transmitter. This transformation was accomplished by feeding the 8,600-foot dipole at a distance of 1,700 feet from the center.

The Q of the antenna was found to be about 12 by determining the two frequencies f_1 and f_2 where the input impedance had a phase angle of 45^o and by using the equation

$$Q = f_o/(f_2 - f_1) \tag{44}$$

where f_o is the resonant frequency.

The radiation pattern has a maximum value directly over the antenna, a fact which makes it especially suitable for vertical-incidence ionospheric sounding.

V. THE PROPAGATION OF ELECTROMAGNETIC WAVES IN THE IONOSPHERE

A. Ray Treatment

Certain problems involving the propagation of an electromagnetic wave in the ionosphere may be solved by a ray treatment similar to that used in geometrical optics. In the ionosphere, the ionization density increases gradually with height, reaches a maximum, and then diminishes. Depending on conditions, there may be several such ionization maxima which are called layers. If the change in ionization is small in the space of a wavelength, the amount of energy reflected as a wave penetrates the medium is small and can be neglected. In such a case, the medium is termed slowly varying, and it is sufficient to consider only the refraction that takes place.

In the derivation of the magneto-ionic equations, $\frac{d\Gamma}{dx}$ is assumed to be negligible. (Γ is the propagation constant, and x is measured in the direction of propagation.) This approximation is equivalent to assuming the variation of the propagation constant to be so gradual that the medium may be considered as homogeneous throughout a distance of a few wavelengths.

In applying the magneto-ionic theory and ray treatment to E-layer propagation problems at low frequencies, the assumption sometimes may be made (e. g., near the equator) that the absorption due to collisions is negligible. This assumption is suggested by the fact that at night the reflection coefficient often approaches unity. The propagation is then of the quasi-transverse type (the terms quasi-transverse and quasi-longitudinal were introduced by Booker in Ref. 8). The authors of this report believe that, under average conditions at low and very-low frequencies in the range of 16 to 70 kc/s, this assumption results in a great oversimplification of the problem. In the lossless case, the Appleton-Hartree equation may be written in the form

$$n^2 = 1 - \frac{x}{1 - \frac{y_T^2}{2(1-x)} \pm \sqrt{\frac{y_T^4}{4(1-x)^2} + y_L^2}} \qquad (45)$$

where

n = refractive index

$x = -\frac{1}{p} = \frac{KN}{f^2}$

$K = \frac{e^2}{4\pi^2 m \epsilon_v}$

N = ionization density

$y_T = -\frac{\gamma_T}{p} = \frac{f_T}{f}$

$y_L = -\frac{\gamma_L}{p} = \pm \frac{f_L}{f}$ (Plus sign used when the positive direction of the earth's magnetic field makes an acute angle with the direction of propagation)

f_T = transverse gyro frequency

f_L = longitudinal tyro frequency

f = wave frequency

At vertical incidence, reflection occurs when the refractive index is reduced to zero. At frequencies below the gyro frequency, $n = 0$ for

$x = 1$ (ordinary component of wave, given by plus sign before radical)

$x = 1 + y$ (extraordinary component of wave, given by minus sign before radical)

where

$y = \frac{f_H}{f}$

f_H = gyro frequency

In this case, the propagation of the ordinary wave is not affected by the earth's magnetic field. The terms ordinary wave and extraordinary wave have been derived from the optical analogy. In double refraction in optics, the ray which follows the ordinary laws of refraction is called the ordinary ray, and the other is called the extraordinary ray.

For the conditions of our experiments, the electronic gyro frequency

f_H = 1,416 kc/s. The ionization density re quired for reflection of the extraordinary component at 50 kc/s is (1,416/50) + 1 or 29.3 times that necessary for reflection of the ord inary component. On entering an ionized region, an electromagnetic wave is split into two components. In our 50-kc/s experiments, the extraordinary component is reflected from a higher region of greater ionization density. The path length of the extraordinary wave in the ionized region is longer; thus, this wave will suffer greater attenuation.

If losses are neglected, the polarizations of the waves may be determined from the expression

$$R = \frac{1}{y_L}\left[\pm\sqrt{\frac{y_T^4}{4(1-x)^2}+y_L^2}-\frac{y_T^2}{2(1-x)}\right] \tag{46}$$

B. Wave Treatment

Helliwell (Ref. 9) has made measurements for determining the vertical ionization gradient of the lower nighttime E-region. He obtained height versus frequency data on 21 April 1949. Measurements were made in 50-kc/s steps from 100 to 400 kc/s. A measurable increase in height occurred between 100 and 400 kc/s. This increase amounted to not more than 2 km. He assumed that the time variation is negligible; that the ionization density increases exponentially with height; that, at the level of reflection, the ionization density is proportional to the square of the frequency; and that the true height change is the same as the virtual height change. The scale height of the layer was determined by using the relation

$$N = N_o e^{\frac{h-h_o}{H}} \tag{47}$$

where

N_c = ionization density at height h_o

N = ionization density at height h

H = scale height of the layer

Helliwell found the scale height to be H = 0.7 km. Thus, in a distance of 0.7 km, the ionization density increased by a factor of 2.7. Helliwell believes that this scale height is typical for the lower sides of the layers in the nighttime E-region. For such layers, it is clear that the slowly varying conditions do not exist at low frequencies, where the wavelength is greater than 1 km. Thus, at low frequencies, the applicability of the magneto-ionic theory and ray treatment is open to serious question. This fact suggests the use of a wave treatment in which the slowly varying approximations are not made.

In a wave treatment, we wish to find solutions to the wave equations when the propagation constant varies appreciably in the space of a wavelength. As yet there is no satisfactory wave treatment that may be applied to low-frequency ionospheric propagation problems. There are several reasons for this fact. In order to develop a wave theory, the ionization gradients in the lower ionospheric regions must be known. There is still considerable question as to the exact nature of these gradients. They cannot be deduced with confidence from theoretical considerations, because there is disagreement as to the exact ionization processes that take place in these regions. Also, there is some doubt as to the proper values of recombination coefficients, collisional frequencies, and temperatures to use. The ionization gradients have not been determined by radio measurements, because the measurements are difficult to make at low frequencies, and because they cannot be properly interpreted without initially having a suitable wave theory.

Another difficulty lies in the mathematical complexity of the nonlinear wave equations. Exact solutions to these equations may be obtained when the ionization gradients are represented by certain mathematical functions. However, these functions do not represent the ionized layers with sufficient accuracy. As an example, the Epstein layer may be treated exactly; however, it does not satisfactorily represent an ionospheric layer.

Approximate solutions to the wave equations may be found by applying the Wentzel-Kramers-Brillouin (WKB) method of quantum mechanics (Ref. 10). Care must be used in applying the WKB method, because the solutions obtained are not valid if the propagation constant changes appreciably in the space of a wavelength. However, an approximate solution can be found by properly matching slowly varying solutions of neighboring regions.

An additional complexity arises when the wave-equation solutions are not independent. In this case, coupled wave equations must be solved. This condition arises when the geomagnetic dip angle assumes

large values or when the ionization gradients are very steep. The coupled wave equations predict a third wave component. This phenomenon, termed ionospheric triple splitting, has been observed and treated by Eckersley (Ref. 11).

Several workers have made contributions toward the development of a wave theory. Booker (Ref. 12) has shown that the ray or slowly varying treatment is a true first-order approximation to the wave solution. Fösterling (Ref. 13) has adapted the WKB method to include coupling terms. He considered general values of the geomagnetic dip angle. His results generally confirm those of Booker, namely, that the significant results of the quasi-homogeneous treatment, such as polarization, are approximately correct. Wilkes (Ref. 14) has obtained a formal solution for the coupled wave equations in the case of a linear variation of electron density, but he does not go beyond the formal solution. Feinstein (Ref. 15) has treated the case of a linear variation of electron density for a general angle of geomagnetic dip. He finds that with high electron-density gradients the ellipticity of the polarization ellipse is greater than that predicted by the slowly varying treatment.

Mallinckrodt (Ref. 16) has considered the problem of propagation in an inhomogeneous medium. His treatment is confined to the case of vertical incidence with a general tilt of the earth's magnetic field. For this case, he has shown that any linear medium has two and only two characteristic waves. The polarizations and complex reflection (or transmission) coefficients of the characteristic waves serve to define completely the effect of the medium on any incident wave. The characteristic waves (of either transmission or reflection) are defined as those waves which suffer no change in polarization on transmission or reflection. In the quasi-homogeneous treatment of the magneto-ionic theory, the characteristic waves are the ordinary and extraordinary wave components.

In the magneto-ionic theory, a very simple relationship exists between the polarizations of the ordinary and extraordinary components. It may be shown that $R_o R_x = 1$ or $R_x = 1/R_o$, where R_o and R_x are the polarizations of the ordinary and extraordinary components. Unfortunately, on the basis of Mallinckrodt's treatment, there is no reason to expect that this reciprocal relationship applies to the inhomogeneous case.

All of the work toward development of a wave treatment has contributed to our qualitative understanding of the properties of rapidly varying ionospheric layers. At present, the quantitative results of this work cannot be readily applied to particular propagation problems.

There are no simple equations by which one can find a wave solution corresponding to a particular set of constants. As a result of this fact, the ray treatment must be used in situations in which it is not strictly applicable. Its use is partially justified by the fact that the results of the quasi-homogeneous treatment give a solution which is at least approximately correct.

VI. THE 50-kc/s IONOSPHERIC DATA

Some 50-kc/s relative virtual-height and sky-wave-polarization measurements were made during several nights in October 1952. These data are presented in Figures 35 through 39. The measuring technique and system employed are described in Sections II and III. The measurements of sky-wave field strength and noise field strength were obtained by using a Stoddart AN-URM-6 field-strength meter. This receiver has a bandwidth of 350 cycles per second at a frequency of 50 kc/s. The large loop antenna which is furnished with this instrument was used. Our own 50-kc/s, dual-conversion superheterodyne receiver was used in making the phase-angle measurements. In these measurements, the phase of the sky wave was compared with a reference phase transmitted over a very-high-frequency link. The orientations of the transmitting and receiving antennae are shown in Figure 5.

A. Atmospheric Noise Data

Atmospheric noise data are given in Figures 35, 37, and 39. The noise field strength increased during the evening hours. It reached its maximum value between 0030 and 0130 PST. During the early morning hours of 0300 to 0400 PST the noise field intensity began to decrease. The atmospheric noise received in the east-west direction reached a much higher maximum value than that received in the north-south direction.

At 50 kc/s, atmospheric noise from distant sources is propagated as a ground wave or as a sky wave by E-layer reflections at oblique incidence. The sky wave suffers great attenuation in passing through the D-layer. The D-layer dissipates during the night. Thus, during the middle of the night, when the noise sky wave is not attenuated by the D-layer, the noise field strength reaches a maximum value. The

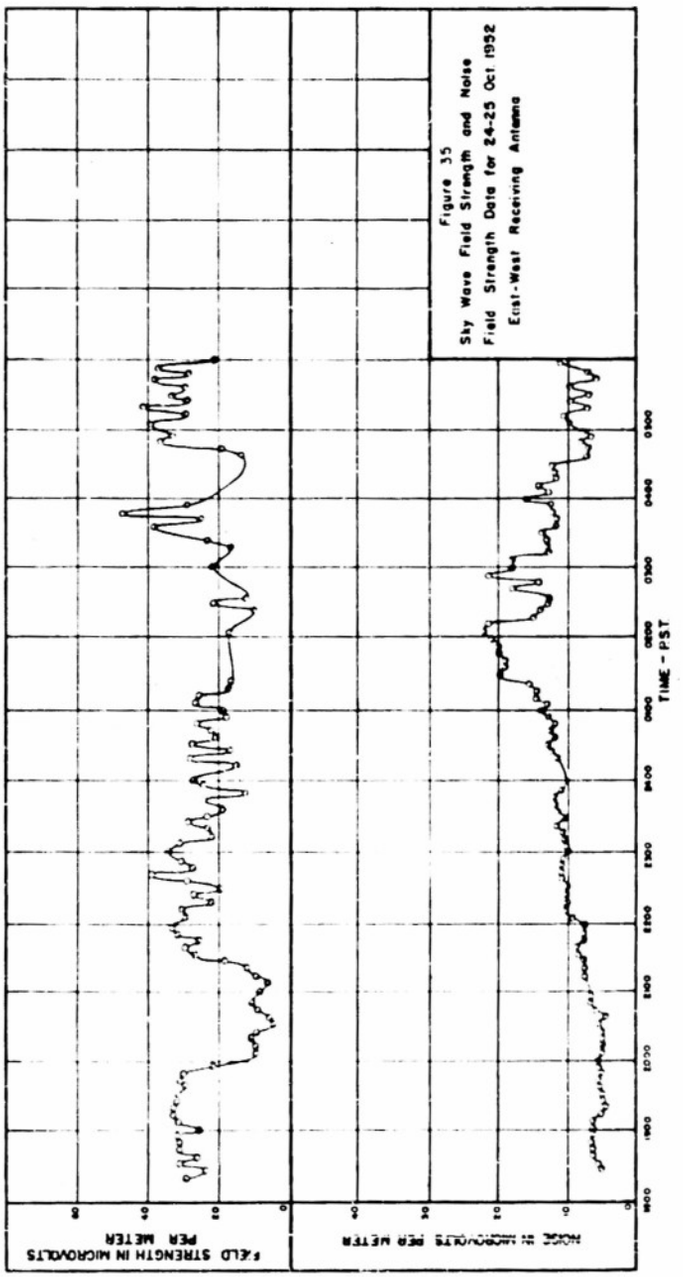
Figure 35
Sky Wave Field Strength and Noise
Field Strength Data for 24-25 Oct 1952
East-West Receiving Antenna
FIELD STRENGTH IN MICROVOLTS PER METER
NOISE IN MICROVOLTS PER METER
TIME - PST

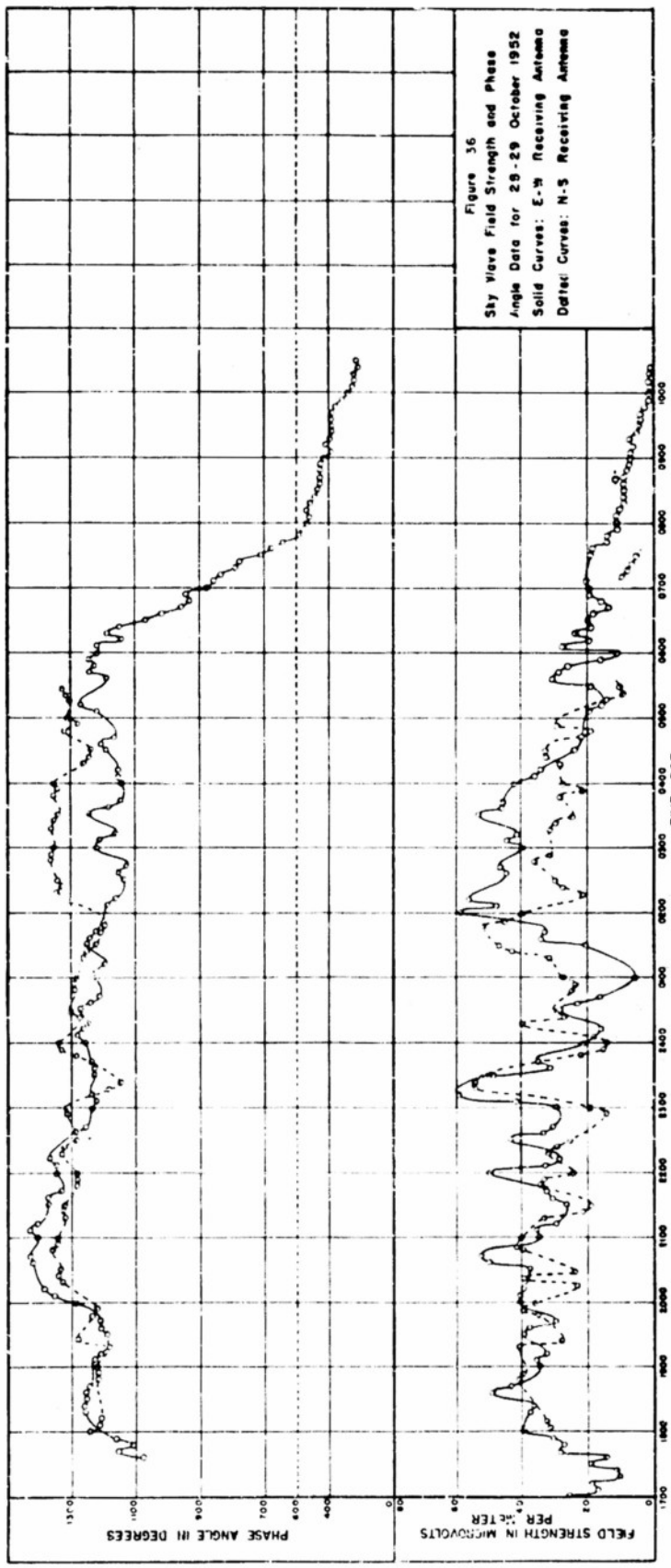
Figure 36
Sky Wave Field Strength and Phase
Angle Data for 28-29 October 1952
Solid Curves: E-W Receiving Antenna
Dotted Curves: N-S Receiving Antenna
PHASE ANGLE IN DEGREES
FIELD STRENGTH IN MICROVOLTS PER METER
TIME - PST

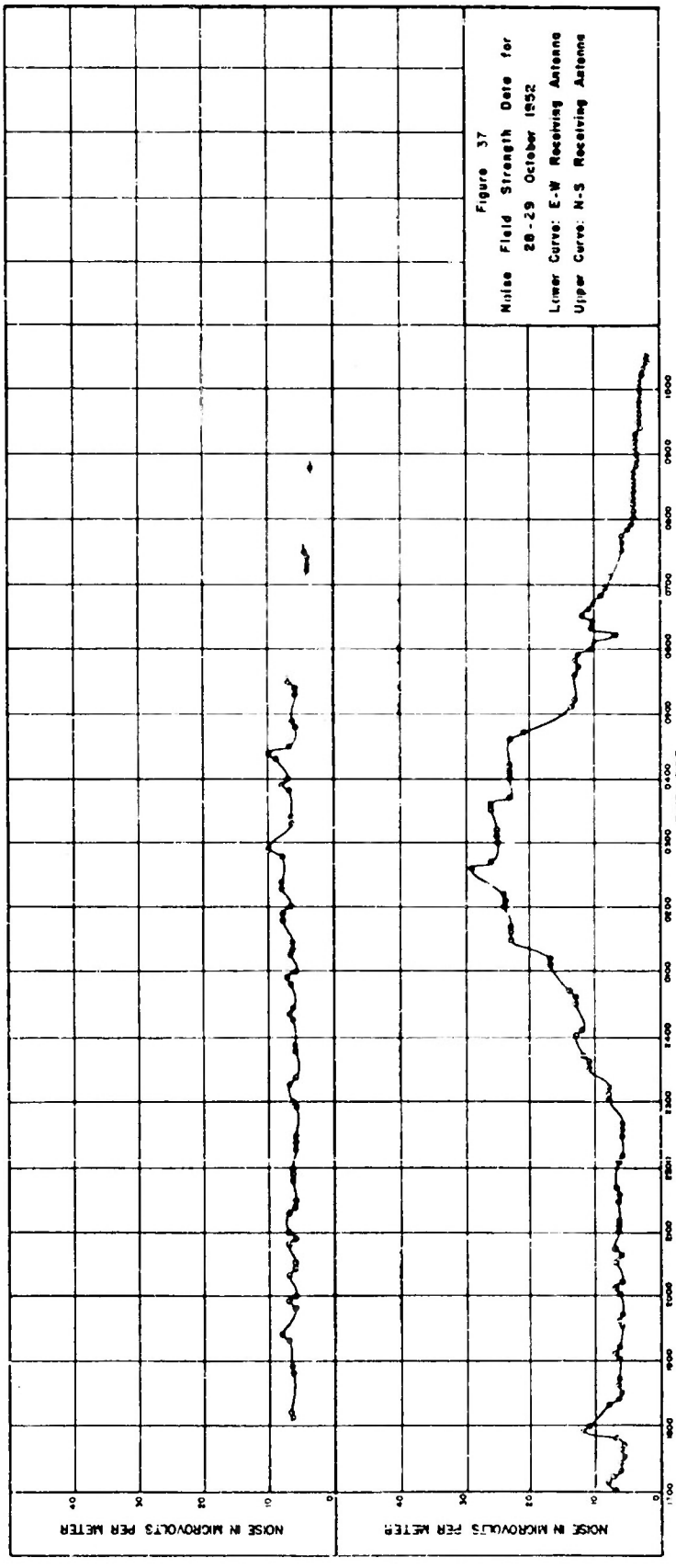
Figure 37
Noise Field Strength Data for
28-29 October 1952
Lower Curve: E-W Receiving Antenna
Upper Curve: N-S Receiving Antenna
NOISE IN MICROVOLTS PER METER
NOISE IN MICROVOLTS PER METER
TIME - PST

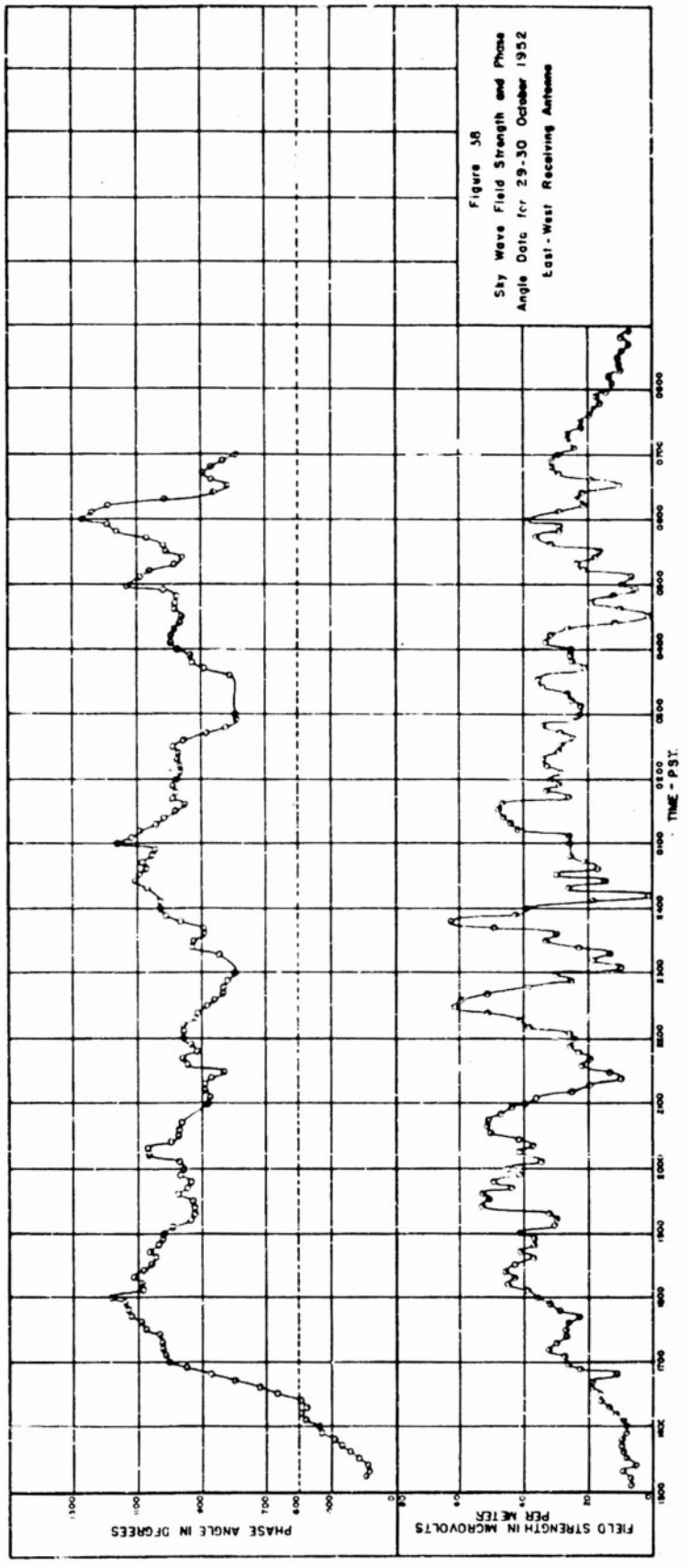
Figure 38
Sky Wave Field Strength and Phase Angle Data for 29-30 October 1932
East - West Receiving Antenna
FIELD STRENGTH IN MICROVOLTS PER METER
PHASE ANGLE IN DEGREES
TIME - PST.

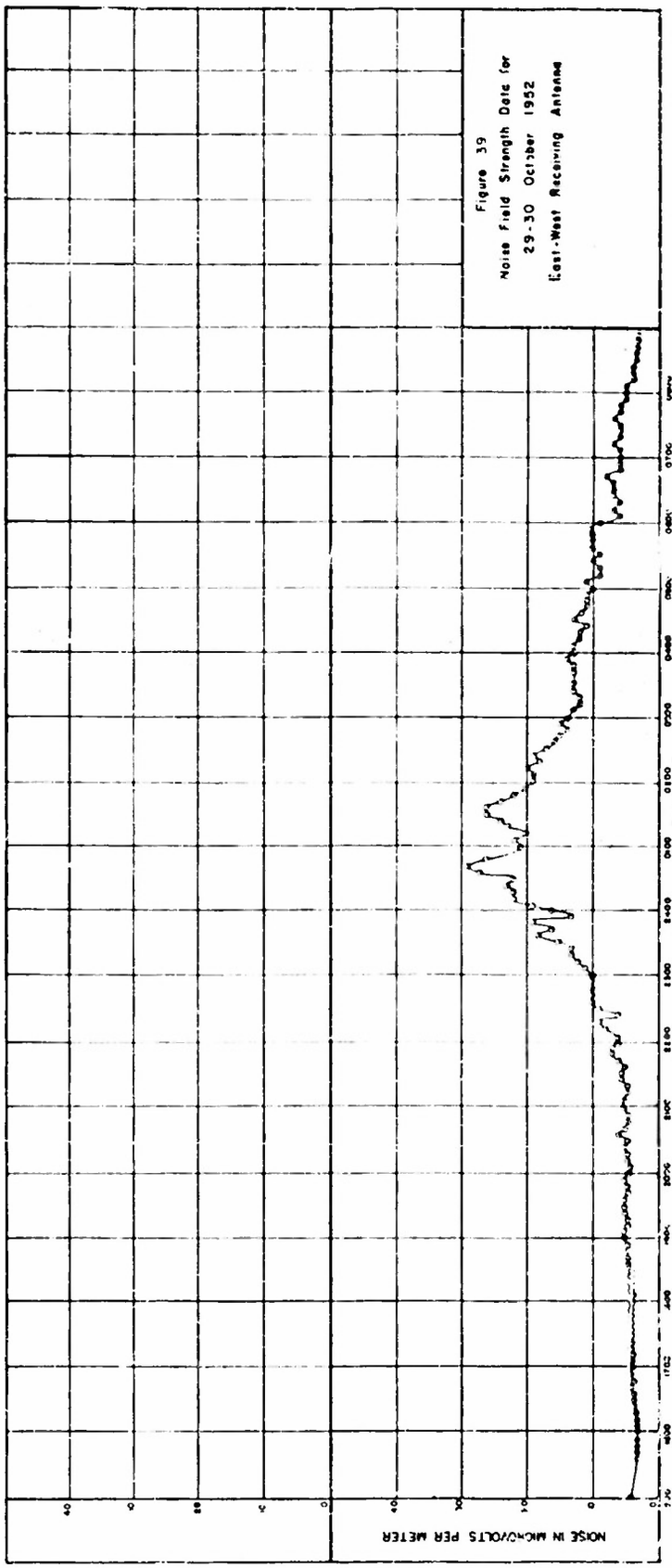
Figure 39
Noise Field Strength Data for
29-30 October 1952
East-West Receiving Antenna
NOISE IN MICROVOLTS PER METER
TIME - PST

authors believe that the higher noise field strengths received in the east-west direction are due to atmospheric noise from tropical storms located in the Gulf of Mexico and the Caribbean Sea.

B. Relative Virtual-Height Data and the Sunrise Effect

Changes in the virtual height of the E-layer may be computed from the changes in the phase angle of the sky wave. Absolute virtual-height measurements could be made by determining the total phase shift of the reference signal.

In Figure 40, the geometry of reflection from the E-layer is given. A nominal height of 90 km is assumed for the reflecting layer. At 50 kc/s, a change of 360° in the

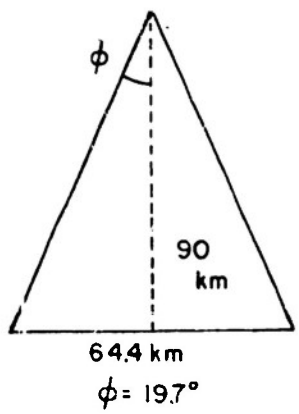

Figure 40. E-Layer Reflection

phase angle of the sky wave corresponds to a change of 2.83 km in the virtual height. A phase change of 5 or 6° can be easily resolved. Thus the resolution of the virtual-height measurements is approximately 0.05 km. The resolution of this continuous-wave system is much higher than that of pulse systems. Pulse systems have an advantage in that two or more partially reflecting layers can be detected if the wavelength is less than the layer separation. There is no advantage in using pulse techniques for making vertical-incidence measurements at very-low frequencies.

During the night, the virtual height of the E-layer fluctuated by about 2 to 3 km. It is possible that at times our signal was reflected from two or more partially reflecting layers rather than from a single layer.

The relative virtual-height measurements made with the two receiving antennae differ. This difference is interpreted as being evidence for strong magneto-ionic splitting. On entering the ionized region, the incident wave must have been split into two parts, presumably the magneto-ionic components. These two wave components travel different paths and are reflected from different heights. This effect would give rise to the phase difference that is observed on the two receiving dipoles.

It should be remembered that the measured phase angles are subject to an uncertainty of an integer times 360 degrees. Therefore, it cannot be concluded that the virtual heights for the reflection of the two components differ only by small amounts or change sign as indicated in Figure 36.

During the late afternoon and early evening (the sunset period), the height of the layer increased by about 7.5 km, and during the morning (the sunrise period), the layer lowered by about 7.5 km. This height change agrees very well with the average values observed in October. Ground sunrise occurred at 0608 PST on 29 October. No significant change in height was observed prior to ground sunrise.

C. Sky-Wave, Field-Strength Data and Relative Reflection Coefficients

Sky-wave, field-strength data are presented in Figures 35, 36 and 38. All measurements were made with a constant input power of 625 watts at the transmitting antenna terminals. The sky-wave field strength is a measure of the E-layer reflection coefficient. The data give the relative changes in the reflection coefficients. By suitably calibrating the system, absolute reflection-coefficient measurements could be made.

Data for two reflection coefficients $_{\perp}R_{\perp}$ and $_{\perp}R_{\parallel}$ were taken. $_{\perp}R_{\perp}$ is measured when the antennae are oriented so that the transmitted signal and received signal are polarized normal to the plane of incidence. $_{\perp}R_{\parallel}$ is a conversion coefficient. It is measured when the antennae are oriented so that the transmitted signal is polarized normal to the plane of incidence and the received signal is polarized parallel to the plane of incidence. By selecting a receiving site in a direction off the end of the transmitting dipole, an additional coefficient $_{\parallel}R_{\perp}$ could be measured. The 50-kc/s ground wave would probably interfere with the measurement of the $_{\parallel}R_{\parallel}$ reflection coefficient.

The 50-kc/s sky wave is attenuated by the D-layer. Thus the field strength is a maximum during the night when the D-layer has dissipated. Between 1100 and 1300 PST (the period of maximum D-layer ionization) the field strength was so low that it could not be measured.

The field-strength data show severe and rapid fluctuations. This is evidence of strong magneto-ionic splitting. The phenomenon of rapid fading during strong magneto-ionic splitting has been observed before (Ref. 17). Several factors possibly contributed to this effect. First, the virtual height was varying considerably. This fact is probably indicative of large fluctuations in the ionization gradients which would cause variations in the reflection coefficients. There may be interference effects due to the presence of two or more partially reflecting layers. Also there may be partial interference between the two magneto-ionic components.

The two amplitude curves tend to fluctuate together. The component in the plane of incidence (N-S antenna) may be larger or smaller than the component normal to the plane of incidence (E-W antenna). At no time is the ratio of the two components either very large or very small. Hence for this particular set of night observations the reflection coefficient $_{\perp}R_{\perp}$ and the conversion coefficient $_{\perp}R_{\parallel}$ are of the same order of magnitude during most of the night. This is rather interesting, particularly since the transmitted signal is definitely plane polarized normal to the plane of incidence.

In Section V-A it was shown that the ionization density required for reflection of the extraordinary component is approximately 29.3 times that necessary for reflection of the ordinary component. With a scale height of 0.7 km, this increase in ionization corresponds to a distance of 2.36 km. This distance is nearly equal to 3 km, the half-wavelength in free space at 50 kc/s. Thus interference effects between the split components should be important. With fluctuating ionization gradients, interference between the magneto-ionic components would give rise to variations in the polarization of the sky wave. The polarization of the sky wave is considered next.

D. Polarization of the Sky Wave

The phase-angle and field-strength data of Figure 36 give all of the information which is necessary for completely describing the polarization of the down-coming wave. The polarization of the sky wave may be described in terms of an electric-polarization ellipse. Let us calculate the ellipticity of this ellipse.

The sky wave is received on crossed dipole antennae. Let the voltage induced in the north-south antenna be given by

$$x = E_{NS} \cos \omega t \tag{48}$$

and let the voltage induced in the east-west antenna be given by

$$y = E_{EW} \cos (\omega t + \delta) \tag{49}$$

where south and east are the $+x$ and $+y$ directions. E_{NS}, E_{EW}, and δ are quantities which are measured in the experiment. Equations 48 and 49 are the parametric equations for an ellipse. By eliminating t in these equations, we obtain

$$\frac{x^2}{E_{NS}^2} + \frac{y^2}{E_{EW}^2} - \frac{2xy}{E_{NS} E_{EW}} \cos \delta = \sin^2 \delta \tag{50a}$$

or

$$E_{EW}^2 x^2 - 2(E_{EW} E_{NS} \cos \delta) xy + E_{NS}^2 y^2 = E_{EW}^2 E_{NS}^2 \sin^2 \delta \tag{50b}$$

The term containing xy in Equation 50b can be eliminated by rotating the coordinate system through an angle ϕ, where ϕ is given by the expression

$$\phi = \frac{1}{2} \tan^{-1} \left(\frac{-2 E_{EW} E_{NS} \cos \delta}{E_{EW}^2 - E_{NS}^2} \right) \tag{51}$$

If this coordinate transformation is performed, it is easy to show that the ellipticity of the polarization ellipse is given by the equation

$$\epsilon_1 = \left(\frac{A - \sqrt{B}}{A + \sqrt{B}} \right)^{\frac{1}{2}} \tag{52}$$

where

$$A = E_{EW}^2 + E_{NS}^2 \tag{53}$$

$$B = E_{EW}^4 - 2 E_{EW}^2 E_{NS}^2 (1 - 2\cos^2\delta) + E_{NS}^4 \tag{54}$$

The ellipticity ϵ_l is defined as the ratio of the minor axis to the major axis of the ellipse. Equation 52 was used in calculating the ellipticity of the polarization ellipse. These data are shown in Figure 41.

The angle ϕ gives the orientation of the minor axis of the electric-polarization ellipse with respect to the x-y coordinate system. By referring to Figure 5, we see that Θ, the angle of the major axis with respect to the geomagnetic coordinates, is given by the expression

$$\Theta = \phi - 90° - 61° = \phi - 151° \tag{55}$$

A curve of Θ as a function of time is given in Figure 42.

Both the ellipticity and orientation of the major axis of the ellipse varied during the night. This fact is to be expected under conditions of strong splitting and fluctuating ionization gradients. However, it is interesting to note that, during most of the night, the major axis was oriented approximately magnetic east-west. The ellipticity, or ratio of the axes of the ellipse, is less than 0.5 for a larger fraction of the time than it is greater than 0.5. Thus, the field tends to be plane polarized rather than circularly polarized.

It is interesting to estimate the limiting polarization. The limiting polarization is the polarization that the magneto-ionic components possess on emergence from the ionosphere. A plane-polarized wave incident on the ionosphere is split into the two magneto-ionic components. These components, if they could retrace their original paths, would on emergence have the same polarization which they possessed on entry into the ionosphere. Thus the limiting polarization may be calculated approximately by letting the ionization density N approach zero in the expression for the polarization. With $N \longrightarrow 0$,

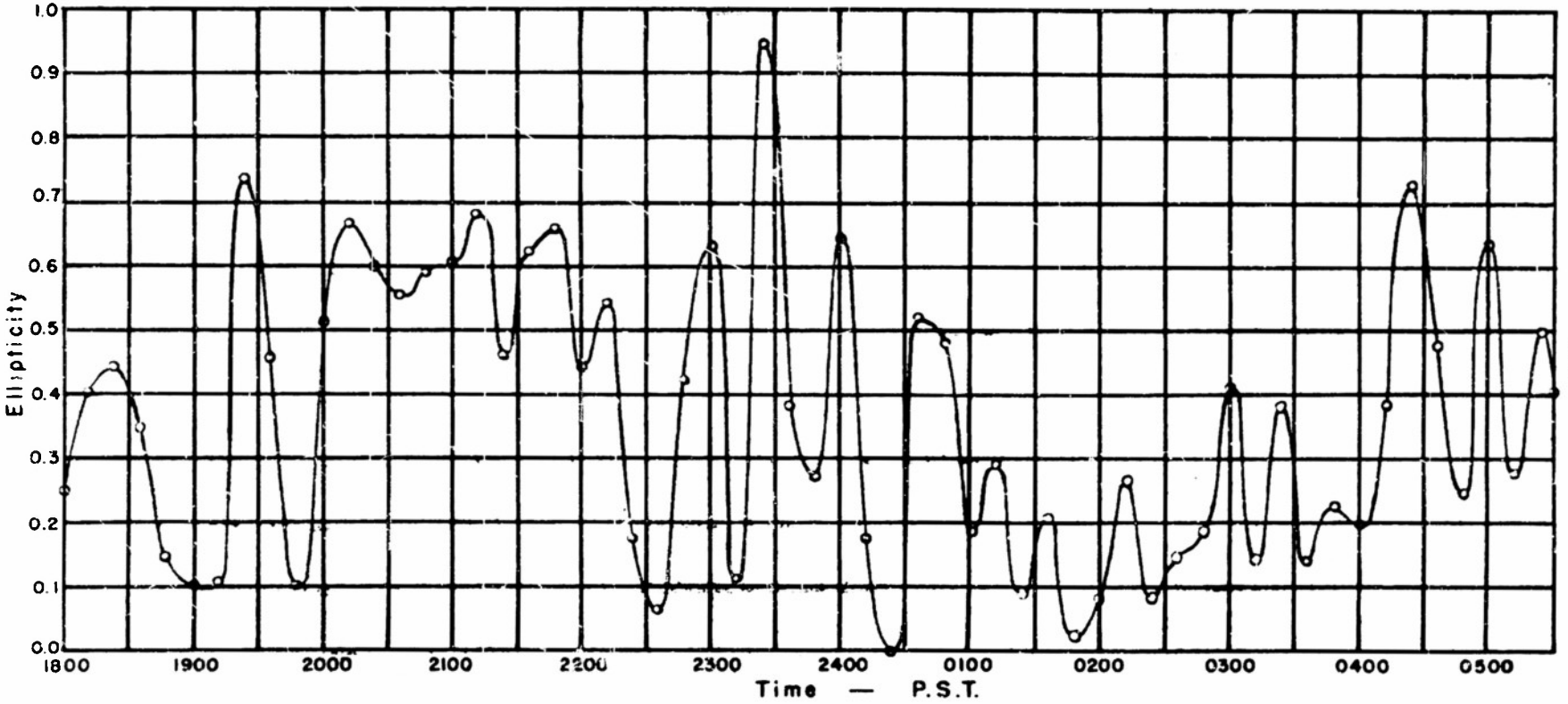

Figure 41. Ellipticity of the Polarization Ellipse October 28-29, 1952

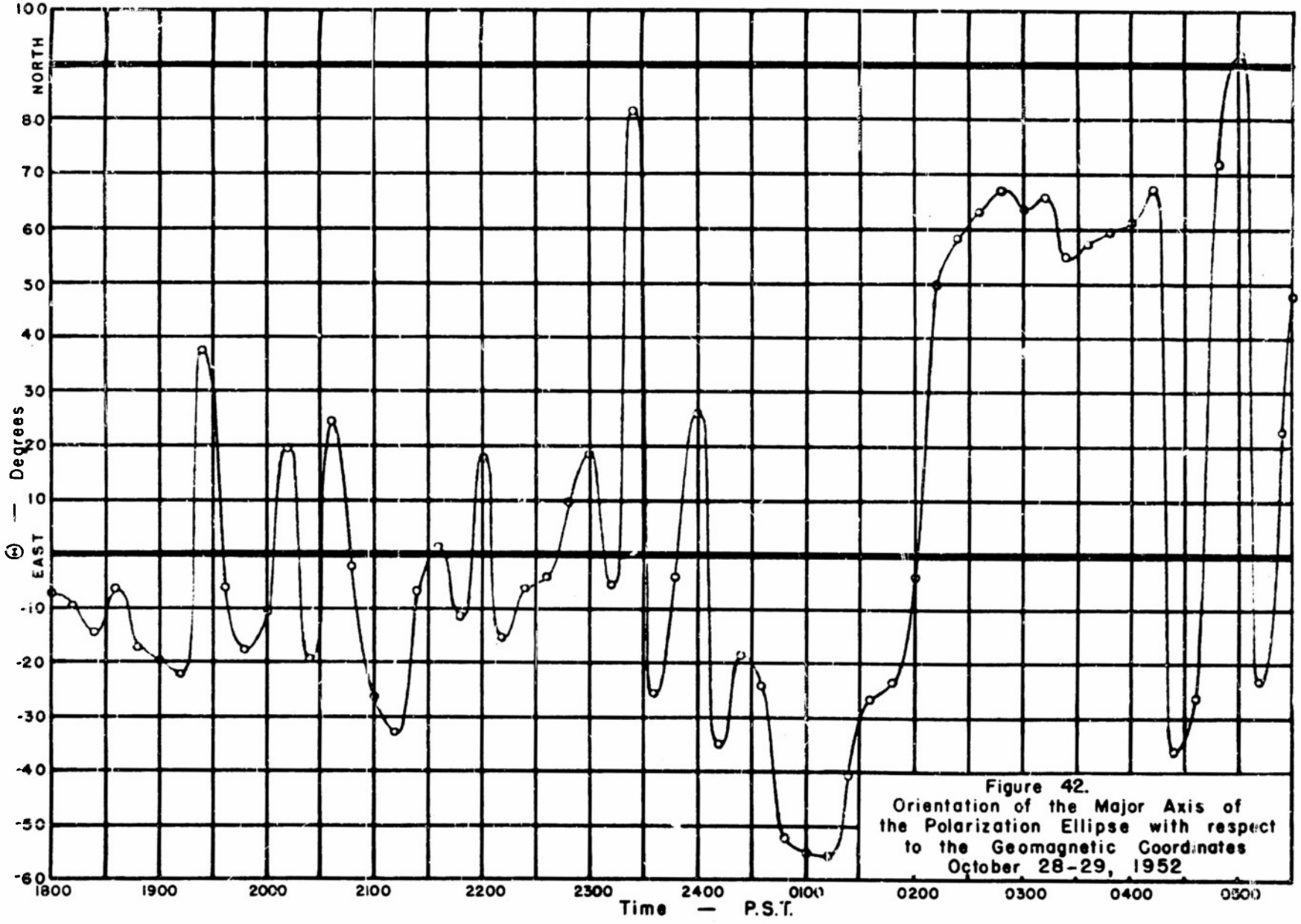

Figure 42.
Orientation of the Major Axis of the Polarization Ellipse with respect to the Geomagnetic Coordinates October 28-29, 1952

$$R_{I_{N\to 0}} = \frac{j}{\mu_v H_L}\left[\frac{\mu_v^2 H_T^2}{\left(-\frac{\omega m}{e}+j\frac{m\upsilon}{e}\right)} \pm \sqrt{\frac{\mu_v^4 H_T^4}{\left(-\frac{\omega m}{e}+j\frac{\omega\nu}{e}\right)^2}+\mu_v^2 H_L^2}\right] \quad (56)$$

By substituting in Equation 96 the values

$H_L = 0.44$ gauss

$H_T = 0.25$ gauss

$\upsilon = 1.56 \times 10^6$ per second (electronic collisional frequency for nighttime at 90 km)

$\omega = \pi \times 10^5$ radians/sec

we obtain for the ordinary wave

$$R_O\Big|_{N=0} = 0.794\, e^{-j\,138.4^\circ} \quad (57)$$

and for the extraordinary wave

$$R_x\Big|_{N=0} = 1.26\, e^{+j\,138.4^\circ} \quad (58)$$

If the collisions of the electrons with other particles are neglected, we obtain for the ordinary wave

$$R_O\Big|_{\substack{N=0\\ \nu=0}} = 0.124\, e^{-j\,90^\circ} \quad (59)$$

and for the extraordinary wave

$$R_x\Big|_{\substack{N=0\\ \upsilon=0}} = 8.06\, e^{+j\,90^\circ} \quad (60)$$

Equations 59 and 60 show that, in the absence of collisions, the ordinary wave is elliptically polarized with the major axis of the electric polarization ellipse magnetic north-south, and the extraordinary wave is elliptically polarized with the major axis of the electric polarization ellipse magnetic east-west. As a result of the electron collisions,

the ellipticity of the polarization ellipses is increased, and the major axes are rotated symmetrically toward the northeast-southwest direction. By referring to Equation 51, we find that the major axes are rotated through an angle of 36.4°

It is somewhat difficult to interpret the polarization data of Figure 42, because the two magneto-ionic components cannot be separated. At any time the two components add together, or partially interfere with one another, to give the resultant signal.

VII. CONCLUSION

The work that has been accomplished has demonstrated the value and flexibility of a new technique for studying the ionosphere at low frequencies. It has been shown that the ground antenna operates as predicted. This antenna has high radiation efficiency; it is easy and inexpensive to construct; it is resonant and readily tunable; and it has an ideal radiation pattern for vertical-incidence ionospheric studies. It should be profitable to carry out both theoretical and experimental work to determine whether or not some antenna of this general nature would be useful for low-frequency communication purposes.

In Northern Canada there is a great need for dependable communication systems. High-frequency and very-high-frequency sky-wave propagation is unreliable, because at these high latitudes there is insufficient ionization in the upper atmosphere. Since most of the atmospheric noise originates in the tropical latitudes, the low-frequency radio noise level is very low. Thus low-frequency, ground-wave propagation should provide a most satisfactory means of communication. Conventional low-frequency antenna systems have the disadvantage of being expensive to construct. The ground-dipole antenna radiates a large ground-wave field. Thus a ground dipole or some modification of it might prove very satisfactory for communication purposes in northern latitudes.

Ground antennae should be useful in oblique-incidence ionospheric studies. The present antenna radiates the major part of its energy vertically upward, a fact which is ideal for vertical-incidence experiments However, for oblique-incidence experiments, the radiation should be at a moderate angle with the horizon. This type of radiation pattern may be achieved by using an array of two parallel dipole antennae or by arranging the antennae in the form of a resonant loop.

It is difficult to draw any definite conclusions from the 50-kc/s data that have been taken, because, statistically, they cannot be regarded as typical or representative. More of the same type of data should be taken both at 50 kc/s and at lower frequencies. The system should be calibrated so that absolute measurements of virtual height and reflection coefficients could be made. It would be of interest to attempt to correlate very-low-frequency ionospheric data with terrestrial magnetic activity and the occurrence of solar flares.

With a moderate amount of additional equipment, the transmitting antenna could be pulsed. It would be of great interest to compare pulse data and continuous-wave data taken under the same conditions and during the same periods of time.

There are no simple methods for separating the two magneto-ionic wave components at the receiving site. However, the polarization of the transmitted signal could be controlled at the transmitter. It is proposed to use crossed transmitting dipoles. By controlling the phase and amplitudes of the currents in the dipoles, either a signal polarized in a manner similar to that of the ordinary component or the extraordinary component could be transmitted. The data obtained would be for the purpose of attempting to understand more fully the mechanism of the interaction of low- and very-low-frequency radio waves with the ionosphere.

The experiments mentioned are but a few of the many that could be performed. Ground antennae and the system described have many outstanding features for use in ionospheric research. It is hoped that a continuation of the research program will result in valuable contributions to the fields of ionospheric physics and radio propagation.

REFERENCES

1. Department of the Army, Technical Manual TM 11-5506.

2. Department of the Army, Technical Manual TM 11-5023.

3. Goldman, S., "Frequency Analysis, Modulation and Noise," 1st ed., New York: McGraw-Hill Book Co., Inc. (1948).

4. Technology Instrument Corp. Instruction Book for Phase Meter Type 320 AB.

5. Sommerfeld, A., and F. Renner, "Strahlungsenergie und Erde Absorption bei Dipole Antennen." Annalen der Physik, vol. 41 (No. 1), pp. 1-36 (1942).

6. Sommerfeld, A., "Partial Differential Equations in Physics," New York: Academic Press Inc. (1949).

7. Hertz, "Die Krafte elecktrischer Schwingungen," Collected Works II, p. 147.

8. Booker, H. G., "Some General Properties of the Formulae of the Magneto-Ionic Theory," Proceedings of the Royal Society, vol. 147, pp. 325-382 (1934).

9. Helliwell, R. A., A. J. Mallinckrodt, F. W. Kruse, and B. A. Wambsganss, Pulse Studies of the Ionosphere at Low Frequencies, Stanford, California: Stanford University, Electronics Research Laboratory (March, 1950).

10. Mott, N. F., "Elements of Wave Mechanics," Cambridge at the University Press (1952).

11. Eckersley, T. L., Proceedings of the Physical Society of London, vol: B-63, p. 49 (1950).

12. Booker, H. G., Proceedings of the Royal Society, vol. A-155, p. 235 (1936).

13. Försterling, H., Hochfrequenz und Elektrotechnik, vol. 59, p. 10 (1942).

14. Wilkes, M. W., Proceedings of the Royal Society, vol. A-189, p. 130 (1947).

15. Feinstein, J., "Ionospheric Wave Propagation at Low Frequencies," IXth General Assembly, Document A. G. 1950/No. 60/Commission III, Zurich, Switzerland: International Scientific Radio Union (1950).

16. Helliwell, R. A., A. J. Mallinckrodt, et al., Interim Progress Report, Ionospheric Research, Stanford, California: Stanford University, Electronics Research Laboratory (March, 1951).

17. Hutchinson, H. P., "Short Period Sky-Wave Fading of CW Emissions, Transactions of the Institute of Radio Engineers, Professional Group on Antennas and Propagation (No. 3), pp. 12-18 (1952).

TECHNICAL REPORTS DISTRIBUTION LIST

Contract Nonr-220 (07)
Project NR 071-261

Addressee	No. of Copies
Chief of Naval Research Department of the Navy Washington 25, D. C. Attn: Code 427	2
Director Naval Research Laboratory Washington, D. C. Attn: Code 2000	6
Code 3460	1
Code 3490	1
Chief, Bureau of Ships Department of the Navy Washington 25, D. C. Attn: Code 838	1
Code 835	1
Chief, Bureau of Aeronautics Department of the Navy Washington 25, D. C. Attn: Code EL 411	1
Chief, Bureau of Ordnance Department of the Navy Washington 25, D. C. Attn: Re4f	1
Chief of Naval Operations Department of the Navy Washington 25, D. C. Attn Op 203Q	1
Op 42	1

Addressee	No. of Copies
Director Naval Air Development Center Johnsville, Pennsylvania Attn: AEEL	1
Director Naval Air Test Center Patuxent, Maryland Attn: Electronics Dept.	1
Director Naval Electronics Laboratory San Diego, Calif. Attn: Dr. J. B. Smyth	1
Director ONR Special Devices Center Port Washington, New York	1
U. S. Naval Post Graduate School Monterey, California Attn: Electronics Engng. Dept.	1
Office of Naval Research Branch Office 346 Broadway New York, N. Y.	1
Office of Naval Research Branch Office 844 North Rush Street Chicago 11, Illinois	1
Office of Naval Research Branch Office 1000 Geary Street San Francisco 9, California	1
Office of the Chief Signal Officer Pentagon Bldg. Washington 25, D. C. Attn: SIGET SIGOL - 2	1 1

Addressee	No. of Copies
Signal Corps Engineering Labs Evans Signal Laboratory Fort Monmouth, New Jersey Attn: Applied Physics Branch	1
Research and Development Board Pentagon Bldg. Washington 25, D. C.	1
Navy Research Section Library of Congress Washington, D. C.	2
Mass. Inst. of Technology Research Laboratory of Electronics Cambridge, Massachusetts Attn: Prof. A. Hill	1
Harvard University Cruft Laboratory Cambridge, Massachusetts Attn: Prof. H. R. Mimno	1
Office of Naval Research Branch Office 1030 East Green Street Pasadena 1, California	2
Officer in Charge Office of Naval Research Navy #100, Fleet Post Office New York, N. Y.	3
Headquarters U. S. A. F. Pentagon Bldg. Washington 25, D. C. Attn: AFDRD-EL5	1
Commanding General Rome Air Development Center Griffis Air Force Base Rome, New York Attn: Technical Library	1

Addressee	No. of Copies
Commanding General Air Force Cambridge Research Laboratory 230 Albany Street Cambridge, Massachusetts	1
Commanding General Wright-Patterson Air Development Center Dayton, Ohio Attn: WCEO	1
Cornell University School of Electrical Engng. Ithaca, New York Attn: Prof. C. R. Burrows	1
University of Illinois Department of Electrical Engineering Urbana, Illinois Attn: Prof. E. Jordan	1
Stanford University Department of Electrical Engineering Stanford, California Attn: Prof. O. G. Villard	1
Dartmouth College Thayer School of Engineering Hanover, New Hampshire Attn: Prof. M. G. Morgan	1
Pennsylvania State College Department of Electrical Engineering State College, Pennsylvania Attn: Prof. A. Waynick	1
University of Texas Department of Electrical Engineering Austin, Texas Attn: Prof. A. W. Straiton	1

Addressee	No. of Copies
National Bureau of Standards Central Radio Propagation Laboratory Washington 25, D. C. Attn: Dr. N. Smith	1
National Bureau of Standards Boulder Laboratory, Radio Division P. O. Box 299 Boulder, Colorado	1
Office of Technical Services Department of Commerce Washington 25, D. C.	1
Armed Services Technical Information Agency Document Service Center Knott Building Dayton 2, Ohio	5